EVENT-TRIGGERED AND AFFINE FORMATION CONTROL OF MULTIPLE ROBOTIC SYSTEMS

by

Zipeng Huang

Submitted in partial fulfillment of the requirements
for the degree of Doctor of Philosophy

at

Dalhousie University
Halifax, Nova Scotia
December 2021

Table of Contents

List of Tables . . . . . **v**

List of Figures . . . . . **vii**

Abstract . . . . . **xi**

List of Abbreviations and Symbols Used . . . . . **xii**

Acknowledgements . . . . . **xiv**

Chapter 1 Introduction **1**

1.1 Research Background 1

1.2 Literature Review on Formation Control 2

1.3 Literature Review on event-triggered control (ETC) 6
1.3.1 ETC Consensus Control 6
1.3.2 Zeno Behavior and Zeno-free Approaches 8

1.4 Thesis Objectives 10

1.5 Thesis Outline and Contributions 11

Chapter 2 Preliminary Theory and Problem Formulation **13**

2.1 Graph Theory 13
2.1.1 Laplacian Matrix 13
2.1.2 Oriented Incidence Matrix 14
2.1.3 Stress Matrix 15

2.2 Matrix Theory 17
2.2.1 Kronecker Product 17
2.2.2 Useful Matrix Inequality and Property 18

2.3 Problem Formulation 19
2.3.1 Event-Triggered Formation Control 19
2.3.2 Affine Formation Control 21

Chapter 3 Experimental Hardware and Software **22**

3.1 Pioneer Mobile Robots 22

3.2 Crazyflie Aerial Robot 25

3.3 Motion Capture Systems 30

3.4 Communication and Control System 31

Chapter 4 Event-Triggered Formation Control with an Autonomous Leader 34

4.1 Controller and Event Generator Design 35
4.1.1 Controller Design 35
4.1.2 Closed-loop Dynamics 36
4.1.3 Event Generator Design 37
4.1.4 Main Results 38

4.2 Simulation Results 45
4.2.1 Effect of Communication Mechanisms 48
4.2.2 Effect of Triggering Threshold ϵ 49

4.3 Experimental Results 50

4.4 Conclusion 56

Chapter 5 Event-Triggered Formation Control with a Non-autonomous Leader 57

5.1 Distributed Event-Triggered Formation Control Strategy 57
5.1.1 Controller Design 58
5.1.2 Closed-loop Dynamics 58
5.1.3 Event Generator Design 60
5.1.4 Main Results 62

5.2 Simulation Results 66
5.2.1 Effect of Communication Mechanisms 67
5.2.2 Effect of Triggering Threshold ϵ 70

5.3 Experimental Results 71

5.4 Conclusion 79

Chapter 6 Edge-Triggered Formation Control 80

6.1 Edge-Triggered Formation Control Strategy 81
6.1.1 Edge-states-based Formation Controller Design 81
6.1.2 Closed-loop Formation Error Dynamics 82

6.2 Edge Event Generator Design 84

6.3 Main Results 87

6.4 Simulation Results 98
6.4.1 Feasibility Region Analysis 99
6.4.2 Effect of Communication Mechanisms 102
6.4.3 Effect of Triggering Threshold ϵ 103

6.5 Experimental Results 104

6.6 Conclusion 112

Chapter 7 Affine Formation Control for Multiple Quadcopters . . 113

7.1 Affine Controller Design 114

7.2 Simulation Results 116

7.3 Conclusion 121

Chapter 8 Conclusions and Future Research 122

8.1 Conclusions 122

8.2 Future Research 123

Bibliography 125

Appendix A Author's Publications 134

List of Tables

1.1 Constraints and tools among displacement-, distance-, and bearing-based formation controllers (p_i and p_j denote the position vectors of two neighboring agents) 5

3.1 Technical specifications of Crazyflie 26

4.1 Simulation results of l_2 norm of formation error (m) 49

4.2 Simulation results of triggering percentage (%) 49

4.3 Simulation results of average communication frequency (Hz) of all agents in (4.1) under 10 Hz sampling frequency with different triggering thresholds 49

4.4 Experimental results of l_2 norm of formation error (m) 52

4.5 Experimental results of triggering percentage (%) 52

5.1 Simulation results of l_2 norm (m) of formation error 70

5.2 Simulation results of triggering percentage (%) 70

5.3 Simulation results of average communication frequency (Hz) of all agents in the team under 10 Hz sampling frequency with different triggering thresholds 70

5.4 Simulation results of l_2 norm (m) of formation error in the team under different triggering thresholds 71

5.5 Experimental results of l_2 norm of formation error (m) 72

5.6 Experimental results of triggering percentage (%) 72

6.1 Simulation results of triggering percentage (%) of edges in Fig. 6.3 under three ECMs 102

6.2 Simulation results of l_2 norm (m) of formation error of system (5.1) under three ECMs 103

6.3 Simulation results of total communication events in system (5.1) under edge-triggered ECM and node-triggered ECM with respect to different triggering thresholds 103

6.4 Simulation results of l_2 norm of formation error of system (5.1) under edge-triggered ECM and node-triggered ECM with respect to different triggering thresholds 104

6.5 Experimental results of triggering percentage (%) of edges in Fig. 6.3 under three ECMs 104

6.6 Experimental results of l_2 norm (m) of the formation error of the system (5.1) under three ECMs 105

List of Figures

1.1 Applications of MASs 1

1.2 An illustrative example of the behavior-based formation control strategy 3

2.1 A bi-directional communication topology with three agents as an example 15

2.2 An illustrative example of a stress matrix with four agents in the unit 16

3.1 Pioneer P3-DX and P3-AT robots 23

3.2 Hand position of a differential drive Pioneer robot 24

3.3 Communication devices of Crazyflie 25

3.4 Crazyflie architecture [1] 26

3.5 The inertial(XYZ) and body($X_BY_BZ_B$) frames of Crazyflie 2.0 (9 cm between diagonal rotors) 27

3.6 Control architecture of Crazyflie's on-board controller 28

3.7 Identification and validation results for roll dynamics 29

3.8 Identification and validation results for pitch dynamics 29

3.9 Validation results for yaw dynamics 30

3.10 OptiTrack motion capture (MoCap) calibration steps 31

3.11 Communication graph of the hovering control of Crazyflie . . . 32

3.12 Network settings for deploying a controller node 33

3.13 Quadcopter control framework in Robot Operating System (ROS) 33

4.1 Schematic diagram of the i^{th} agent: formation control with event triggered communication 38

4.2 Communication topology of a mobile robot system with an autonomous leader 45

4.3 Simulation results of the evolution of the team with $\epsilon = 0.0005$ 46

4.4	Simulation results of formation error profile	47
4.5	Simulation results of snapshots of the system (4.1) in the X-Y plane at: a) t=0 *sec*, b) t=3.3 *sec*, c) t=6.6 *sec*, d) t=10 *sec* .	47
4.6	Simulation results of triggering instants	48
4.7	Simulation results of the evolution of the team with $\epsilon = 2$ . . .	50
4.8	Experimental results of the evolution of the team with $\epsilon = 0.0005$	51
4.9	Initial and final positions of Pioneer robots	52
4.10	Experimental results of formation error profile	52
4.11	Experimental results of snapshots in the X-Y plane at: a) t=0 *sec*, b) t=6.6 *sec*, c) t=13.3 *sec*, d) t=20 *sec*	53
4.12	Experimental results of triggering instants	53
4.13	Experimental results of the evolution of the team under PCM	54
4.14	Experimental results of formation error profile under PCM . .	54
4.15	Experimental results of snapshots under PCM in the X-Y plane at: a) t=0 *sec*, b) t=6.6 *sec*, c) t=13.3 *sec*, d) t=20 *sec*	55
4.16	Experimental results of triggering instants under PCM	55
5.1	Simulation results of the formation evolution (5.1) with $\epsilon = 0.0005$	68
5.2	Simulation results of formation error profile	68
5.3	Simulation results of snapshots in the X-Y plane at: a) t=0 *sec*, b) t=4.6 *sec*, c) t=9.3 *sec*, d) t=14 *sec*	69
5.4	Simulation results of triggering instants	69
5.5	Experimental results of the formation evolution under estimate-error-based ECM	72
5.6	Experimental results of the formation error under estimate-error-based ECM	73
5.7	Experimental results of snapshots under estimate-error-based ECM in the X-Y plane at: a) t=0 *sec*, b) t=4.6 *sec*, c) t=9.3 *sec*, d) t=14 *sec*	73
5.8	Experimental results of triggering instants under estimate-error-based ECM	74

5.9 Experimental results of the formation evolution under state-error-based ECM 74

5.10 Experimental results of the formation error under state-error-based ECM 75

5.11 Experimental results of snapshots under state-error-based ECM in the X-Y plane at: a) t=0 *sec*, b) t=4.6 *sec*, c) t=9.3 *sec*, d) t=14 *sec* 75

5.12 Experimental results of triggering instants under state-error-based ECM 76

5.13 Experimental results of the formation evolution under PCM . 76

5.14 Experimental results of the formation error under PCM 77

5.15 Experimental results of snapshots under PCM in the X-Y plane at: a) t=0 *sec*, b) t=4.6 *sec*, c) t=9.3 *sec*, d) t=14 *sec* 77

5.16 Experimental results of triggering instants under PCM 78

6.1 Node and edge triggered schemes (red arrow denotes a communication edge is enabled) 80

6.2 A schematic illustration of the steps in (6.40) 94

6.3 A leader-follower communication topology with edges labeled . 98

6.4 Simulation results of the formation evolution of the system (5.1) under edge-triggered ECM 99

6.5 Simulation results of the formation error profile of the system (5.1) under edge-triggered ECM 100

6.6 Simulation results of snapshots of the system (5.1) under edge-triggered ECM in the X-Y plane at: a) t=0 *sec*, b) t=4.6 *sec*, c) t=9.3 *sec*, d) t=14 *sec* 100

6.7 Simulation results of triggering instants of the system (5.1) under edge-triggered ECM 101

6.8 Feasibility region of (6.28) over $\rho_1, \rho_2, \alpha \in [0, 2]$ 101

6.9 Feasibility region of (6.28) over $\rho_1, \rho_2 \in [0, 2]$ when $\alpha = 1$ . . . 102

6.10 Experimental results of formation evolution of system (5.1) under the edge-triggered estimate-error-based ECM 105

6.11 Experimental results of the formation error system (5.1) under the edge-triggered estimate-error-based ECM 106

6.12 Experimental results of snapshots of the system (5.1) under edge-triggered estimate-error-based ECM in the X-Y plane at: a) t=0 *sec*, b) t=4.6 *sec*, c) t=9.3 *sec*, d) t=14 *sec* 106

6.13 Experimental results of triggering instants of the system (5.1) under the edge-triggered estimate-error-based ECM 107

6.14 Experimental results of the formation evolution of the system (5.1) under the edge-triggered state-error-based ECM 107

6.15 Experimental results of the formation error of the system (5.1) under the edge-triggered state-error-based ECM 108

6.16 Experimental results of snapshots of the system (5.1) under the edge-triggered state-error-based ECM in the X-Y plane at: a) t=0 *sec*, b) t=4.6 *sec*, c) t=9.3 *sec*, d) t=14 *sec* 108

6.17 Experimental results of triggering instants of the system (5.1) under the edge-triggered state-error-based ECM 109

6.18 Experimental results of the formation evolution of the system (5.1) under the edge-based PCM 109

6.19 Experimental results of the formation error of the system (5.1) under the edge-based PCM 110

6.20 Experimental results of snapshots of the system (5.1) under the edge-based PCM in the X-Y plane at: a) t=0 *sec*, b) t=4.6 *sec*, c) t=9.3 *sec*, d) t=14 *sec* 110

6.21 Experimental results of the triggering instants of the system (5.1) under the edge-based PCM 111

7.1 Nominal formation configuration with three leaders (in red) and three followers (in blue) 117

7.2 Simulation results of the formation evolution in X-Y plane . . 118

7.3 Simulation results of the affine formation error 119

7.4 Simulation results of snapshots of the group formation in the X-Y plane at: a) t=0 *sec*, b) t=10 *sec*, c) t=20 *sec*, d) t=30 *sec* 119

7.5 Simulation results of the formation evolution in 3D 120

Abstract

This thesis investigates the time-invariant and time-varying formation tracking control strategies for multi-agent systems (MASs). The time-invariant formation tracking control strategies are studied for multi-robotic systems with general linear agent dynamics under sampled-data-based event-triggered communication settings. Unlike traditional time-triggered communication strategies, event-triggered communication strategies (event generators) are designed in this thesis to adaptively regulate the inter-agent communication with the goal to reduce unnecessary communication while maintaining acceptable system performance. The formation tracking controllers are then designed based on the event-regulated information so that the formation control problem can be transformed into a stability analysis problem of the closed-loop formation error dynamics. Sufficient conditions in the form of linear matrix inequalities (LMIs) that ensure asymptotic convergence of the closed-loop formation error dynamics are derived for systems with an autonomous leader using Lyapunov-based stability analysis methods, and the event generator and controller gains are co-designed such that the derived conditions are feasible. Under a similar structure, a new event generator and a controller are then developed for systems with a non-autonomous leader to enable more general and practical formation maneuverings. A novel edge-based event-triggering strategy is further investigated to reduce communication resources while maintaining comparable system performance. Sufficient conditions that ensure an exponential convergence of the formation error dynamics are derived, where the convergence rate is explicitly expressed and can be tuned based on convergence speed requirements. The developed formation controllers and event generators are validated in simulations and experiments using a group of mobile robots with linearized dynamics. This thesis also studies the time-varying formation control problem for a group of quadcopters with experimentally identified dynamics using a two-layer affine formation control strategy, where a linear affine formation controller is designed based on the virtual translational dynamics in the formation layer and a finite-time controller is designed to track the virtual inputs in the local control layer.

List of Abbreviations and Symbols Used

Abbreviations

DOF	degree-of-freedom.
ECM	event-triggered communication mechanism.
ETC	event-triggered control.
IMU	inertial measurement unit.
LMI	linear matrix inequality.
MAS	multi-agent system.
MIET	minimum inter-event time.
MoCap	motion capture.
PCM	periodic communication mechanism.
PID	proportional-integral-derivative.
ROS	Robot Operating System.
TTC	time-triggered control.

Symbols

I_n	$n \times n$ identity matrix sort.
$\|\cdot\|$	Euclidean norm of a vector.
$\otimes$	Kronecker product.
$\mathcal{Z}_{\geq 0}$	nonnegative integer set.
$\rightarrow$	tends to.
$\mathcal{G}$	graph.
$\mathcal{A}$	adjacency matrix.
$\mathcal{D}$	in-degree matrix.
$\mathcal{E}$	edge set of a graph.
$\mathcal{V}$	node set of a graph.
$\mathcal{L}$	Laplacian matrix.
$\mathcal{N}_i$	neighor set of a node i.

$\mathbf{I}_{inc}$	oriented incidence matrix.
$\mathcal{R}^{M\times N}$	set of $M \times N$ real matrices.
$\mathcal{R}^{N}$	set of $N \times 1$ real vectors.
Ω	stress matrix.
∞	infinity.
$\in$	belongs to.
A^{-1}	inverse of matrix A.
A^{T}	transpose of matrix A.
$\sum$	summation.
$A > 0$	positive definite matrix A.
$\lambda_i(\cdot)$	eigenvalue of a matrix.
$*$	transpose of the off-diagonal block in a block matrix.
$\tau(t)$	time-varying delay.
ϵ	triggering threshold.
$\lvert\cdot\rvert$	cardinality of set.
inf	infimum of a set.
$A(i,:)$	i^{th} row of the matrix A.

Acknowledgements

First of all, I would like to express my sincere gratitude to my supervisors Dr. Ya-Jun Pan and Dr. Robert Bauer of the Mechanical Engineering Department for their continued dedication and availability during the course of my PhD program. It would have been impossible to reach my doctoral milestones without their constant help and encouragement.

Besides my supervisors, I would like to thank my supervisory committee members Dr. Ted Hubbard, Dr. Jason Gu and Dr. Hugh H.T. Liu for their invaluable feedback and advice. I would also like to thank the Advanced Controls and Mechatronics Laboratory research group for their suggestions and comments over the years.

I gratefully acknowledge the financial support from the Nova Scotia Graduate Scholarship (NSGS), the Natural Sciences and Engineering Research Council of Canada (NSERC), and the Department of Mechanical Engineering at Dalhousie University.

Last but not the least, I would like to thank my parents and my fiancée for supporting me spiritually throughout the writing of this thesis and my life in general.

Chapter 1

Introduction

1.1 Research Background

MASs are large-scale systems consisting of multiple intelligent autonomous agents that can achieve coordinated tasks by interacting with each other through exchanging information. The word "agent" can represent a mobile robot, an aerial robot, or a sensor node depending on the control context. MASs can potentially offer higher efficiency, lower cost and more operational capability than a single agent system in achieving tasks that are difficult for a single agent to complete such as search and rescue, border surveillance, payload transportation (as in Fig. 1.1a) and assembly (as in Fig. 1.1b).

(a) Payload transportation [2]

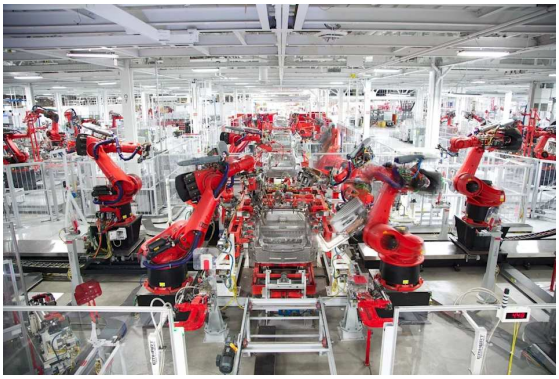

(b) Assembly [3]

Figure 1.1: Applications of MASs

Coordination between the agents is mandatory for the MAS to achieve tasks as a group. Traditionally, coordinating algorithms in MASs are developed using centralized structures where a central computer is responsible for collecting information and scheduling control tasks for all agents; however, the computation and communication power required by centralized structures can grow rapidly as the number of agents increases. Centralized structures are also susceptible to unanticipated failures in the

network, where whole system fails if there is a failure in the central agent. Recently, a substantial amount of work has been conducted on developing distributed coordination control strategies for MASs. In distributed structures, each agent is equipped with microprocessors, sensors and actuators, which enables it to collect data from networks, plan its own tasks, and execute control actions.

Consensus and formation control are two fundamental coordination problems in the study of MASs. A consensus control problem refers to the design of a controller for each agent only based on the information locally available (locally-computable) such that the group of agents can reach an agreement on certain quantities of interest (e.g. position, velocity, and heading). Formation control aims to design distributed controllers that drive the whole group to achieve and maintain a certain geometric pattern of interest. If there is a group reference, the formation control design can generally be classified as a formation tracking design, otherwise it is referred to as a formation producing design.

Continuous information exchange is often assumed in the conventional consensus and formation control studies in MASs; however, this assumption is unrealistic in practical applications since all communication networks have a limit on bandwidth. One possible strategy is to use a periodic communication mechanism (PCM) (time-triggered) where inter-agent communication occurs at regular equally-spaced sampling instants. This strategy can often lead to unnecessary consumption of both network and computation resources, especially as the system approaches its equilibrium and there are no external disturbances. Event-triggered communication mechanisms (ECMs) have recently received considerable attention among researchers due to their potential advantages in saving communication network resources while still maintaining comparable control performances. The underlying idea in event triggered broadcasting is to have agents broadcast and update their sampled states only when necessary. The following sections provide a detailed literature review on formation control, and event-triggered control (ETC).

1.2 Literature Review on Formation Control

Formation strategies, such as birds migrating in a V-shaped formation to improve aerodynamic efficiency [4], have been observed in many biological systems. In recent

years, these formation tactics have also been applied to robotic systems by many researchers in the control and robotics communities to accomplish various tasks including payload transportation [2], object search [5], and forest fire monitoring [6].

Early formation control approaches, such as virtual-structure [7] and behavior-based [8] have been found to be successful in accomplishing many complicated formation control tasks with complex agent dynamics and constraints. In the virtual-structure approach, robots are treated as particles in a physical rigid body, and the geometric relationship (virtual structure) between robots are enforced by human made control systems. Group motion is enabled when a virtual force field is exerted on the virtual structure and individual robot will then move in the direction of the force; however, this approach requires a centralized formulation, and therefore it is difficult to control the robots in a distributed manner. In a behavior-based formation control approach, several behaviors are prescribed for each agent, and the final control input can be determined as a weighted average of the control input from each behavior. This approach is relatively straightforward to implement, but the convergence of the whole system is not guaranteed and stability analysis is very challenging. Fig. 1.2 shows an illustrative example of a behavior-based control strategy, where the control objective for the group of robots is to move from their initial positions to some desired positions while maintaining the triangular formation. Each robot in the system has two behaviors: move to the goal, and maintain the formation. The final control input is then computed as the weighted average of the inputs from these two behaviors.

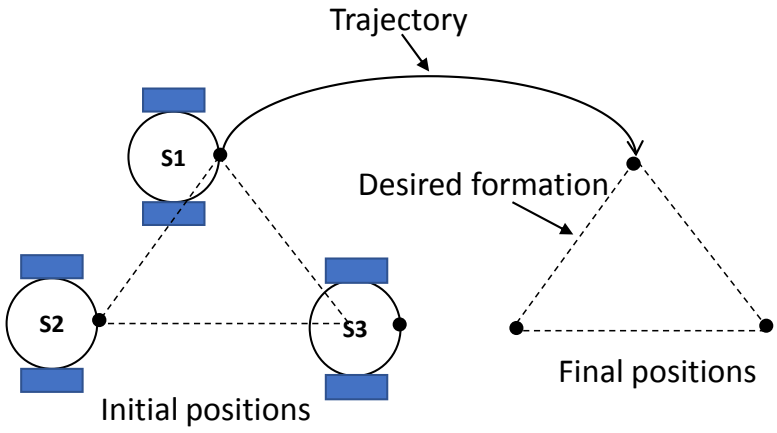

Figure 1.2: An illustrative example of the behavior-based formation control strategy

Distributed formation controllers that can guarantee the overall system convergence have received increased attention from researchers given the early success of applying distributed consensus-based control approaches to the formation control of mobile robots [9, 10]. For MASs with simple integrator-type agents, consensus-based formation controllers can generally be categorized as displacement-based [11, 12], distance-based [13,14], or bearing-based [15,16] in accordance with the constant inter-agent displacement, distance, or bearing constraints that are employed to establish the desired group formation. The group formation maneuverability is largely dependent on the constraints imposed on the system. For example, displacement-based formation controllers can only be applied to track formations with time-varying translations since the constant displacement constraint also implicitly imposes constant orientation and scale constraints on the group formation. In comparison, distance-based controllers are applicable to tasks where both time-varying translations and orientations are desired, but not applicable to tasks that require time-varying scales, while bearing-based controller can be applied to track formations with time-varying translations and scales, but not with time-varying orientations. Table 1.1 summarizes the constant constraints imposed on the group formation along with the common tools used to develop the control algorithm among these three types of formation controllers. Modifications of these controllers have been carried out to overcome some of the limitations induced by the constant formation constraints in the literature. For instance, [17] incorporated a formation scaling factor for the formation size in a displacement-based setup. The scaling factor is only known to a subset of the agents (leaders), and can be estimated by the remaining agents though a formation-scale estimation mechanism. In the distance-based control scheme, [18] demonstrated that it is possible to achieve a resized formation by only changing the desired distance of the leader edge. Nevertheless, additional sensing or communication abilities are often required in order to apply these modifications, and the resultant controller or estimator is usually complicated.

Recently, new time-varying formation controllers have been developed in the literature based on various constraints such as barycentric coordinates [19], complex Laplacians [20], graphical Laplacians [21], and stress matrices [22] that define the

Table 1.1: Constraints and tools among displacement-, distance-, and bearing-based formation controllers (p_i and p_j denote the position vectors of two neighboring agents)

Formation Controllers	Constant Constraint	Theoretical Tools
Displacement-based	$p_i - p_j$	Connected graphs
Distance-based	$\|p_i - p_j\|$	Rigid graphs
Bearing-based	$\frac{p_i - p_j}{\|p_i - p_j\|}$	Bearing Laplacians

target formations. Among these new formation controllers, affine formation controller [23], which is based on constant stress matrices, is a promising method to solve general time-varying formation control problems. In an affine formation control design, the group target formation is defined as an affine transformation (translation, rotation, scaling, shear, or combinations of them) of the nominal formation, and the controllers are designed based on the property that the stress matrices (determined from nominal configuration and underlying communication structure) are invariant to affine transformations. In addition, leader-follower strategies are often adopted in affine formation control design, and the followers' desired positions can be uniquely determined from the leaders' position if the leaders are properly chosen.

Formation control problems for MASs with general linear dynamic agents have also been investigated in the literature. The time-invariant formation producing problem (leaderless) for MASs with linear agents was initially studied in [24] using the Nyquist stability criterion. The more general time-varying formation producing problem was investigated in [25–28] under various settings. A distributed time-delayed formation controller was designed in [25] considering the existence of constant delays in the communication channels. The authors in [26] developed sub-formation controllers based on the solutions from algebraic Riccati equations for general linear MASs that can be partitioned into sub-groups. Sufficient and necessary formation feasibility conditions along with a time-varying formation protocol were presented in [27] for MASs under switching directed communication topologies. Fully distributed time-varying formation controllers were studied using adaptive gain scheduling techniques in [28] for MASs with directed and undirected communication topologies. Apart from formation producing problems, the formation tracking problems (leader-follower) where the entire group is expected to track certain reference trajectories have also been researched.

The authors in [29] studied robust time-varying formation tracking control for a general homogeneous linear MAS in the presence of parameters uncertainties and external disturbances. In particular, controllers were designed such that the closed-loop system is asymptotically stable and the control gains were adaptively adjusted using the σ-modification method to avoid potential unbounded gains. This research was later extended to robust output formation tracking control of heterogeneous linear MASs in [30]. It should be noted that the group formation in [25–30] are defined based on some prespecified time-based formation vectors. Defining time-varying group target formations that can dynamically adapt to changes in the environment for high-order linear MASs is still an open research problem.

1.3 Literature Review on ETC

Different from the traditional time-triggered control (TTC) scheme where sampling and control updates are executed at a fixed period, ETC schemes provide an adaptive way of determining when to sample the system and when to update the control input. This process is usually governed by some pre-designed triggering conditions that depend on system states and performance levels, which are continuously monitored or periodically checked. Although ETC strategies have been historically presented under different names (adaptive sampling, minimum attention control), it is only over the past decade that they have gained their popularity especially in the MAS communities. This section mainly reviews ETC strategies in the context of consensus control of MASs.

1.3.1 ETC Consensus Control

The research in ETC consensus control can generally be categorized based on: agent dynamics, interaction topology, trigger response, event detection, and trigger dependence [31]. ETC was initially studied for single-integrator MASs with asymptotic convergence speed in [32], and a finite-time consensus controller was proposed in [33] using nonlinear ETC strategies. A less conservative triggering function (allowing for larger inter-event time) was proposed in [34] using an integral based Lyapunov approach. The authors in [35] soon extended ETC strategies to double-integrator MASs using a time-dependent triggering function. In addition, the method proposed in [35]

also eliminates the requirements of continuous state information as in [32–34]. To expand the applications and to include more realistic physical system dynamics, ETC strategies have been developed for general linear MASs with [36] or without [37–39] external disturbances, and MASs with Euler-Lagrange agents [40]. In general, developing ETC strategies for nonlinear MASs is very challenging and only a few results are available in the literature. Interaction topologies between agents play important roles in the consensus control of MASs. It is acknowledged that the consensus design for MASs under directed topologies is generally harder than that for MASs under undirected topologies. Early works [32–34, 41] of ETC consensus control were primarily conducted for MASs under undirected topologies. The authors in [42] studied the ETC average consensus problem under a weight-balanced directed communication topology. Results of ETC under more general directed topologies were presented in [43]. In addition to fixed-topologies, some preliminary studies on ETC design for MASs with time-varying topolgies were published in [44, 45].

Trigger response, event detection, and trigger dependence are related to the event generator design and the assumptions placed on the agents' communication/computation abilities. Trigger response refers to what action will be triggered if an event is detected. There are generally three different communication actions: information push [32–36,38,40], information pull [46,47], and information exchange [48,49]. In the information push scheme, an agent broadcasts its state information to neighboring agents and it is assumed that all neighbors can successfully receive the broadcasted information. This communication action is the most common trigger response in ETC studies. The information pull scheme is closely related to the self-triggered formulation [46] where an agent determines its next triggering instant based only on information currently available, and the agent sends a request to its neighbors for new information when a trigger is activated. The information exchange scheme is often assumed in edge-based ETC design, where triggering functions are designed for the communication links and agents connected by a link exchange/swap information when the link triggering condition is violated. Trigger detection refers to how the triggering function evaluations (events) are monitored. Most of the early studies in ETC design assumed that the triggering function can be monitored continuously, which is not practical from an implementation point of view. To eliminate the constraint

of continuous monitoring in hardware implementation, periodic monitoring schemes, where triggering functions are periodically checked, have been developed in [50, 51] by using sampled-data system formulations, or artificially forcing a minimum positive inter-event time. Aperiodic monitoring methods have also been proposed recently in [52] to alleviate the requirement of synchronization from periodic monitoring methods. Trigger dependence refers to how a triggering function is designed and what information is required. In general, triggering functions can be static or dynamic. The static triggering functions can further be classified as state-dependent [32,34] or time-dependent [35, 36, 48]. Dynamic triggering functions [53, 54] depend on internal dynamic variables with their own dynamics that can be designed separately to satisfy certain design requirements.

Alternatively, research in ETC of MASs may be classified into four types of schemes [55]: event-based sampling [32], model-based [37], sampled-data-based [50], and self-triggered [46]. In event-based sampling schemes, systems sample the current measurement only when pre-designed events are triggered. The main drawback of this scheme is that continuous monitoring of events is usually required. Furthermore, this scheme cannot be generalized for agents with time-varying equilibrium trajectories. In model-based schemes, state estimators are designed using model knowledge, and the estimated states are used instead of the true states in the triggering evaluation. This scheme can eliminate the requirements of continuous monitoring; however, the main disadvantage is that an explicit and accurate system model (e.g. system matrix A in linear systems) must be known *a priori*. The sampled-data-based scheme is similar to the periodic event detection method, and the main drawback is the requirement of sampling synchronization across all agents. The self-triggered scheme overlaps with the information pull scheme classified by trigger response. The main disadvantage is that the self-triggered rule design is very complex and is usually system specific.

1.3.2 Zeno Behavior and Zeno-free Approaches

ETC systems are special types of switching systems where they are discontinuous at triggering instants and continuous otherwise. As byproducts of switching systems, Zeno behaviors where infinite switches (jumps/triggers) take place in a finite time interval can also occur in ETC systems. In other words, Zeno behavior can cause an

accumulation point (deadlock) in the system. Therefore, it is of utmost importance to theoretically rule out Zeno behaviors for a valid ETC design. It should be noted that simply enforcing positive inter-event time ($t_{k+1} - t_k > 0$) does not necessarily exclude Zeno behaviors. In addition, ruling out Zeno behavior does not guarantee a minimum inter-event time (MIET) ($t_{k+1} - t_k > c, \forall k \in \mathcal{Z}_{\geq 0}$, where c is a small positive constant value). Nevertheless, a positive MIET is required for an ETC algorithm to be fully implementable since all devices have a limit on operating frequency. To clearly demonstrate these concepts, consider the following examples [31]:

Example 1.1. *Consider a sequence of triggering instants defined by*

$$t_k = \sum_{i=1}^{k} \frac{1}{i^2},\ k \in \mathcal{Z}_{\geq 0}.$$

It is clear that $t_{k+1} - t_k \to 0$ as $k \to \infty$. Further analysis reveals that the sequence $\{t_k\}$ actually has an accumulation point (Zeno behavior occurs) as $t_k \to \frac{\pi^2}{6}$ as $k \to \infty$.

Example 1.2. *Consider a sequence of triggering instants defined by*

$$t_k = \sum_{i=1}^{k} \frac{1}{i},\ k \in \mathcal{Z}_{\geq 0}.$$

It can be observed that Zeno behavior does not occur since $t_k \to \infty$ as $k \to \infty$, and there does not exist a positive MIET because of $t_{k+1} - t_k \to 0$ as $k \to \infty$.

Example 1.3. *Consider a sequence of triggering instants defined by*

$$t_k = \sum_{i=1}^{k} \frac{1}{i} + ck,\ k \in \mathcal{Z}_{\geq 0},$$

where c is a small positive constant. It can be observed that the inter-event time is lower bounded as $t_{k+1} - t_k > c$. Therefore, this triggering sequence has a positive MIET and the Zeno behavior is naturally excluded.

Zeno-free methods have been developed in the literature. The first method involves modifying the triggering function $f(t)$ by adding a strictly positive time-dependent continuous function $h(t)$ (e.g. an exponential decay function) [35, 56]. Then the Zeno

behavior can be excluded by showing that the inter-event time is lower bounded by a positive function dependent on $h(t)$; however, this method does not generate a MIET. Similarly, a strictly constant c can be integrated in the triggering function design [57, 58]. There usually exists a MIET by using this method, but the system performance is deteriorated since the system can only achieve consensus with bounded error that is dependent of the value of c. These two methods are often used together in the literature [59]. Another method uses a time-regulated trigger condition [46, 60]. The next triggering instant t_{k+1} is defined as $t_{k+1} = t_k + \max\{d, \tau_k\}$, where t_k is the latest triggering instant, d is a positive constant, and τ_k is generated from a regular triggering function. This method simply enforces a MIET of d between two consecutive events and therefore rules out Zeno behavior when the inter-event time computed from the regular triggering function is less than d. Notwithstanding this straightforward idea to exclude Zeno behavior, determination of d that ensures overall system convergence is very challenging especially for MASs with complex agent dynamics or communication topologies. Theories from hybrid systems [61] have also been adopted in [54, 62] to study Zeno-free controllers. In particular, the ETC system is reformulated as a hybrid system and the triggering function is designed based on an internal dynamic variable. The asymptotic system convergence can be proved using the invariance principle for hybrid systems, and this method guarantees a MIET. Nevertheless, this method is mainly developed for average consensus of single-integrator MASs and whether it can be extended to MASs with more complex agent dynamics still remains as an open problem. The last method uses a sampled-data-based scheme [50,63], where triggering functions are only evaluated at each sampling instant. A positive MIET is inherently guaranteed as the sampling period, thus the Zeno behavior is completely ruled out. This method inherits the drawbacks from sampled-data systems. For example, some useful information may be ignored when a large sampling interval is used.

1.4 Thesis Objectives

Based on the literature review, it should be noted that the ETC formation control problem is still new and few results are available in the literature. The event-triggered formation producing problem for general linear MASs has been investigated in [64]. Although the event-triggered consensus tracking problem – which is closely related to

the formation tracking problem – has been studied in [65] and [66], the ETC formation tracking problem has not yet been addressed in the literature.

Therefore, the objectives of this thesis are mainly to achieve the time-invariant formation tracking of general linear MASs (which includes the popular single- and double-integrator type agents in formation control studies) with an autonomous and a non-autonomous leader using sampled-data-based ETC strategies applied to wheeled mobile robots. In addition, this thesis also conducts some preliminary affine formation control studies applied to a multi-quadcopter system.

1.5 Thesis Outline and Contributions

This chapter provided a general literature review of the research topics in this thesis along with the thesis objectives. Chapter 2 presents the background theories needed throughout this thesis, along with the research problems studied in this thesis, while Chapter 3 introduces the hardware and software used for conducting experiments in this thesis. Chapter 4 studies ETC formation tracking control for general linear MASs with an autonomous leader. Chapter 5 extends the work from Chapter 4 and studies the ETC formation tracking control for general linear MASs with a non-autonomous leader. Chapter 6 studies the same ETC formation tracking control problem as in Chapter 5 using an edge-based triggering strategy. Chapter 7 studies affine formation control strategies for a multi-quadcopter system, while Chapter 8 summarizes the main results of this thesis and suggests areas for future research.

The main contributions of this thesis are summarized as follows:

1. While conventional formation controllers [25–30] assume continuous data communication, this thesis studies the formation tracking problem using sample-data-based ETC strategies. As a result, the network communication load is significantly reduced.

2. The developed triggering condition and formation protocols use combined measurement of all neighbors' states as opposed to a specific neighbor's information (as used by [59, 65]) when the agent does not have direct access to the leader's information. Consequently, the formulated sufficient conditions for the controller and event generator design can be equivalently decomposed into a set

of low-dimensional conditions, thereby greatly reducing the complexity of the computations.

3. The dynamic non-autonomous leader is taken into consideration when designing the formation protocols in Chapter 5. As a result, the proposed method can accomplish more general and practical leader-follower group formations.

4. A new estimate-error-based triggering condition is developed to effectively reduce the unnecessary communication events that often occur when using a state-error-based triggering condition [64]. A new closed-loop state estimator along with a new tracking controller are proposed to cope with the introduction of a non-autonomous leader in Chapter 5. New sufficient feasibility conditions based on the proposed controller that ensure an asymptotic convergence are derived.

5. A novel edge-based ETC strategy, as opposed to the conventional node-based approaches, is proposed in Chapter 6 to reduce the consumption of communication resources while maintaining comparable performance. New controllers and event generators that are based on the edge-triggered states are proposed. Sufficient conditions that guarantee both asymptotic and exponential convergences are derived. In addition, the exponential convergence speed is explicitly formulated in the derived sufficient conditions.

6. For the first time, this thesis applies the affine formation control strategies to study the time-varying formation control problem for a group of quadcopter agents. A two-layer (affine formation layer and local control layer) affine formation control design scheme given by the underactuated nature of quadcopters is proposed in Chapter 7. The affine formation control tasks can then be achieved by properly designing the controller gains in both layers.

Note that the author's publications are listed in Appendix A, where jounal papers 1-4 and conference papers 1-3 are related to this thesis.

Chapter 2

Preliminary Theory and Problem Formulation

In this Chapter, preliminary theories used in the thesis are introduced. The problem formulations on event-triggered formation control and affine formation control needed for Chapter 3 to Chapter 7 are presented with the MAS formulation.

2.1 Graph Theory

Directed or undirected graphs are naturally adopted to model the information exchange between interacting agents in MASs. A directed graph (digraph) is usually denoted by $\mathcal{G}(\mathcal{V}, \mathcal{E})$ where $\mathcal{V} = 1, \cdots, N$ denotes the node set which symbolizes the agents, and $\mathcal{E} \subseteq \{(i, j) : i, j \in \mathcal{V}, j \neq i\}$ represents the edge set which symbolizes the available communication channels. The edges in digraphs are unidirectional such that an edge $(j, i) \in \mathcal{E}$ indicates that agent i (child node) can receive information from agent j (parent node) but not necessarily vice versa. In addition, the node j is called a neighbor of node i and $\mathcal{N}_i = \{j \in \mathcal{V} \mid (j, i) \in \mathcal{E}\}$ denotes the neighboring set of node i. In contrast to digraphs, edges in undirected graphs are bidirectional, i.e. $(i, j) \in \mathcal{E}$ implies $(j, i) \in \mathcal{E}$. Thus an undirected graph can be viewed as a special case of directed graphs. A directed path from nodes i_1 to i_k is a sequence of ordered edges of the form (i_l, i_{l+1}), $l = 1, \cdots, k-1$. A digraph has a directed spanning tree if it contains at least one node called the root which has no parent node and has directed paths from that node to every other node [10].

2.1.1 Laplacian Matrix

The adjacency matrix $\mathcal{A} = [a_{ij}]$ of a graph is defined such that a_{ij} is a positive weight if $(j, i) \in \mathcal{E}$ and $a_{ij} = 0$ otherwise. Note that $a_{ii} = 0$ since a self-edge is not allowed. Throughout this thesis, we assign $a_{ij} = 1$ if $(j, i) \in \mathcal{E}$. The associated in-degree matrix $\mathcal{D}$ is a diagonal matrix with its diagonal entry given by $d_{ii} = \sum_{j=1}^{N} a_{ij}, i = 1, \cdots, N$. The Laplacian matrix of the graph $\mathcal{G}$ is then defined as $\mathcal{L} = \mathcal{D} - \mathcal{A}$, which is always

symmetric for an undirected graph. Leader-follower-type communication topologies are adopted throughout this thesis and the following assumption holds if not explicitly stated hereafter. Example 2.1 shows the Laplacian matrix for an undirected topology.

Assumption 2.1. *The leader agent has a directed path to all follower agents but does not receive information from any of them. In addition, the communication among follower agents are assumed to be bidirectional.*

It follows that the Lapalacian matrix $\bar{\mathcal{L}}$ for a leader-follower-type topology with one leader (agent 0) and N followers (agent $1, \cdots, N$) has the following form

$$\tilde{\mathcal{L}} = \left[\begin{array}{c|c} 0 & 0_{1\times N} \\ \hline -\mathbf{d} & L_{ff}, \end{array}\right], \tag{2.1}$$

where the element d_i in $\mathbf{d}$ is 1 if agent i can receive information from the leader and d_i is 0 otherwise. Moreover, $L_{ff} = \mathcal{L} + diag\{d_1, \cdots, d_N\}$, where $\mathcal{L}$ characterizes the communication among follower agents.

Lemma 2.1. [67] *For a leader-follower-type communication topology under Assumption 2.1, L_{ff} is positive definite.*

2.1.2 Oriented Incidence Matrix

Incidence matrices are often used to encode the relation between edges and node-node pairs in graph theory. The oriented incidence matrix of a directed graph is denoted as $\mathbf{I}_{inc} \in \mathcal{R}^{M\times N}$, where M and N are the numbers of available edges and nodes, respectively. An incidence matrix can then be defined such that $\mathbf{I}_{inc}[ij] = 1$ if node j is the head of edge i, $\mathbf{I}_{inc}[ij] = -1$ if node j is the tail of edge i, and $\mathbf{I}_{inc}[ij] = 0$ if edge i and node j are not incident. In addition, the head incidence matrix $\mathbf{I}_H \in \mathcal{R}^{M\times N}$ is defined such that $\mathbf{I}_H[ij] = 1$ if node j is a head of edge i and $\mathbf{I}_H[ij] = 0$ otherwise. The tail incidence matrix $\mathbf{I}_T \in \mathcal{R}^{M\times N}$ is defined in the same manner. Clearly, $\mathbf{I}_{inc} = \mathbf{I}_H - \mathbf{I}_T$. Moreover, it can be verified that the Laplacian matrix $\mathcal{L}$ for a bi-directional communication topology can be expressed as $\frac{1}{2}\mathbf{I}_{inc}^T\mathbf{I}_{inc}$ [68].

Example 2.1. *For the bidirectional communication topology shown in Fig. 2.1, the head incidence matrix, tail incidence matrix, and orientated incidence matrix are*

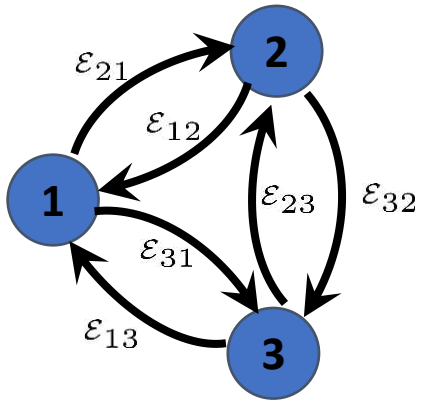

Figure 2.1: A bi-directional communication topology with three agents as an example

given as

$$\mathbf{I}_H = \begin{bmatrix} 1 & 0 & 0 \\ 1 & 0 & 0 \\ 0 & 1 & 0 \\ 0 & 1 & 0 \\ 0 & 0 & 1 \\ 0 & 0 & 1 \end{bmatrix}, \mathbf{I}_T = \begin{bmatrix} 0 & 1 & 0 \\ 0 & 0 & 1 \\ 1 & 0 & 0 \\ 0 & 0 & 1 \\ 1 & 0 & 0 \\ 0 & 1 & 0 \end{bmatrix}, \mathbf{I}_{inc} = \begin{bmatrix} 1 & -1 & 0 \\ 1 & 0 & -1 \\ -1 & 1 & 0 \\ 0 & 1 & -1 \\ -1 & 0 & 1 \\ 0 & -1 & 1 \end{bmatrix}.$$

In addition, the Laplacian matrix can be obtained as

$$\mathcal{L} = \begin{bmatrix} 2 & -1 & -1 \\ -1 & 2 & -1 \\ -1 & -1 & 2 \end{bmatrix} = \frac{1}{2}\mathbf{I}_{inc}^T\mathbf{I}_{inc}.$$

2.1.3 Stress Matrix

The stress matrix Ω for an undirected graph $\mathcal{G}(\mathcal{V}, \mathcal{E})$ is defined such that $\Omega_{ij} = -\omega_{ij}$ if $i \neq j, (i,j) \in \mathcal{E}$, $\Omega_{ii} = \sum_{k \in \mathcal{N}_k} \omega_{ij}$, and $\Omega_{ij} = 0$ otherwise. From a mechanical system perspective, $\omega_{ij} > 0$ can be interpreted as an attracting force between node i and node j, whereas $\omega_{ij} < 0$ represents a repelling force. Different from the Laplacian matrix where the weight on an edge is usually positive or zero, the weight (stress) can be positive, negative, or zero in a stress matrix. A stress matrix is in equilibrium for a configuration $P = \left[p_1^T, \cdots, p_N^T\right]^T$ if $\sum_{j \in \mathcal{N}_i} \omega_{ij}(p_j - p_i) = 0$, $i \in \mathcal{V}$ [69]. The key

property of a stress matrix is that it is invariant to any affine transformation (such as rotation, scaling and shearing) of the nominal formation configuration.

Example 2.2. *Fig. 2.2 shows a graph with configuration*

$$p_1 = \begin{bmatrix} -1 \\ 1 \end{bmatrix}, p_2 = \begin{bmatrix} 1 \\ 1 \end{bmatrix}, p_3 = \begin{bmatrix} 1 \\ -1 \end{bmatrix}, p_4 = \begin{bmatrix} -1 \\ -1 \end{bmatrix},$$

and an equilibrium stress matrix

$$\Omega = \begin{bmatrix} 1 & -1 & 1 & -1 \\ -1 & 1 & -1 & 1 \\ 1 & -1 & 1 & -1 \\ -1 & 1 & -1 & 1 \end{bmatrix}.$$

In addition, the stress matrix for a formation with multiple leaders and multiple followers can be partitioned as

$$\Omega = \left[\begin{array}{c|c} \Omega_{ll} & \Omega_{lf} \\ \hline \Omega_{fl} & \Omega_{ff,} \end{array}\right]. \tag{2.2}$$

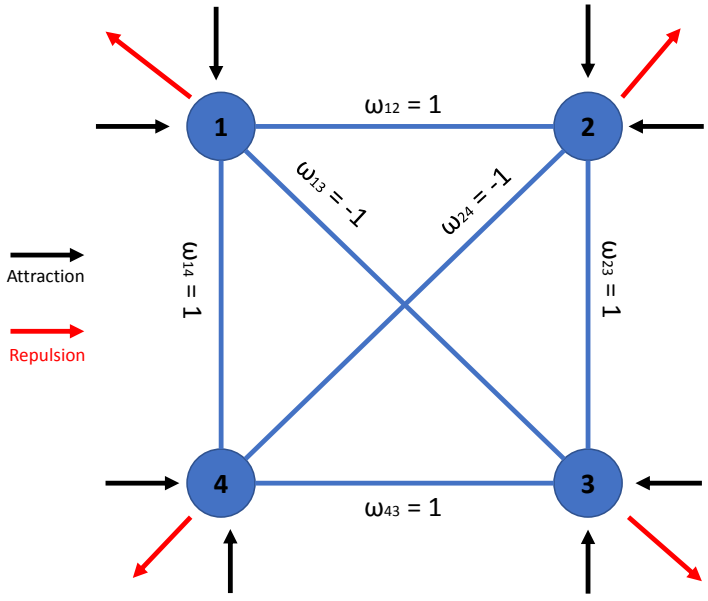

Figure 2.2: An illustrative example of a stress matrix with four agents in the unit

Definition 2.1. [69, 70] *Two formations* $(\mathcal{G}, P)$, $(\mathcal{G}, P')$ *in* $\mathcal{R}^d$ *are equivalent if* $\|p_i - p_j\| = \|p_i' - p_j'\|$ *for all* $(i,j) \in \mathcal{E}$, *and congruent if* $\|p_i - p_j\| = \|p_i' - p_j'\|$ *for all* $i, j \in \mathcal{V}$. *The formation* $(\mathcal{G}, P)$ *is globally rigid if its equivalent formations are also congruent to it. The formation* $(\mathcal{G}, P)$ *is universally rigid if it is globally rigid in any* $\mathcal{R}^{d_1}$, *where* $d_1 \geq d$.

Definition 2.2. *A set of points* $p_1, \cdots, p_n$ *in* $\mathcal{R}^d$ *affinely span* $\mathcal{R}^d$ *if their affine span defined by*

$$S = \Big\{ \sum_{i=1}^{n} a_i p_i : \forall a_i \in \mathcal{R} \text{ and } \sum_{i=1}^{n} a_i = 1 \Big\}$$

has a dimension of d.

Assumption 2.2. *For a nominal formation* $(\mathcal{G}, r)$, *we assume the communication graph* $\mathcal{G}$ *is universally rigid and the leader configuration set* $\{r_i\}_{i \in \mathcal{V}_l}$ *(*$\mathcal{V}_l$ *denotes the leader node set) in* $\mathcal{R}^d$ *affinely span* $\mathcal{R}^d$.

Lemma 2.2. [23] *For a multi-leader-multi-follower formation* $(\mathcal{G}, r)$ *under Assumption 2.2,* Ω_{ff} *in (2.2) is positive definite.*

2.2 Matrix Theory

This section introduces matrix notations and properties commonly used throughout this thesis.

2.2.1 Kronecker Product

For $A \in \mathcal{R}^{m \times n}$, $B \in \mathcal{R}^{p \times q}$, the kronecker product of A and B, $A \otimes B$, is a $mp \times nq$ matrix defined as

$$A \otimes B = \begin{bmatrix} a_{11}B & a_{12}B & \cdots & a_{1n}B \\ a_{21}B & a_{22}B & \cdots & a_{2n}B \\ \vdots & \vdots & \ddots & \vdots \\ a_{m1}B & a_{m2}B & \cdots & a_{mn}B \end{bmatrix}.$$

The Kronecker product satisfies the following rules of calculation [71]:

$$\begin{aligned}(kA) \otimes B &= A \otimes (kB) = k(A \otimes B)\\ (A+B) \otimes C &= A \otimes C + B \otimes C\\ A \otimes (B \otimes C) &= (A \otimes B) \otimes C\\ (A \otimes B)(C \otimes D) &= (AC) \otimes (BD)\\ (A \otimes B)^T &= A^T \otimes B^T\\ (A \otimes B)^{-1} &= A^{-1} \otimes B^{-1},\end{aligned}$$

where k is a constant and the last property holds if and only if both A and B are invertible. In addition, the eigenvalues of $A \otimes B$ can be fully characterized as $\lambda_i \mu_j$, where λ_i denotes an eigenvalue of A and μ_j is an eigenvalue of B.

2.2.2 Useful Matrix Inequality and Property

Lemma 2.3. *For a full column rank matrix $B \in \mathcal{R}^{n\times m}$, there exists a non-singular matrix $Y = \begin{bmatrix}\tilde{B}^T & \bar{B}^T\end{bmatrix}^T \in \mathcal{R}^{n\times n}$ such that $\tilde{B}B = \mathbf{I}_m$ and $\bar{B}B = 0_{(n-m)\times m}$.*

Proof. Since B has full column rank, there exists an elemental matrix E such that $EB = \begin{bmatrix}\mathbf{I}_m^T & 0_{(n-m)\times m}^T\end{bmatrix}^T$. We can choose $\tilde{B}$ as $\begin{bmatrix}\mathbf{I}_m & 0_{m\times(n-m)}\end{bmatrix} E$ to get $\tilde{B}B = \mathbf{I}_m$, and choose $\bar{B}$ as $\begin{bmatrix}0_{m\times(n-m)} & \mathbf{I}_{(n-m)\times(n-m)}\end{bmatrix} E$ to get $\bar{B}B = 0_{(n-m)\times m}$. The matrix Y can then be written as

$$Y = \begin{bmatrix}\mathbf{I}_m & 0_{m\times(n-m)}\\ 0_{(n-m)\times m} & \mathbf{I}_{n-m}\end{bmatrix} E.$$

Since E is non-singular, we can conclude that Y is non-singular. □

Lemma 2.4 (Schur Complement Lemma)**.** [72] *Consider a symmetric block matrix*

$$M = \begin{bmatrix}A & B\\ B^T & D\end{bmatrix},$$

if $D < 0$, then the Schur complement of M given by $A - BD^{-1}B^T$ is negative semi-definite if and only if $M \leq 0$.

Lemma 2.5. *For matrices $A > 0$ and $B > 0$, the matrix inequality $\rho^2 A^T B A - 2\rho A + B^{-1} \geq 0$ holds for any positive constant ρ.*

Proof. The positive semi-definiteness comes from the fact the term $\rho^2 A^T B A - 2\rho A + B^{-1}$ can be written as $(\rho B^{\frac{1}{2}} A - B^{-\frac{1}{2}})^T (\rho B^{\frac{1}{2}} A - B^{-\frac{1}{2}})$. □

Lemma 2.6 (Generalized Quadratic Inequality)**.** *For arbitrary matrices A, B, and a positive definite matrix F with compatible dimensions, the matrix inequality $A^T F B + B^T F A \leq \rho A^T F A + \rho^{-1} B^T F B$ holds for any positive constant ρ.*

Proof. This Lemma can be proved by showing $(\sqrt{\rho} A - \sqrt{\rho^{-1}} B)^T F (\sqrt{\rho} A - \sqrt{\rho^{-1}} B) \geq 0$. □

2.3 Problem Formulation

Two formation control problems have been studied in the thesis with simulation and experimental results.

2.3.1 Event-Triggered Formation Control

We consider a MAS consisting of N homogeneous linearized mobile-follower-robot agents with dynamics given by

$$\dot{\mathbf{x}}_i = A\mathbf{x}_i + B\mathbf{u}_i, \;\; i = 1, \cdots, N, \tag{2.3}$$

and an autonomous leader

$$\dot{\mathbf{x}}_0 = A\mathbf{x}_0, \tag{2.4}$$

or a non-autonomous leader

$$\dot{\mathbf{x}}_0 = A\mathbf{x}_0 + B\mathbf{u}_0, \tag{2.5}$$

where $\mathbf{x}_i \in \mathcal{R}^n$ is the state of follower i, $\mathbf{x}_0 \in R^n$ denotes the leader's states, $\mathbf{u}_i \in \mathcal{R}^m$ represents the followers' control inputs to be designed, and u_0 is leader's control input. A, B are known system and control matrices with compatible dimensions. In addition, B is assumed to have full rank.

Definition 2.3. *The formation control problem for a leader-follower MAS is solved asymptotically if the formation error vectors* $\eta_i = \mathbf{x}_i - f_i - \mathbf{x}_0$ *satisfy the following condition:*

$$\lim_{t\to\infty} \|\eta_i\| = 0,\ i = 1, \cdots, N. \tag{2.6}$$

The formation control problem is solved with bounded error if

$$\lim_{t\to\infty} \|\eta_i\| \leq \sigma,\ i = 1, \cdots, N, \tag{2.7}$$

where σ *is a small positive tunable parameter, and* f_i *is a pre-designed formation vector that characterizes the desired relative position of agent* i *with respect to the leader.*

Remark 2.1. *In the special case that* $f_i = 0$ *for all* $i \in \mathcal{V}$*, the formation tracking control problem can be reduced to a leader-follower consensus tracking problem.*

The formation control problem is studied in this thesis under a sampled-data environment. While the individual agents' control system is sampled at a periodic rate (having regular equally-spaced sampling instants), the inter-agent communication is governed by some pre-designed triggering conditions, which are evaluated at each sampling instant. In other words, an agent broadcasts its sampled states to neighbors only when certain conditions are satisfied. The event-triggered formation control problems studied in this thesis can be summarized as follows:

Research Problem 2.1. *Develop distributed controllers as well as locally-computable event-triggering communication mechanisms such that the formation control problem for the MAS (2.3)-(2.4) with a communication topology satisfying Assumption 2.1 can be achieved.*

Research Problem 2.2. *Under the same conditions as in Research Problem 2.1, develop controllers and event-triggering mechanisms for the MAS with followers (2.3) and a non-autonomous leader (2.5).*

Remark 2.2. *Note that event-triggered formation controllers in this thesis are designed for linear follower agents. The developed method can also be implemented to systems where the agents dynamics are nonlinear through linearization.*

2.3.2 Affine Formation Control

Definition 2.4. [23] *The target formation of the nominal formation $(\mathcal{G}, r)$ in $\mathcal{R}^d$ can be defined as*

$$\begin{bmatrix} p_l^*(t) \\ p_f^*(t) \end{bmatrix} = [\mathbf{I}_n \otimes A(t)] \begin{bmatrix} r_l \\ r_f \end{bmatrix} + \mathbf{1}_n \otimes b(t), \tag{2.8}$$

where $A(t) \in \mathcal{R}^{d\times d}$, $b(t) \in \mathcal{R}^d$ and $r = [r_l^T, r_f^T]^T$ (the subscript l denotes leader set and f denotes follower set) is the nominal configuration. $p^* = [p_l^{*T}, p_f^{*T}]^T$ represents a time-varying affine transformation of the nominal formation.

The affine formation control objective is then to design controllers for a formation $(\mathcal{G}, p)$ such that $p(t) \to p^*(t)$, as $t \to \infty$. Since the leader set is usually small and may be directly controlled by human operators or other high-level intelligent controllers, we assume $p_l(t) = p_l^*(t)$ can be realized at all times. Therefore, the affine formation control objective becomes to design controllers for follower agents such that $p_f(t) \to p_f^*(t)$, as $t \to \infty$. Note that the desired follower target configuration $p_f^*(t)$ for a nominal formation under Assumption 2.2 can be uniquely determined from the leader configuration $p_l^*(t)$ as

$$p_f^*(t) = -\bar{\Omega}_{ff}^{-1}\bar{\Omega}_{fl}p_l^*(t), \tag{2.9}$$

where $\bar{\Omega}_{ff} = \Omega_{ff} \otimes \mathbf{I}_d$ and $\bar{\Omega}_{fl} = \Omega_{fl} \otimes \mathbf{I}_d$.

Definition 2.5. *The affine formation control problem for a multi-leader-multi-follower MAS is achieved if the affine formation error vector*

$$\delta_p(t) = p_f(t) + \bar{\Omega}_{ff}^{-1}\bar{\Omega}_{fl}p_l^*(t), \tag{2.10}$$

satisfies $\lim_{t\to\infty} \|\delta_p(t)\| = 0$.

The objective of the affine formation control problems studied in this thesis can be summarized as follows.

Research Problem 2.3. *Design controllers such that the affine formation control problem for a multi-quadcopter system satisfying the conditions in Assumption 2.2 can be achieved.*

Chapter 3

Experimental Hardware and Software

This Chapter introduces the hardware and software used for conducting the experiments in this thesis.

3.1 Pioneer Mobile Robots

Two Pioneer P3-DX[1] robots and one Pioneer P3-AT[2] robot from the Advanced Control and Mechatronics Lab (ACM Lab) at Dalhousie University are used in experiments described in Chapters 4 to 6. The P3-DX shown in Fig. 3.1a is a two-wheel two-motor differential drive robot (with a caster), and it can reach a maximum linear speed of $1.2\,m/s$ and a maximum angular speed of 300 deg $/s$. In addition, it has a maximum payload of $17\,kg$. The Pioneer P3-AT shown in Fig. 3.1b is a four-wheel four-motor skid-steer robot. It can reach a maximum linear speed of $0.7\,m/s$ and a maximum angular speed of 140 deg $/s$ and has a maximum payload of $12\,kg$. Both robots have onboard micro-controllers that can communicate with external computers through serial ports. Moreover, these robots come with a software development kit which include a set of software applications. ARIA[3] is a core open-source software that provides a platform for controlling and receiving data from all Pioneer robots. MobileSim[4] is the native simulation environment that enables simulating multiple Pioneer robots simultaneously.

[1] https://www.generationrobots.com/media/Pioneer3DX-P3DX-RevA.pdf

[2] https://www.generationrobots.com/media/Pioneer3AT-P3AT-RevA-datasheet.pdf

[3] https://www.eecs.yorku.ca/course_archive/2009-10/W/4421/doc/pioneer/aria/main.html

[4] http://vigir.missouri.edu/~gdesouza/Research/MobileRobotics/Software/MobileSim/README.html

(a) Pioneer P3-DX ($0.46 \times 0.38 \times 0.24$ in meters)

(b) Pioneer P3-AT($0.51 \times 0.50 \times 0.28$ in meters)

Figure 3.1: Pioneer P3-DX and P3-AT robots

The kinematic model of a Pioneer robot can be given as

$$\begin{cases} \dot{x} = v\cos(\theta) \\ \dot{y} = v\sin(\theta) \\ \dot{\theta} = w, \end{cases} \tag{3.1}$$

where x, y represent the position in X and Y-directions, θ denotes the robot orientation, and v, w are the linear and angular velocity inputs, respectively. Note that (3.1) is an under-actuated non-holonomic system and there exists no smooth static stabilizing controllers at a point [73]. To simplify the networked formation controller design in MASs, we linearize (3.1) around a hand position $P_h = \begin{bmatrix} P_{hx} & P_{hy} \end{bmatrix}^T$ that is $d\,m$ away from the robot centroid as shown in Fig. 3.2. The hand position can then be expressed as

$$\begin{cases} P_{hx} = x + d\cos(\theta) \\ P_{hy} = y + d\sin(\theta), \end{cases}$$

and their time derivatives are given as

$$\begin{bmatrix} \dot{P}_{hx} \\ \dot{P}_{hy} \end{bmatrix} = \begin{bmatrix} \cos(\theta) & -d\sin(\theta) \\ \sin(\theta) & d\cos(\theta) \end{bmatrix} \begin{bmatrix} v \\ w \end{bmatrix}. \tag{3.2}$$

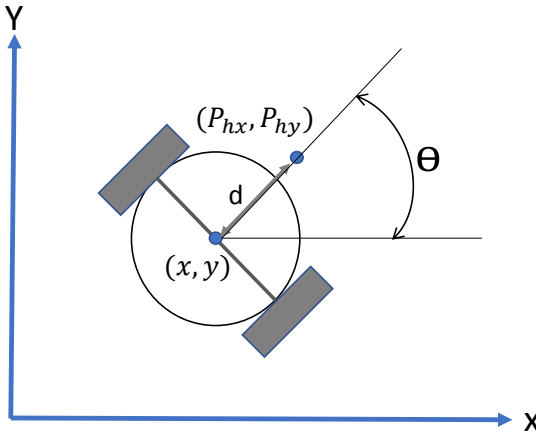

Figure 3.2: Hand position of a differential drive Pioneer robot

By designing

$$\begin{bmatrix} v \\ w \end{bmatrix} = \begin{bmatrix} \cos(\theta) & \sin(\theta) \\ -\frac{1}{d}\sin(\theta) & \frac{1}{d}\cos(\theta) \end{bmatrix} \begin{bmatrix} u_x \\ u_y \end{bmatrix},$$

(3.2) becomes the following linear system

$$\begin{bmatrix} \dot{P}_{hx} \\ \dot{P}_{hy} \end{bmatrix} = \begin{bmatrix} u_x \\ u_y \end{bmatrix}, \tag{3.3}$$

which can be generalized by the linear state-space equation $\dot{\mathbf{x}} = A\mathbf{x} + B\mathbf{u}$ with

$$\mathbf{x} = \begin{bmatrix} P_{hx} \\ P_{hy} \end{bmatrix}, \mathbf{u} = \begin{bmatrix} u_x \\ u_y \end{bmatrix}, A = \begin{bmatrix} 0 & 0 \\ 0 & 0 \end{bmatrix}, B = \begin{bmatrix} 1 & 0 \\ 0 & 1 \end{bmatrix}.$$

Remark 3.1. *The kinematic model of the hand position is holonomic (can move in all directions). Formation controllers will be developed based on the hand position model (3.3) in this thesis. It is possible to design formation controllers based on the robot centroid by choosing small d; however, there may exist a singularity in computing the actual inputs if the hand position is infinitely close to the centroid.*

3.2 Crazyflie Aerial Robot

The Crazyflie[5] aerial robot is used for the simulation work carried out in Chapter 7. As shwon in Fig. 3.5, Crazyflie is an open-source (both hardware and software) nano-quadcopter platform that can be integrated into third-party software such as Matlab® and Robot Operating System (ROS). It has a battery life around seven minutes at a weight of 27 grams. Its small size makes it suitable for indoor flight and dense formations. It has high survivability in crashes and poses little risk for humans because of its miniature size; the author had several crashes from a height of 2 m to a concrete floor with only damage to the replaceable propellers and motor mounts. In addition, it has a 10 degree-of-freedom (DOF) inertial measurement unit (IMU) and contains a 32-bit, 168-MHz ARM microcontroller with floating-point unit that is capable of performing significant computations onboard. Communication between the Crazyflie client in Fig. 3.3a and Crazyflie is enabled through a 2.4 GHz USB radio in Fig. 3.3b that transmits up to 2 Mb/s in 32-byte packets. Moreover, reliable communication can be established by properly adjusting the communication channel and data rate using the Crazyflie client. Table 3.1 summarizes the main technical specifications of Crazyflie, and the hardware architecture is shown in Fig. 3.4.

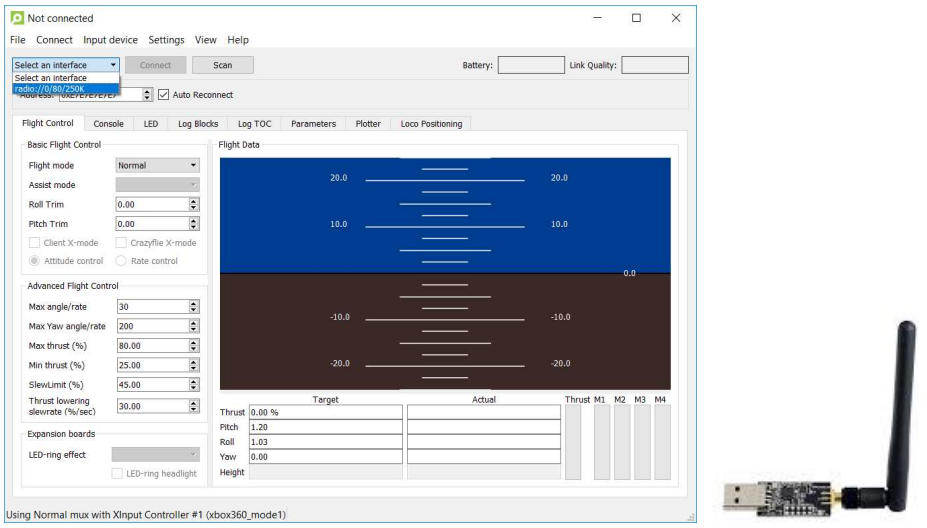

(a) Crazyflie client [6]

(b) Crazyradio PA

Figure 3.3: Communication devices of Crazyflie

[5] https://www.bitcraze.io/products/old-products/crazyflie-2-0/
[6] https://www.bitcraze.io/2018/03/crazyflie-clients/

Table 3.1: Technical specifications of Crazyflie

STM32F405	main microcontroller, used for state-estimation, control, and handling extensions
nRF51822	radio and power management microcontroller
MPU9250	9-axis inertial measurement unit
LPS25H	pressure sensor
USB	charging and wired communication

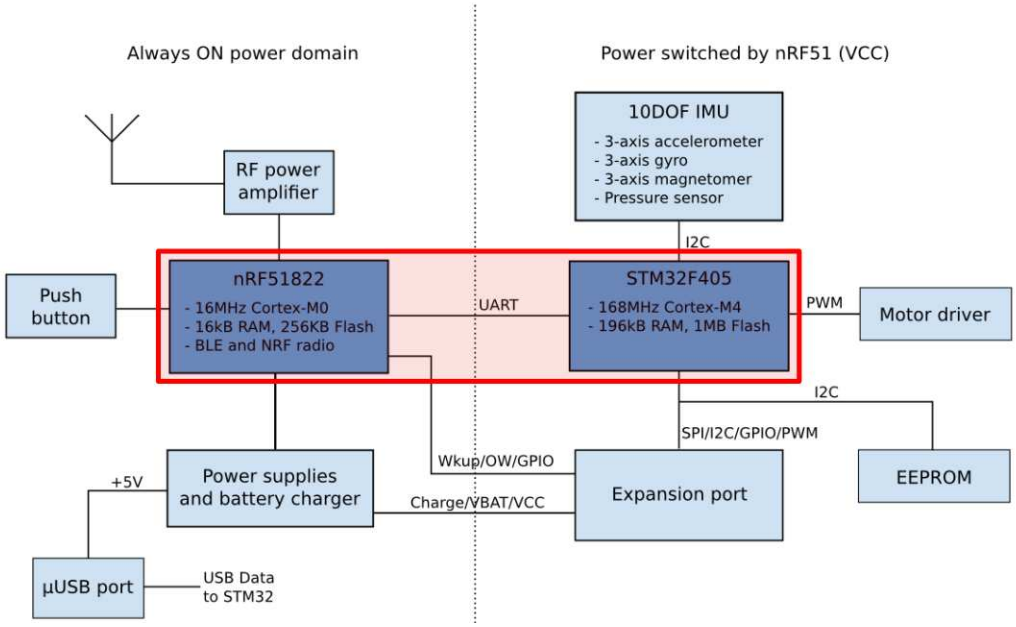

Figure 3.4: Crazyflie architecture [1]

A Crazyflie with the coordinate system defined in Fig. 3.5 can be modeled using Newton-Euler equations [74] or Euler-Lagrange equations [75]. An ideal Newton-Euler model without considering external disturbances and gyroscopic forces is then given as

$$\begin{bmatrix} \ddot{x} \\ \ddot{y} \\ \ddot{z} \end{bmatrix} = -g \begin{bmatrix} 0 \\ 0 \\ 1 \end{bmatrix} + \frac{T}{m} \begin{bmatrix} C_\psi S_\theta C_\phi + S_\psi S_\phi \\ S_\psi S_\theta C_\phi - C_\psi S_\phi \\ C_\theta C_\phi \end{bmatrix}, \tag{3.4a}$$

$$\begin{bmatrix} \dot{p} \\ \dot{q} \\ \dot{r} \end{bmatrix} = \begin{bmatrix} \frac{I_{yy}-I_{zz}}{I_{xx}} qr + \frac{\tau_\phi}{I_{xx}} \\ \frac{I_{zz}-I_{xx}}{I_{yy}} pr + \frac{\tau_\theta}{I_{yy}} \\ \frac{I_{xx}-I_{yy}}{I_{zz}} pq + \frac{\tau_\psi}{I_{zz}} \end{bmatrix}, \tag{3.4b}$$

where x, y, z are the linear positions defined in the inertial frame and ϕ, θ, ψ are

the roll, pitch, and yaw Euler angles defined using the current-frame Yaw-Pitch-Roll convention [76]. States p, q, r correspond to the angular velocities along the X_B, Y_B, and Z_B body frame axes, respectively. Parameter g is the gravity constant, m denotes the mass, and I_{xx}, I_{yy}, I_{zz} are the moments of inertia with respect to their principal axis in the body frame. $T, \tau_\phi, \tau_\theta, \tau_\psi$ are the external thrust force and rolling, pitching, and yawing moments, respectively. In addition, the Euler rates and the angular velocities are related by the following equation

$$\begin{bmatrix} \dot{\phi} \\ \dot{\theta} \\ \dot{\psi} \end{bmatrix} = \begin{bmatrix} 1 & S_\phi T_\theta & C_\phi T_\theta \\ 0 & C_\phi & -S_\phi \\ 0 & S_\phi / C_\theta & C_\phi / C_\theta \end{bmatrix} \begin{bmatrix} p \\ q \\ r \end{bmatrix}, \theta \neq \pm \frac{\pi}{2}, \tag{3.5}$$

where C_x, S_x, T_x represent $\cos(x)$, $\sin(x)$ and $\tan(x)$. Note that quaternions [77] can also be applied to represent quadcopter orientations.

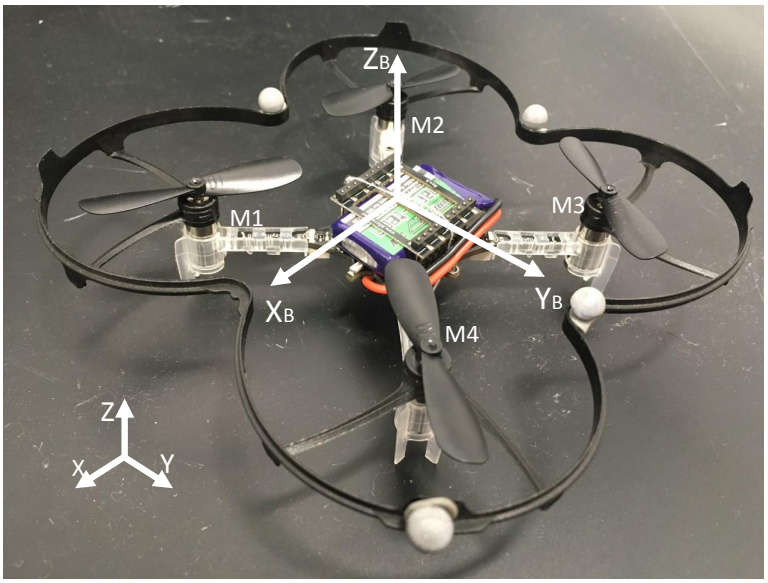

Figure 3.5: The inertial(XYZ) and body($X_B Y_B Z_B$) frames of Crazyflie 2.0 (9 cm between diagonal rotors)

Cascade control structures are often employed to fully stabilize a quadcopter in real-world implementations because of a quadcopter's highly nonlinear and unstable behaviors [78]. Most cascade structures consist of an attitude controller for stabilizing orientations and a position controller for stabilizing positions. Attitude controllers are typically implemented on-board and use the feedback from an on-board IMU for fast

control updates. Position controllers, which can be either on-board or off-board, often use the feedback from exteroceptive sensors, such as GPS and on/off-board cameras. In our system, a cascade on-board PD controller was provided for attitude control by the vendor, and we design off-board position controllers using measurements from the OptiTrack MoCap available in the host lab. Fig. 3.6 shows Crazyflie's onboard control architecture, where $\phi_c, \theta_c, \psi_c, \Omega_c$ denote the desired inputs to the on-board controller.

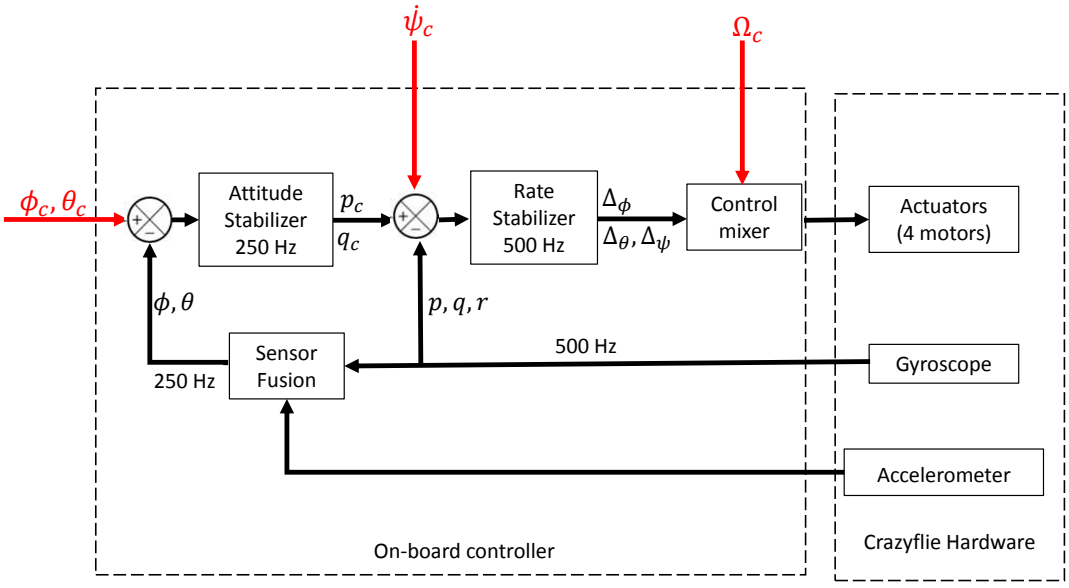

Figure 3.6: Control architecture of Crazyflie's on-board controller

To obtain an explicit attitude model (including the onboard controller) for controller design of the multiple quadcopter system, we assumed small operating angle conditions and independently identified the attitude dynamics in roll, pitch and yaw directions using a closed-loop system identification method. It was discovered that first-order dynamics, which are relatively simple for controller design, could sufficiently capture Crazyflie's roll and pitch dynamic behavior. The predicted roll and pitch angle responses using the identified first-order dynamics are superimposed on the actual experimentally measured response in Fig. 3.7 and Fig. 3.8, respectively. The experimental data collected in first 15 seconds was used for model identification while the data in the last 15 seconds was used for model validation. Fig. 3.9 shows the open-loop predicted (simple integrator) and closed-loop actual (under proportional-integral-derivative (PID) controller) system responses from a 20-degree step yaw angle

input. It can be concluded that a simple integrator can approximately represent the yaw dynamics. More details can be found from the author's publication in [79].

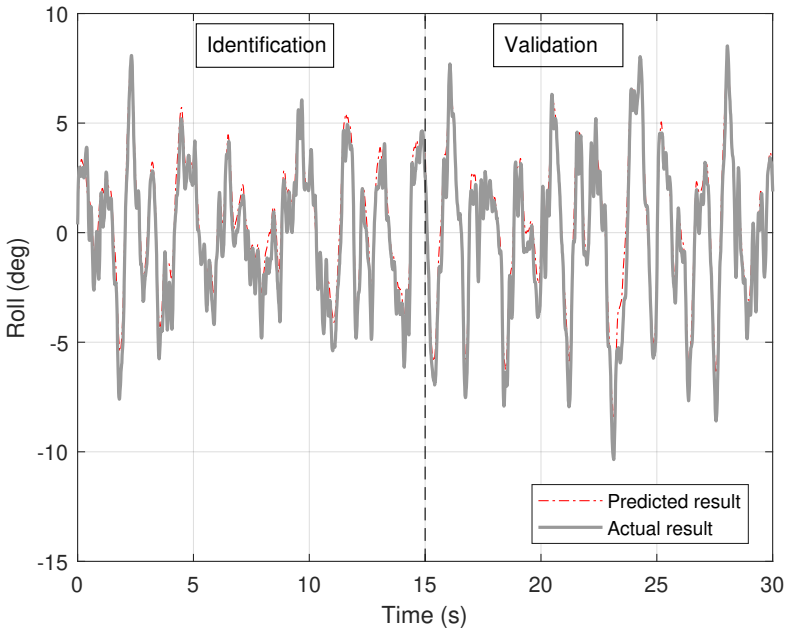

Figure 3.7: Identification and validation results for roll dynamics

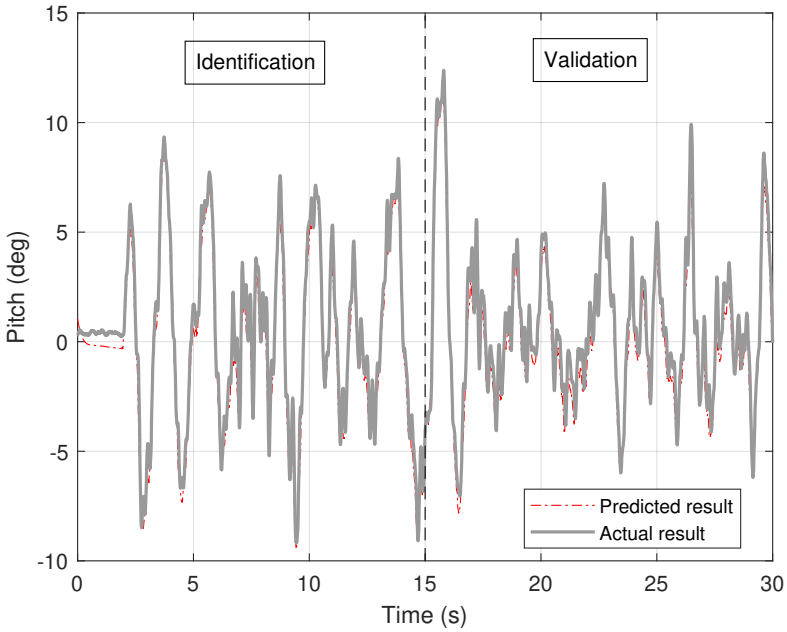

Figure 3.8: Identification and validation results for pitch dynamics

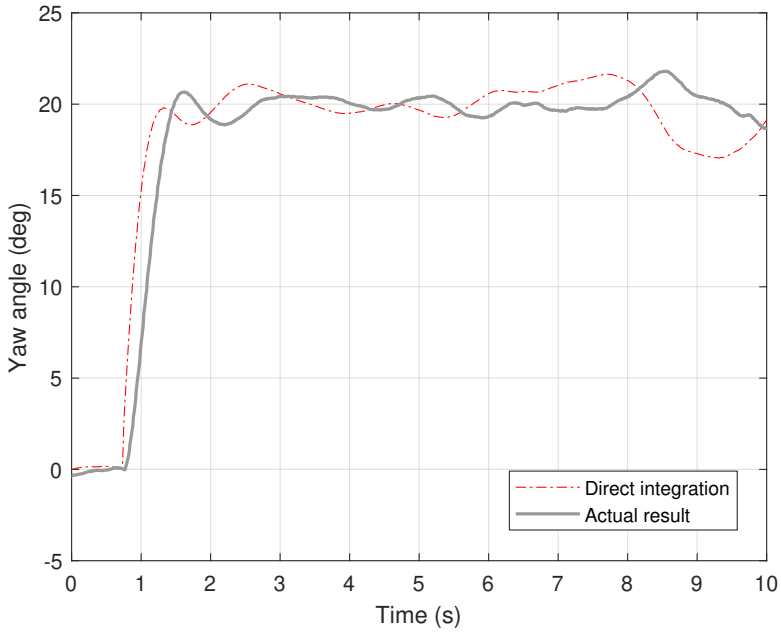

Figure 3.9: Validation results for yaw dynamics

The identified attitude dynamics are then summarized as

$$\begin{cases} \dot{\phi} = \frac{1}{\tau_\phi}(-\phi + k_\phi \phi_c), \\ \dot{\theta} = \frac{1}{\tau_\theta}(-\theta + k_\theta \theta_c), \\ \dot{\psi} = \psi_c, \end{cases} \tag{3.6}$$

where $\tau_\phi = 0.1993$, $k_\phi = 1.043$, $\tau_\theta = 0.1967$, and $k_\theta = 1.085$.

3.3 Motion Capture Systems

A MoCap system measures the position and orientation of objects in a physical space. The OptiTrack[7] MoCap system used in this thesis consists of multiple cost-effective Flex 13[8] cameras to measure the position and orientation of Crazyflie for control purposes. The Flex 13 camera has a resolution of 1.3 megapixels and a capturing rate of 120 frames per second, and uses USB 2.0 for connectivity. Note that OptiTrack is an optical-passive system, where reflective markers are placed on an object of interest and the position for each marker is triangulated with the measurements from multiple

[7] `https://optitrack.com/`
[8] `https://optitrack.com/cameras/flex-13/`

fixed high speed cameras. Fig. 3.5 shows a Crazyflie with reflective markers.

The OptiTrack system comes with a Motive[9] software interface for camera calibration and data streaming. Calibration is essential for OptiTrack to achieve accurate position and orientation readings. The calibration process roughly consists of five steps: preparing and optimizing the setup, masking in grayscale mode (Fig. 3.10a), wanding in precision mode (Fig. 3.10b), analyzing results (Fig. 3.10c), and grounding (Fig. 3.10d). After calibration, the rigid body data can be streamed into various client applications (Matlab®/Simulink®/ROS) from Motive (server).

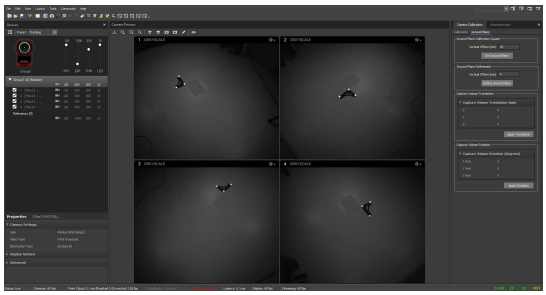

(a) Grayscale image of a rigid body

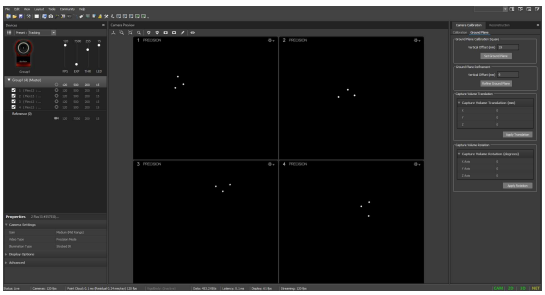

(b) Precision mode

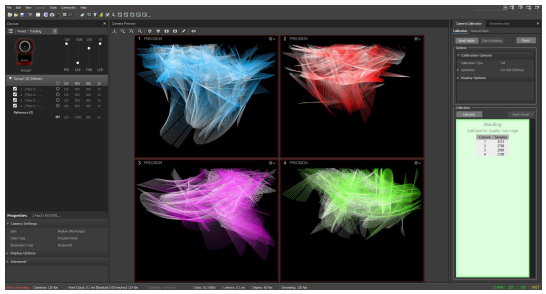

(c) Collect wanding samples

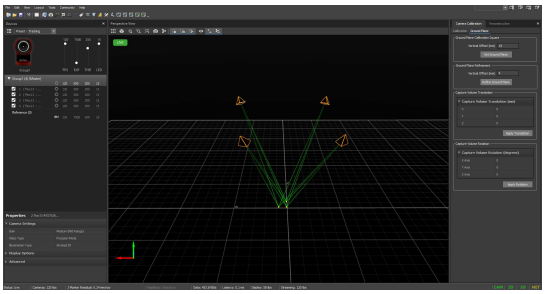

(d) Ground plane

Figure 3.10: OptiTrack MoCap calibration steps

3.4 Communication and Control System

The distributed algorithms developed in this thesis are validated using centralized realizations in the ROS environment. ROS[10] is an open-source software platform for robot software developers with the intention to ease some significant challenges, such as distributed computation, software reuse, and rapid testing [80]. Components, such

[9] `https://optitrack.com/software/motive/`
[10] `http://wiki.ros.org/`

as controllers and sensors, in a control system are abstracted as nodes (executables) in ROS and the communication between nodes are enabled through Topics (broadcast) or Services (request-reply).

ROS also provides a graphical way of viewing the relationship between nodes and topics. Fig. 3.11 shows a typical communication graph of hovering control of a single Crazyflie. The node `/crazyflie/joy` takes human input from a joystick controller and publishes messages to the topic `/crazyflie/joy`. The node `/crazyflie/vrpn` publishes the camera measurement to the topic `/tf` and then to the controller node `/crazyflie/controller`. The desired hovering control inputs are computed in the controller node and published to the topic `/crazyflie/cmd_vel`, which then sends to node `/crazyflie_server` to communicate with the Crazyflie though Crazyradio. More comprehensive materials about ROS can be found in [81] and [82].

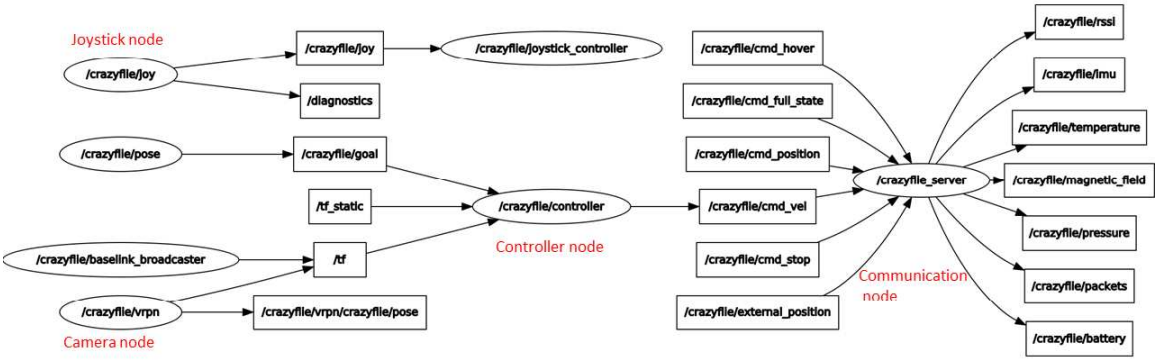

Figure 3.11: Communication graph of the hovering control of Crazyflie

The following ROS libraries are used in this thesis.

- `crazyflie_ros`[11] [83]: ROS communication driver for Crazyflie.
- `ROSARIA`[12]: provides a ROS interface (receiving control commands and publish sensor measurements) for Pioneer robots.
- `vrpn_client_ros`[13]: streams rigid body data (position and attitude) to ROS.

In all experiments, controllers are coded in Simulink® and then directly compiled and deployed to the target hardware as ROS nodes using the Matlab® ROS toolbox[14]

[11] `https://github.com/whoenig/crazyflie_ros`
[12] `http://wiki.ros.org/ROSARIA`
[13] `http://wiki.ros.org/vrpn_client_ros`
[14] `https://www.mathworks.com/products/ros.html`

by appropriately setting the network properties (e.g. IP address of the ROS Master device). Fig. 3.12 shows an interface for setting the ROS and network properties under Hardware Implementation in Simulink®, and Fig. 3.13 illustrates a typical quadcopter control framework in ROS.

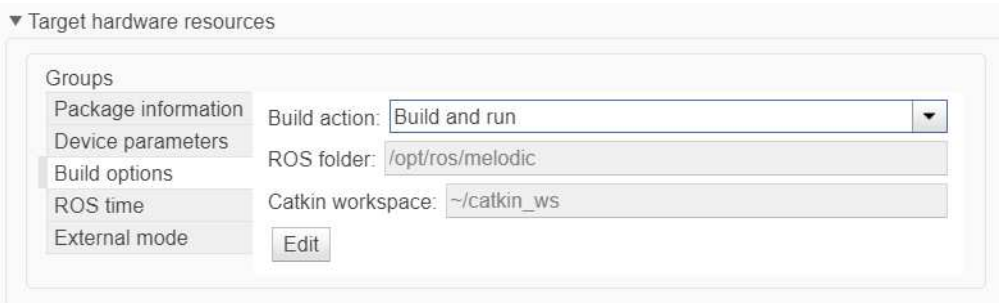

Figure 3.12: Network settings for deploying a controller node

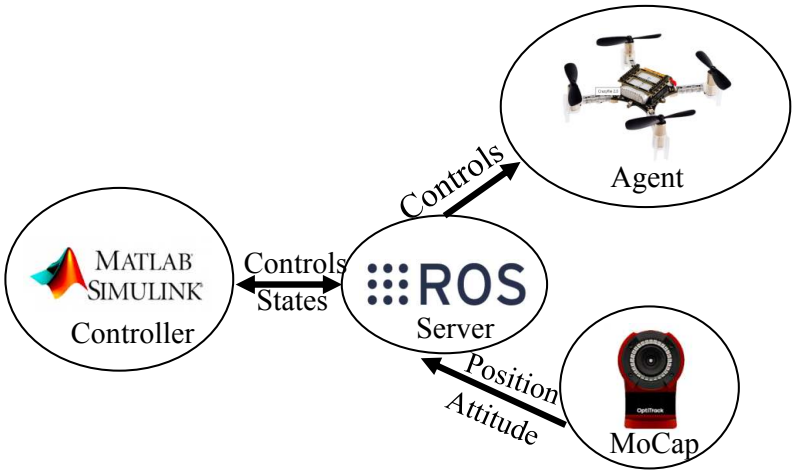

Figure 3.13: Quadcopter control framework in ROS

Chapter 4

Event-Triggered Formation Control with an Autonomous Leader

This Chapter is dedicated to solving Research Problem 2.1 as described in the problem formulation section of Chapter 2. In particular, a locally-computable state-estimate-based ECM along with a distributed controller are designed for the leader-follower MAS (4.1) under a sampled-data setting.

$$\begin{cases} \dot{\mathbf{x}}_i &= A\mathbf{x}_i + B\mathbf{u}_i,\ i = 1, \cdots, N, \\ \dot{\mathbf{x}}_0 &= A\mathbf{x}_0. \end{cases} \tag{4.1}$$

The formation control problem is transformed into a stability analysis problem of a closed-loop system under the proposed formation protocol and ECM. Sufficient conditions that guarantee the co-existence of a valid formation controller and an event-triggered communication mechanism are derived using a Lyapunov-based method and LMI techniques. In addition, equivalent low dimensional (agent-sized) sufficient conditions are obtained to reduce the computational complexity. Lastly, the developed controller and ECM are analyzed in numerical simulations and validated in experiments using a group of three Pioneer mobile robots.

The following Lemma, which is a direct consequence of Jensen's inequality [84] and the reciprocal convexity lemma [85], is useful in the sufficient condition formulation in this thesis.

Lemma 4.1. *Given a positive definite matrix $R \in R^{n\times n}$, if there exists an arbitrary matrix $S \in R^{n\times n}$ such that*

$$\begin{bmatrix} R & * \\ S^T & R \end{bmatrix} \geq 0, \tag{4.2}$$

then for any $\tau \in [0, h]$*, the following inequality holds*

$$-h\int_{t-h}^{t}\dot{\eta}^T(\upsilon)(\mathbf{I}_N\otimes R)\dot{\eta}(\upsilon)d\upsilon \leq -\phi_1^T(\mathbf{I}_N\otimes R)\phi_1 - \phi_2^T(\mathbf{I}_N\otimes R)\phi_2 - \phi_1^T(\mathbf{I}_N\otimes S)\phi_2 - \phi_2^T(\mathbf{I}_N\otimes S^T)\phi_1, \quad (4.3)$$

where $\phi_1 = \eta(t-\tau) - \eta(t)$*, and* $\phi_2 = \eta(t-h) - \eta(t-\tau)$*.*

4.1 Controller and Event Generator Design

A distributed controller as well as an ECM are proposed to address Research Problem 2.1 in this section. The controller and event generator are co-designed based on the sufficient LMI conditions that ensure system convergence.

4.1.1 Controller Design

For $t \in [vh, (v+1)h)$, the distributed control input for agent i is proposed as

$$\mathbf{u}_i = -\mu_i + K(\sum_{j\in N_i} a_{ij}(\hat{\mathbf{x}}_i(vh) - \hat{\mathbf{x}}_j(vh) - f_i + f_j) + d_i(\hat{\mathbf{x}}_i(vh) - f_i - \mathbf{x}_0)), \quad (4.4)$$

where μ_i is the formation compensation input to be determined, $\hat{\mathbf{x}}_i(vh)$ and $\hat{\mathbf{x}}_j(vh)$ are the estimated states of agents i and j at the latest sampling instant vh. It is assumed that the state estimate evolves following the dynamics $\hat{\mathbf{x}}_i(t) = e^{A(t-t_k^i h)}\mathbf{x}_i(t_k^i h)$ and $\hat{\mathbf{x}}_j(t) = e^{A(t-t_{\tilde{k}}^j h)}\mathbf{x}_j(t_{\tilde{k}}^j h)$ where $t_k^i h$ and $t_{\tilde{k}}^j h$ represent the latest released (available to their neighbors) sampling instants for agents i and j, respectively. Therefore, the estimates follow the dynamics $\dot{\hat{\mathbf{x}}}_i(t) = A\hat{\mathbf{x}}_i(t)$ and $\dot{\hat{\mathbf{x}}}_j(t) = A\hat{\mathbf{x}}_j(t)$ and the estimates at each sampling instants may be evaluated as $\hat{\mathbf{x}}_i(vh) = e^{A(vh-t_k^i h)}\mathbf{x}_i(t_k^i h)$ and $\hat{\mathbf{x}}_j(vh) = e^{A(vh-t_{\tilde{k}}^j h)}\mathbf{x}_j(t_{\tilde{k}}^j h)$. In addition, K is a static gain matrix that will be designed based on the sufficient conditions that ensure system stability. In addition, there exists a matrix $\tilde{B}$ such that $\tilde{B}B = \mathbf{I}_m$ from Lemma 2.3. The formation compensation input μ_i can then be designed as $\tilde{B}Af_i$.

Remark 4.1. *Note that the formation controller (4.4) reduces to a conventional consensus controller where* $f_i = 0$*. Therefore, the proposed method in this Chapter can also be applied to solve conventional consensus problems of general linear MASs.*

4.1.2 Closed-loop Dynamics

The closed-loop dynamics of follower agent i under control input (4.4) are, therefore

$$\dot{\mathbf{x}}_i = A\mathbf{x}_i + BK(\sum_{j\in N_i} a_{ij}(\hat{\mathbf{x}}_i(vh) - \hat{\mathbf{x}}_j(vh) - f_i + f_j) + d_i(\hat{\mathbf{x}}_i(vh) - f_i - \mathbf{x}_0(vh))) - B\mu_i. \quad (4.5)$$

The closed-loop formation error dynamics are then given as

$$\dot{\eta}_i = A\eta_i + BK(\sum_{j\in N_i} a_{ij}(\hat{\mathbf{x}}_i(vh) - \hat{\mathbf{x}}_j(vh) - f_i + f_j) + d_i(\hat{\mathbf{x}}_i(vh) - f_i - \mathbf{x}_0(vh))) + (Af_i - B\mu_i). \quad (4.6)$$

The purpose of the formation compensation input μ_i in (4.6) is to compensate for the effect of the formation vector f_i. Different from the formation protocols for MAS with low-order agents (single/double-integrators), it was shown in [86] that distributed formation protocols may not exist in general linear agent cases given certain desired formations. In this work, we assume the following assumption on the formation vectors f_i holds true.

Assumption 4.1. *$\bar{B}Af_i = 0$ is satisfied for all formation vectors.*

Under Assumption 4.1, we have $\bar{B}Af_i - \bar{B}B\mu_i = 0$, and $\tilde{B}Af_i - \tilde{B}B\mu_i = 0$. Therefore, the term $Af_i - B\mu_i$ in (4.6) is nullified and the closed-loop formation error dynamics (4.6) are therefore reduced to

$$\dot{\eta}_i = A\eta_i + BK(\sum_{j\in N_i} a_{ij}(\hat{\mathbf{x}}_i(vh) - \hat{\mathbf{x}}_j(vh) - f_i + f_j)d_i(\hat{\mathbf{x}}_i(vh) - f_i - \mathbf{x}_0(vh)). \quad (4.7)$$

Definition 4.1. *Define an estimate error vector for agent i as $\mathbf{e}_i(vh) = \hat{\mathbf{x}}_i(vh) - \mathbf{x}_i(vh)$, where vh represents the last sampling instant. Similarly, we define $\mathbf{e}_j(vh) = \hat{\mathbf{x}}_j(vh) - \mathbf{x}_j(vh)$. Then, $\hat{\mathbf{x}}_i(vh) = \mathbf{e}_i(vh) + \mathbf{x}_i(vh)$, and $\hat{\mathbf{x}}_j(vh) = \mathbf{e}_j(vh) + \mathbf{x}_j(vh)$.*

Definition 4.2. *An artificial delay $\tau(t)$ is defined as $\tau(t) = t - vh$, $t \in [vh, (v+1)h)$, which is a time-varying sawtooth-type delay with a constant slope of 1.*

Remark 4.2. *The artificial delay in Definition 4.2 is commonly used in analyzing sampled-data systems [87]. With this definition, the last sample instant vh can be represented as $t - \tau(t)$, and analysis methods in delay systems can be adopted to*

analyze the stability of the formation control problem. Note $\tau(t)$ will be simply written as τ for brevity hereafter.

Under the assumptions and definitions stated above, the closed-loop formation error dynamics for the i^{th} follower agent can be rewritten as

$$\dot{\eta}_i = A\eta_i + BK(\sum_{j\in N_i} a_{ij}(\eta_i(t-\tau) - \eta_j(t-\tau) + \mathbf{e}_i(t-\tau) - \mathbf{e}_j(t-\tau)) + d_i(\mathbf{e}_i(t-\tau) + \eta_i(t-\tau)). \tag{4.8}$$

Then, the overall system can be written as

$$\dot{\eta} = (\mathbf{I}_N \otimes A)\eta + (L_{ff} \otimes BK)\eta(t-\tau) + (L_{ff} \otimes BK)\mathbf{e}(t-\tau), \tag{4.9}$$

where η, $\eta(t-\tau)$, and $\mathbf{e}(t-\tau)$ are the stacked form of η_i, $\eta_i(t-\tau)$, and $\mathbf{e}_i(t-\tau)$, respectively.

4.1.3 Event Generator Design

Event generators are designed to regulate the communication among agents. In brief, agents do not transmit their sampled state information to their neighbors unless certain triggering conditions are met (node-based broadcast scheme). Fig. 4.1 shows the structure of the proposed formation controller with event-triggered communication. Similar to the idea of combined measurement [88], we define the combined formation error for agent i as follows

$$\begin{aligned}\mathbf{q}_i(vh) &= \sum_{j\in N_i} a_{ij}(\hat{\mathbf{x}}_i(vh) - \hat{\mathbf{x}}_j(vh) - f_i + f_j) + d_i(\hat{\mathbf{x}}_i(vh) - f_i - \mathbf{x}_0(vh) \\ &= \sum_{j\in N_i} a_{ij}(\eta_i(vh) + \mathbf{e}_i(vh) - \eta_j(vh) - \mathbf{e}_j(vh)) + d_i(\eta_i(vh) + \mathbf{e}_i(vh)).\end{aligned} \tag{4.10}$$

Then, a quadratic triggering function can be designed as

$$F_i(vh) = \mathbf{e}_i(vh)^T \Psi \mathbf{e}_i(vh) - \mathbf{q}_i(vh)^T \Phi \mathbf{q}_i(vh) - \epsilon^2, \tag{4.11}$$

where Ψ and Φ are positive definite matrices to be determined, and ϵ is a small positive constant. The next event release instant for agent i can then be determined

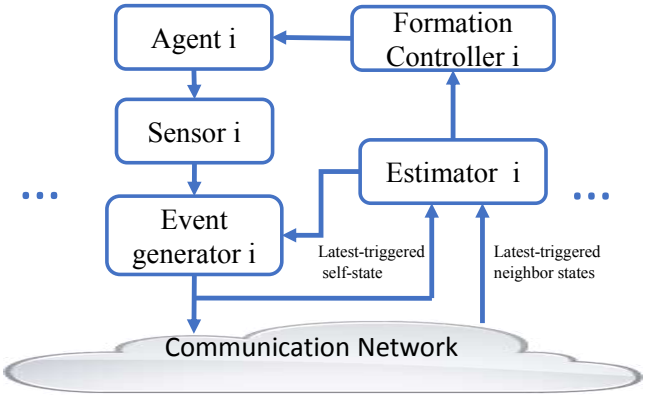

Figure 4.1: Schematic diagram of the i^{th} agent: formation control with event triggered communication

as follows

$$t^i_{k+1}h = inf\{vh > t_k h |\ F_i(vh) > 0\}. \tag{4.12}$$

Note that inter-agent communications are only enabled when the triggering rules are activated, at which point the error estimate $\mathbf{e}_i$ will be reset to zero. Therefore, $F_i(vh) \leq 0$ can be enforced for all agents at all sampling instants, and $\sum_{i=1}^{N} F_i(vh) \leq 0$. This inequality can be rewritten in the following quadratic form

$$\begin{bmatrix} \mathbf{e}(vh) \\ \eta(vh) \end{bmatrix}^T \begin{bmatrix} \mathbf{I}_N \otimes \Psi - L_{ff}^T L_{ff} \otimes \Phi & * \\ -L_{ff}^T L_{ff} \otimes \Phi & -L_{ff}^T L_{ff} \otimes \Phi \end{bmatrix} \begin{bmatrix} \mathbf{e}(vh) \\ \eta(vh) \end{bmatrix} \leq N\epsilon^2. \tag{4.13}$$

Remark 4.3. *The small positive threshold ϵ is introduced to account for the numerical error associated with the triggering condition evaluations. It is expected that larger values of ϵ will result in fewer triggering instants—at the expense of system performance. In addition, asymptotic convergence can be obtained theoretically if we choose $\epsilon = 0$. There will be more discussions on the effects of ϵ when the simulation results are presented in Section 4.2.*

4.1.4 Main Results

Sufficient conditions that ensure the existence of a valid event generator and formation controller for Research Problem 2.1 are established in Theorem 4.1.

Theorem 4.1. *The system (4.1) achieves formation with bounded error under control*

law (4.4) and communication regulation condition (4.12) if, for given positive scalars ρ, β, *and* ϵ, *there exist symmetric positive definite matrices* $\tilde{\Phi}$, $\tilde{\Psi}$, $\tilde{P}$, $\tilde{Q}$, $\tilde{R} \in \mathbb{R}^{n\times n}$, *as well as arbitrary matrices* $\tilde{S} \in \mathbb{R}^{n\times n}$ *and* $Y \in \mathbb{R}^{m\times n}$, *such that*

$$\begin{bmatrix} \tilde{R} & * \\ \tilde{S}^T & \tilde{R} \end{bmatrix} \geq 0, \tag{4.14}$$

$$\hat{H}_i = \begin{bmatrix} \hat{H}_{i_{11}} & * & * & * & * \\ \hat{H}_{i_{21}} & \hat{H}_{i_{22}} & * & * & * \\ \hat{H}_{i_{31}} & \hat{H}_{i_{32}} & \hat{H}_{i_{33}} & * & * \\ \hat{H}_{i_{41}} & \hat{H}_{i_{42}} & \hat{H}_{i_{43}} & \hat{H}_{i_{44}} & * \\ \hat{H}_{i_{51}} & \hat{H}_{i_{52}} & \hat{H}_{i_{53}} & \hat{H}_{i_{54}} & \hat{H}_{i_{55}} \end{bmatrix} < 0, i \in 1, \cdots, N, \tag{4.15}$$

where

$$\begin{aligned}
\hat{H}_{i_{11}} &= \tilde{P}A^T + A\tilde{P} + \tilde{Q} - \tilde{R} + \beta\mathbf{I}_n, & \hat{H}_{i_{42}} &= \lambda_i^2\tilde{\Phi}, \\
\hat{H}_{i_{21}} &= \lambda_i Y^T B^T + \tilde{R} - \tilde{S}^T, & \hat{H}_{i_{44}} &= -\tilde{\Psi} + \lambda_i^2\tilde{\Phi}, \\
\hat{H}_{i_{22}} &= -2\tilde{R} + \tilde{S} + \tilde{S}^T + \lambda_i^2\tilde{\Phi}, & \hat{H}_{i_{51}} &= hA\tilde{P}, \\
\hat{H}_{i_{31}} &= \tilde{S}^T, & \hat{H}_{i_{52}} &= h\lambda_i BY, \\
\hat{H}_{i_{32}} &= \tilde{R} - \tilde{S}^T, & \hat{H}_{i_{54}} &= h\lambda_i BY, \\
\hat{H}_{i_{33}} &= -\tilde{Q} - \tilde{R}, & \hat{H}_{i_{55}} &= \rho^2\tilde{R} - 2\rho\tilde{P} \\
\hat{H}_{i_{41}} &= \lambda_i Y^T B^T
\end{aligned}$$

and λ_i *is the* i^{th} *eigenvalue of the matrix* L_{ff} *in an ascending order. Then, the controller gain* K *can be computed as* $Y\tilde{P}^{-1}$, *and the matrices* Φ *and* Ψ *in the triggering conditions are obtained as* $\tilde{P}^{-1}\tilde{\Phi}\tilde{P}^{-1}$ *and* $\tilde{P}^{-1}\tilde{\Psi}\tilde{P}^{-1}$, *respectively. In addition, the formation error is ultimately bounded by*

$$\|\eta\| \leq \sqrt{\frac{N}{\beta}}\epsilon. \tag{4.16}$$

Proof. Consider the following continuous Lyapunov functional candidate on the interval $t \in [vh, (v+1)h)$ for the lumped formation error dynamics

$$V(t) = V_1(t) + V_2(t) + V_3(t), \tag{4.17}$$

where

$$V_1(t) = \eta(t)^T(\mathbf{I}_N \otimes P)\eta(t), \tag{4.18}$$

$$V_2(t) = \int_{t-h}^{t} \eta^T(s)(\mathbf{I}_N \otimes Q)\eta(s)ds, \tag{4.19}$$

$$V_3(t) = h\int_{t-h}^{t}\int_{s}^{t} \dot{\eta}^T(\upsilon)(\mathbf{I}_N \otimes R)\dot{\eta}(\upsilon)d\upsilon ds, \tag{4.20}$$

and $P, Q, R \in R^{n\times n}$ are symmetric positive definite matrices. Taking the time derivative of the Lyapunov functional candidate along the closed-loop formation error dynamics (4.9) yields,

$$\begin{aligned}\dot{V}_1 = {} & 2\eta^T(t-\tau)(L_{ff}^T \otimes K^T B^T P)\eta(t) + 2\mathbf{e}^T(t-\tau)(L_{ff}^T \otimes K^T B^T P)\eta(t) \\ & + \eta(t)^T(\mathbf{I}_N \otimes (A^T P + PA))\eta(t),\end{aligned} \tag{4.21}$$

$$\dot{V}_2 = \eta^T(t)(\mathbf{I}_N \otimes Q)\eta(t) - \eta^T(t-h)(\mathbf{I}_N \otimes Q)\eta(t-h), \tag{4.22}$$

$$\begin{aligned}\dot{V}_3 &= -h\int_{t-h}^{t} \dot{\eta}^T(\upsilon)(\mathbf{I}_N \otimes R)\dot{\eta}(\upsilon)d\upsilon + h\int_{t-h}^{t}\frac{\partial}{\partial t}\int_{s}^{t} \dot{\eta}^T(\upsilon)(\mathbf{I}_N \otimes R)\dot{\eta}(\upsilon)d\upsilon ds \\ &= -h\int_{t-h}^{t} \dot{\eta}^T(\upsilon)(\mathbf{I}_N \otimes R)\dot{\eta}(\upsilon)d\upsilon + h^2\dot{\eta}^T(t)(\mathbf{I}_N \otimes R)\dot{\eta}(t).\end{aligned} \tag{4.23}$$

If there exist an arbitrary matrix S with compatible dimension such that

$$\begin{bmatrix} R & * \\ S^T & R \end{bmatrix} \geq 0, \tag{4.24}$$

then, from Lemma 4.1 we have

$$\begin{aligned}\dot{V}_3 \leq {} & -\phi_1^T(\mathbf{I}_N \otimes R)\phi_1 - \phi_2^T(\mathbf{I}_N \otimes R)\phi_2 - \phi_1^T(\mathbf{I}_N \otimes S)\phi_2 \\ & - \phi_2^T(\mathbf{I}_N \otimes S^T)\phi_1 + h^2\dot{\eta}^T(t)(\mathbf{I}_N \otimes R)\dot{\eta}(t).\end{aligned} \tag{4.25}$$

Define $\xi(t)$ and ζ as

$$\xi(t) = \begin{bmatrix} \eta(t)^T & \eta(t-\tau)^T & \eta(t-h)^T & \mathbf{e}(t-\tau)^T \end{bmatrix}^T,$$
$$\zeta = \begin{bmatrix} \mathbf{I}_N \otimes A & L_{ff} \otimes BK & 0 & L_{ff} \otimes BK \end{bmatrix}.$$

Then the closed-loop dynamics (4.9) can be expressed as $\dot{\eta}(t) = \zeta\xi(t)$, and $\dot{V}_3$ is upper bounded by

$$\begin{aligned} \dot{V}_3 \leq & -\phi_1^T(\mathbf{I}_N \otimes R)\phi_1 - \phi_2^T(\mathbf{I}_N \otimes R)\phi_2 - \phi_1^T(\mathbf{I}_N \otimes S)\phi_2 \\ & - \phi_2^T(\mathbf{I}_N \otimes S^T)\phi_1 + h^2\xi(t)^T(\zeta^T(\mathbf{I}_N \otimes R)\zeta)\xi(t). \end{aligned} \tag{4.26}$$

Combining results from $\dot{V}_1, \dot{V}_2, \dot{V}_3$, we have

$$\dot{V} = \dot{V}_1 + \dot{V}_2 + \dot{V}_3 \leq \xi^T(t)\Omega\xi(t) + h^2\xi(t)^T(\zeta^T(\mathbf{I}_N \otimes R)\zeta)\xi(t), \tag{4.27}$$

where

$$\Omega = \begin{bmatrix} \Omega_{11} & * & * & * \\ \Omega_{21} & \Omega_{22} & * & * \\ \Omega_{31} & \Omega_{32} & \Omega_{33} & * \\ \Omega_{41} & 0 & 0 & 0 \end{bmatrix}, \tag{4.28}$$

with 0 denoting a zero matrix with compatible dimensions and

$$\begin{aligned} \Omega_{11} &= \mathbf{I}_N \otimes (A^TP + PA + Q - R), & \Omega_{32} &= \mathbf{I}_N \otimes (R - S^T), \\ \Omega_{21} &= L_{ff}^T \otimes K^TB^TP + \mathbf{I}_N \otimes (R - S^T), & \Omega_{33} &= -\mathbf{I}_N \otimes (Q + R), \\ \Omega_{22} &= \mathbf{I}_N \otimes (-2R + S + S^T), & \Omega_{41} &= L_{ff}^T \otimes K^TB^TP. \\ \Omega_{31} &= \mathbf{I}_N \otimes S^T, \end{aligned}$$

In addition, the triggering enforced inequality (4.13) can be rewritten as

$$\xi^T(t)\bar{\Omega}\xi(t) \leq N\epsilon^2, \tag{4.29}$$

where

$$\bar{\Omega} = \begin{bmatrix} 0 & * & * & * \\ 0 & \bar{\Omega}_{22} & * & * \\ 0 & 0 & 0 & * \\ 0 & \bar{\Omega}_{42} & 0 & \bar{\Omega}_{44} \end{bmatrix}, \tag{4.30}$$

with

$$\begin{aligned} \bar{\Omega}_{22} &= -L_{ff}^T L_{ff} \otimes \Phi, \\ \bar{\Omega}_{42} &= -L_{ff}^T L_{ff} \otimes \Phi, \\ \bar{\Omega}_{44} &= \mathbf{I}_N \otimes \Psi - L_{ff}^T L_{ff} \otimes \Phi. \end{aligned}$$

Then, using (4.29), $\dot{V}$ in (4.27) can be enlarged and rewritten as

$$\dot{V} \leq \xi(t)^T \Xi \xi(t) + N\epsilon^2 - \beta \eta^T \eta. \tag{4.31}$$

where β is a small positive number and

$$\Xi = \Omega - \bar{\Omega} + h^2 \zeta^T (\mathbf{I}_N \otimes R)\zeta + \beta E_1^T E_1, \tag{4.32}$$

with $E_1 = \begin{bmatrix} \mathbf{I}_n & 0 & 0 & 0 \end{bmatrix}$. It can be shown that the formation error η will be ultimately bounded as $\|\eta\| \leq \sqrt{\frac{N}{\beta}}\epsilon$ if $\Xi \leq 0$, which is equivalent using Lemma 2.4 to

$$\begin{bmatrix} \Omega - \bar{\Omega} + \beta E_1^T E_1 & * \\ h(\mathbf{I}_N \otimes R)\zeta & -\mathbf{I}_N \otimes R \end{bmatrix} < 0. \tag{4.33}$$

We pre- and post-multiply the inequality (4.33) by $diag\{\mathbf{I}_N \otimes \tilde{P}, \mathbf{I}_N \otimes \tilde{P}, \mathbf{I}_N \otimes \tilde{P}, \mathbf{I}_N \otimes \tilde{P}, \mathbf{I}_N \otimes R^{-1}\}$, where $\tilde{P} = P^{-1}$. In addition, define $\tilde{Q} = \tilde{P}Q\tilde{P}$. $\tilde{R}, \tilde{S}, \tilde{\Psi}, \tilde{\Phi}$ are defined analogously. Then the inequality in (4.33) is equivalent to

$$\begin{bmatrix} \tilde{\Omega} & * \\ h\zeta(\mathbf{I}_N \otimes \tilde{P}) & -\mathbf{I}_N \otimes R^{-1} \end{bmatrix} < 0, \tag{4.34}$$

where,

$$\tilde{\Omega}_{11} = \mathbf{I}_N \otimes (\tilde{P}A^T + A\tilde{P} + \tilde{Q} - \tilde{R} + \beta\mathbf{I}_n), \qquad \tilde{\Omega}_{33} = -\mathbf{I}_N \otimes (\tilde{Q} + \tilde{R}),$$
$$\tilde{\Omega}_{21} = L_{ff}^T \otimes \tilde{P}K^T B^T + \mathbf{I}_N \otimes (\tilde{R} - \tilde{S}^T), \qquad \tilde{\Omega}_{41} = L_{ff}^T \otimes \tilde{P}K^T B^T,$$
$$\tilde{\Omega}_{22} = \mathbf{I}_N \otimes (-2\tilde{R} + \tilde{S} + \tilde{S}^T) + (L_{ff}^T L_{ff} \otimes \tilde{\Phi}), \quad \tilde{\Omega}_{42} = (L_{ff}^T L_{ff} \otimes \tilde{\Phi}),$$
$$\tilde{\Omega}_{31} = \mathbf{I}_N \otimes \tilde{S}^T, \qquad \tilde{\Omega}_{44} = -\mathbf{I}_N \otimes \tilde{\Psi} + (L_{ff}^T L_{ff} \otimes \tilde{\Phi}).$$
$$\tilde{\Omega}_{32} = \mathbf{I}_N \otimes (\tilde{R} - \tilde{S}^T),$$

To address the nonlinear term $-\mathbf{I}_N \otimes R^{-1}$ in (4.34), we apply Lemma 2.5 and conclude that $-\mathbf{I}_N \otimes R^{-1} \leq \rho^2 \mathbf{I}_N \otimes \tilde{R} - 2\rho(\mathbf{I}_N \otimes \tilde{P})$ for any positive constant $\rho > 0$. Therefore, it is sufficient to ensure the inequality in (4.34) if

$$H = \begin{bmatrix} \tilde{\Omega} & * \\ h\zeta(\mathbf{I}_N \otimes \tilde{P}) & \rho^2 \mathbf{I}_N \otimes \tilde{R} - 2\rho(\mathbf{I}_N \otimes \tilde{P}) \end{bmatrix} < 0, \tag{4.35}$$

is satisfied. In what follows, the inequality (4.35) will be equivalently decomposed into a set of inequalities with lower dimensions corresponding to the size of a single agent. Since $L_{ff} > 0$, there exists an orthonormal matrix U such that $U\Lambda U^T$, where $\Lambda = diag\{\lambda_1, \cdots, \lambda_N\}$ with λ_i denoting the i^{th} eigenvalue of matrix L_{ff} in an ascending order. Then define a non-singular matrix $W = \mathbf{I}_5 \otimes (U \otimes \mathbf{I}_n)$, and note that $H < 0$ is equivalent to

$$\tilde{H} = WHW^T < 0, \tag{4.36}$$

where

$$\tilde{H}_{11} = \mathbf{I}_N \otimes (\tilde{P}A^T + A\tilde{P} + \tilde{Q} - \tilde{R} + \beta\mathbf{I}_n),$$
$$\tilde{H}_{21} = \Lambda \otimes \tilde{P}K^T B^T + \mathbf{I}_N \otimes (\tilde{R} - \tilde{S}^T),$$
$$\tilde{H}_{22} = \mathbf{I}_N \otimes (-2\tilde{R} + \tilde{S} + \tilde{S}^T) + \Lambda^2 \otimes \tilde{\Phi},$$

$$\tilde{H}_{31} = \mathbf{I}_N \otimes \tilde{S}^T, \qquad \tilde{H}_{44} = -\mathbf{I}_N \otimes \tilde{\Psi} + \Lambda^2 \otimes \tilde{\Phi},$$
$$\tilde{H}_{32} = \mathbf{I}_N \otimes (\tilde{R} - \tilde{S}^T), \qquad \tilde{H}_{51} = h(\mathbf{I}_N \otimes A\tilde{P}),$$
$$\tilde{H}_{33} = -\mathbf{I}_N \otimes (\tilde{Q} + \tilde{R}), \qquad \tilde{H}_{52} = h(\Lambda \otimes BK\tilde{P}),$$

$$\tilde{H}_{41} = \Lambda \otimes \tilde{P}K^T B^T, \qquad \tilde{H}_{54} = h(\Lambda \otimes BK\tilde{P}),$$
$$\tilde{H}_{42} = \Lambda^2 \otimes \tilde{\Phi} \qquad \tilde{H}_{55} = \rho^2(\mathbf{I}_N \otimes \tilde{R}) - 2\rho(\mathbf{I}_N \otimes \tilde{P}),$$

and terms in $\tilde{H}$ not specified are all zeros. In addition, since all elements in $\tilde{H}$ are block diagonal, it follows that $\tilde{H} < 0 \Leftrightarrow \hat{H}_i < 0$, for all $i = 1, \cdots, N$, where the terms in $\hat{H}_i$ are defined as in (4.15) with $Y = K\tilde{P}$. Then we can solve for the control gain matrix as $K = Y\tilde{P}^{-1}$, and positive definite matrices Ψ, Φ in the triggering condition can be obtained as $\tilde{P}^{-1}\Psi\tilde{P}^{-1}, \tilde{P}^{-1}\Phi\tilde{P}^{-1}$. □

Remark 4.4. *From (4.16), smaller N, ϵ and larger β could result in a smaller ultimate formation error bound; however, smaller ϵ tends to induce more frequent triggering instants, and larger β and N can reduce the feasibility of the developed sufficient LMI conditions in (4.15).*

Remark 4.5. *It can be verified that the set of LMIs is convex in $\lambda_i \in [\lambda_1, \lambda_N]$. Therefore, $\hat{H}_i < 0$, $i = 1, \cdots, N$ is equivalent to $\hat{H}_1 < 0$ and $\hat{H}_N < 0$. This property implies that only two low-dimensional LMI conditions need to be evaluated as opposed to a single high-dimensional LMI conditions as in [65] and [59], thus significantly reducing the numerical complexity when considering a large group formation. It should be noted that, while the developed method also applies to MASs with directed communication topologies, the resultant LMI condition will possess a very large amount of decision variables and can become intractable rapidly when the number of agents increases.*

Remark 4.6. *The results developed in this section can be further extended to time-varying communication topology cases where finite arbitrary topology switches can occur within a set of connected topologies in a finite-time interval. Specifically, in addition to the communication events governed by triggering conditions, an agent would also broadcast its information to all of its neighbors whenever a new neighboring agent is introduced. One limitation of the method proposed in this thesis is that it requires the lower and upper bounds of the eigenvalues of L_{ff}, which may not always be available. Nevertheless, the eigenvalue estimation methods in [89, 90] can be possibly used to estimate those eigenvalue bounds.*

Remark 4.7. *The underlying assumption of the synchronized sampling scheme poses a limitation of the developed method. In practical applications, distributed clock*

synchronization algorithms can be applied to synchronize the clocks across multiple agents [91].

4.2 Simulation Results

In this section, the newly-developed event-triggering formation control algorithm is applied in numerical simulations to a group of four Pioneer robots (one virtual leader denoted as node 0 and three followers as nodes $1, 2, 3$) with linearized dynamics (3.3) under the communication shown in Fig. 4.2. Note that a static leader was chosen from (4.1) and the system matrix in (3.3) is a zero matrix. The desired group formation (triangle formation) is defined by the formation vectors $f_1 = \begin{bmatrix} 1 & 0 \end{bmatrix}^T$, $f_2 = \begin{bmatrix} -0.7 & 0.7 \end{bmatrix}^T$, and $f_3 = \begin{bmatrix} -0.7 & -0.7 \end{bmatrix}^T$. The sampling interval is chosen as $h = 0.1\ sec$ and the triggering threshold ϵ is 0.0005. It can be verified that Assumption 2.1 and Assumption 4.1 are satisfied with the selected communication topology and formation vectors.

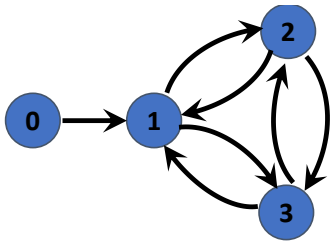

Figure 4.2: Communication topology of a mobile robot system with an autonomous leader

The control gain matrix K and event generator gain matrices Φ and Ψ can be obtained by evaluating the feasibility of (4.15) given parameters ρ and β. Therefore, the controller and event-generator design largely depend on the selections of ρ and β. It is observed in simulations that inappropriate selections of ρ and β often result in poor system performances or even infeasible controllers. In this Chapter, the parameter selection problem is formulated as an optimization problem. In particular, a cost function is defined as $\sqrt{\int_0^{t_{sim}} \|\eta(t)\|^2 dt}$ (l_2 norm of formation error) if a feasible controller exists, whereas a large penalty is assigned to the cost function in scenarios with no feasible controllers. Then, ρ and β are optimized such that the cost function

is minimized. For the simulation conditions stated above, the optimal parameters are obtained using Matlab®'s *fmincon*[1] solver as $\rho = 0.6082$ and $\beta = 0.2839$. Simulations are then carried out using the selected parameters. The control gain matrix K and the event generator gain matrices Ψ and Φ can be computed as

$$K = \begin{bmatrix} -1.1483 & 0 \\ 0 & -1.1483 \end{bmatrix}, \Psi = \begin{bmatrix} 70.2332 & 0 \\ 0 & 70.2332 \end{bmatrix}, \Phi = \begin{bmatrix} 0.0277 & 0 \\ 0 & 0.0277 \end{bmatrix}. \tag{4.37}$$

In a 10 *sec* simulation run, Fig. 4.3 shows the time evolution of the system that, in conjunction with the formation error profile in Fig. 4.4, clearly illustrates that the desired group formation can be achieved with bounded error with the formation controller (4.4), the event triggering rule (4.12) and the control gains in (4.37). Fig. 4.5 demonstrates the snapshots of the group formation (desired formations in solid lines and actual formations in dashed lines) in the X-Y plane at t = 0 sec, 3.3 sec, 6.6 sec, and 10 sec, respectively. Fig. 4.6 shows the communication instants on each agent over the span of the simulation. In addition, the average triggering percentage for followers 1-3 are computed as 78%, 75%, and 75%, respectively.

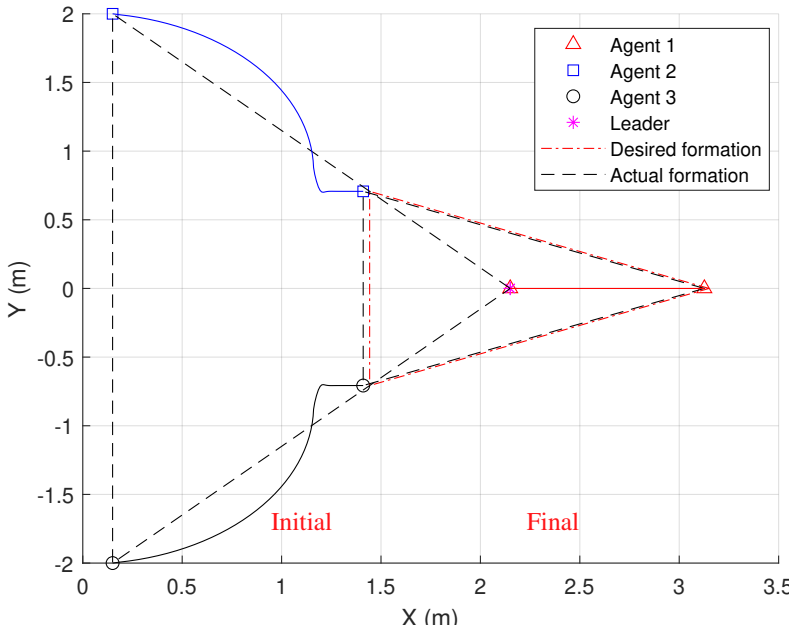

Figure 4.3: Simulation results of the evolution of the team with $\epsilon = 0.0005$

[1] `https://www.mathworks.com/help/optim/ug/fmincon.html`

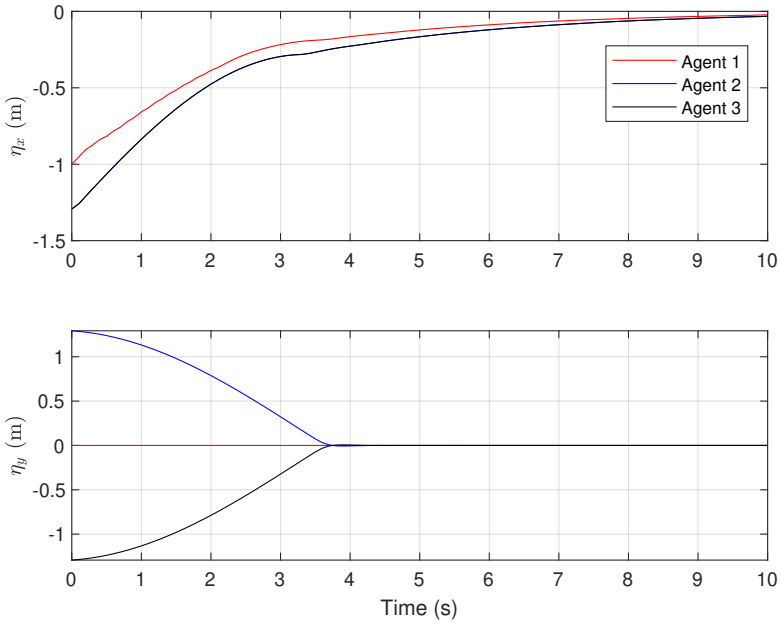

Figure 4.4: Simulation results of formation error profile

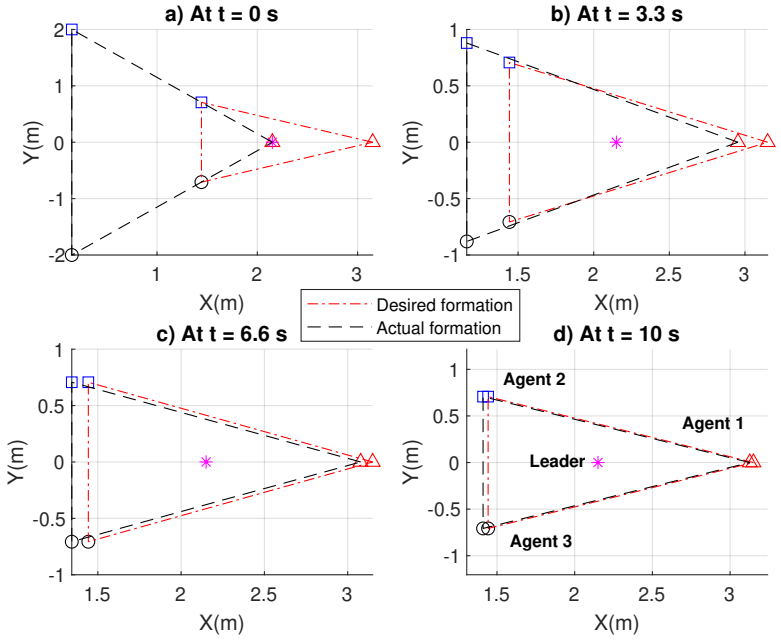

Figure 4.5: Simulation results of snapshots of the system (4.1) in the X-Y plane at: a) t=0 *sec*, b) t=3.3 *sec*, c) t=6.6 *sec*, d) t=10 *sec*

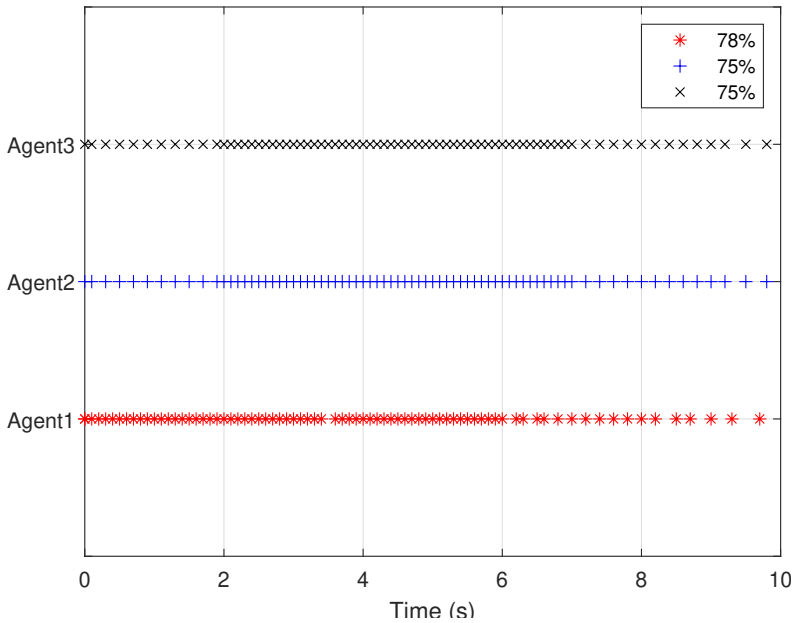

Figure 4.6: Simulation results of triggering instants

4.2.1 Effect of Communication Mechanisms

Note that the system matrix A for a linearized mobile robot is a zero matrix and the estimated state $\hat{\mathbf{x}}_i(vh)$ is equal to the latest triggered state $\mathbf{x}_i(t_k^i h)$ for agent i, and the estimate-error-based event generator becomes a traditional state-error-based generator as in [64]. Therefore, for this case the developed estimate-error-based ECM need only be compared with (not compared with the state-error-based ECM) a PCM where communication occurs at regular equally-spaced sampling instants at a frequency of $10\,Hz$. To compare the system performances under these two communication mechanisms, simulations are conducted under the same conditions except that the triggering rule is discarded in the PCM case.

The l_2 norms of the formation errors of each follower agent under different communication mechanisms are summarized in Table 4.1. The indistinguishable l_2 norms of each follower under the estimate-error-based ECMs and the PCM indicate that similar formation performance can be achieved. Nevertheless, the corresponding average communication frequencies which are listed in Table 4.2 indicate that the newly-developed estimate-error-based ECM requires reduced communication resources.

Table 4.1: Simulation results of l_2 norm of formation error (m)

Mechanisms	Agent 1	Agent 2	Agent 3
Estimate-error-based ECM	1.08	2.21	2.21
PCM	1.06	2.21	2.21

Table 4.2: Simulation results of triggering percentage (%)

Mechanisms	Agent 1	Agent 2	Agent 3
Estimate-error-based ECM	78	75	75
PCM	100	100	100

4.2.2 Effect of Triggering Threshold ϵ

Simulations are conducted to study the effects of different communication triggering threshold values on both system performance and communication demand. The average communication frequency results for the proposed estimate-based ECM with respect to different threshold values are summarized in Table 4.3. It can be concluded that using a larger threshold generally results in less network communication resources (7.6 Hz with $\epsilon = 0.0005$, 1.3 Hz with $\epsilon = 2$). However, as seen by the system evolution under a triggering threshold $\epsilon = 2$ shown in Fig. 4.7, larger thresholds can lead to a degraded system performance (compare to the system evolution with a threshold of 0.0005 as shown in Fig. 4.3). Therefore, there is a trade-off between communication resources and system performance when choosing a triggering threshold ϵ.

Table 4.3: Simulation results of average communication frequency (Hz) of all agents in (4.1) under 10 Hz sampling frequency with different triggering thresholds

Mechanisms	For threshold ϵ=				
	0.0005	0.001	0.01	0.1	2
Estimate-error-based ECM	7.6	6.8	4.4	2.8	1.3

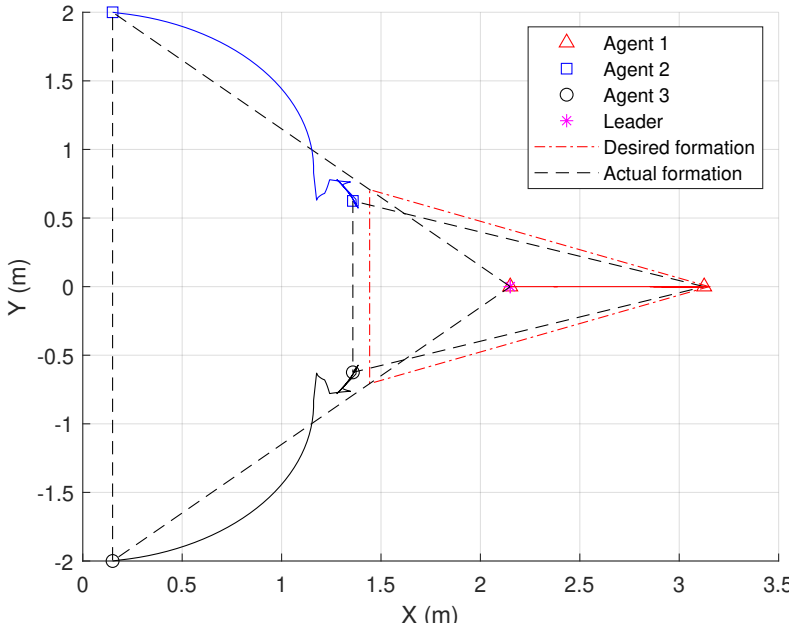

Figure 4.7: Simulation results of the evolution of the team with $\epsilon = 2$

4.3 Experimental Results

Additional simulations were carried out using high-fidelity robotics simulators such as MobileSim[2] and V-REP (currently known as CoppeliaSim) [92] prior to implementing the proposed contol approach on the hardware. Experimental validation was then conducted using a group of Pioneer robots (shown in Fig. 3.1) each driven by a Raspberry Pi[3] in the ROS environment.

Fig. 4.8 shows the system evolution of the Pioneer robots in a 20 *sec* experiment run under the proposed controller (4.4), communication triggering rule (4.12), and gains in (4.37). Fig. 4.9 shows screenshots of the initial and final positions of the Pioneer robots. It can be observed from the experimental results that two follower robots momentarily moved away from the desired formation before reaching the formation during the transition phase. This is largely because of the overshot in the Y-direction resulting from large control inputs. Fig. 4.11 depicts the snapshots of the Pioneer group formation at $t = 0\,sec$, $t = 6.6\,sec$, $t = 13.3\,sec$ and $t = 20\,sec$, respectively. Fig. 4.10 illustrates the formation error evolution for each agent in the

[2] `http://vigir.missouri.edu/~gdesouza/Research/MobileRobotics/Software/MobileSim/README.html`

[3] `https://www.raspberrypi.com/products/raspberry-pi-4-model-b/`

X and Y directions. The communication instants on each Pioneer robot are given in Fig. 4.12. The system evolution, formation error profile, group formation snapshots, and triggering instants for the Pioneer robot system under PCM are shown in Figs. 4.13 to 4.16, respectively. The l_2 norm of formation errors and communication triggering percentage of all Pioneer robots under the proposed estimate-error-based ECM and PCM are summarized in Table 4.4 and Table 4.5, which conclude that the proposed method is able to produce a comparable system performance (l_2 norms are slightly larger) while using reduced communication resources (only requires around 60% of the resources). It can be observed from the experimental results of triggering instants in Fig. 4.12 that there is a short period of time at the beginning of the experiment where no communication triggered. This result is different from the simulations where communication triggering started immediately at the beginning of the simulation as shown in Fig. 4.6. The reason for this discrepancy is that the motor dynamics were neglected in the simulations and the system can therefore achieve the commanded velocities immediately, whereas motor dynamics (inertia) exist in the actual hardware that can introduce a lag between the commanded input and actual motor output. The same reason can explain why there were more oscillations observed in the experiments (Fig. 4.10) than in the simulations Fig. 4.4.

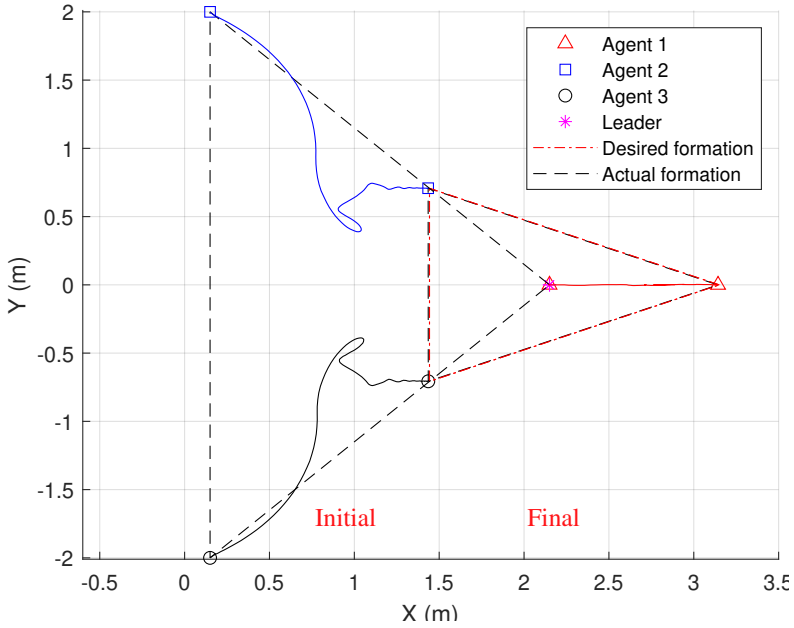

Figure 4.8: Experimental results of the evolution of the team with $\epsilon = 0.0005$

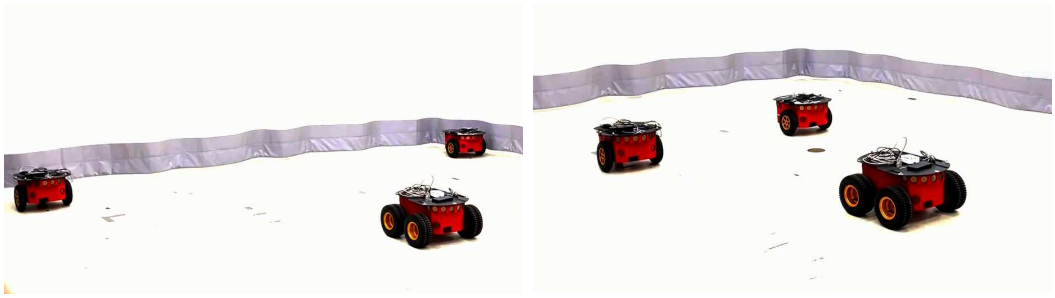

(a) Initial positions (b) Final positions

Figure 4.9: Initial and final positions of Pioneer robots

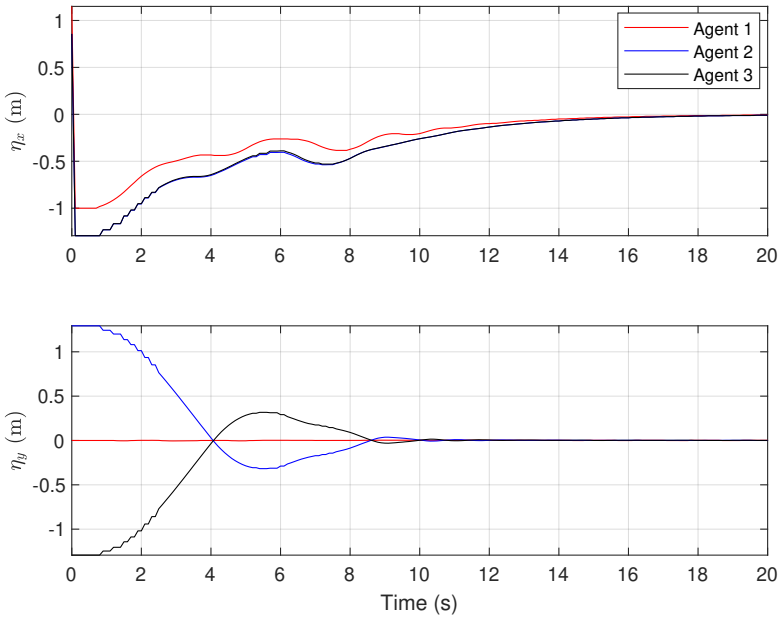

Figure 4.10: Experimental results of formation error profile

Table 4.4: Experimental results of l_2 norm of formation error (m)

Mechanisms	Agent 1	Agent 2	Agent 3
Estimate-error-based ECM	1.71	3.04	3.04
PCM	1.69	3.00	3.00

Table 4.5: Experimental results of triggering percentage (%)

Mechanisms	Agent 1	Agent 2	Agent 3
Estimate-error-based ECM	61	65	65
PCM	100	100	100

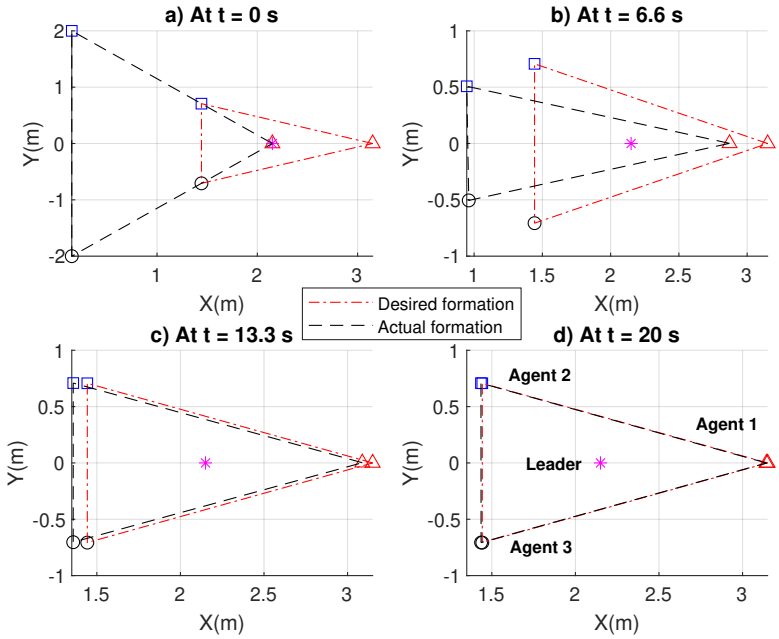

Figure 4.11: Experimental results of snapshots in the X-Y plane at: a) t=0 *sec*, b) t=6.6 *sec*, c) t=13.3 *sec*, d) t=20 *sec*

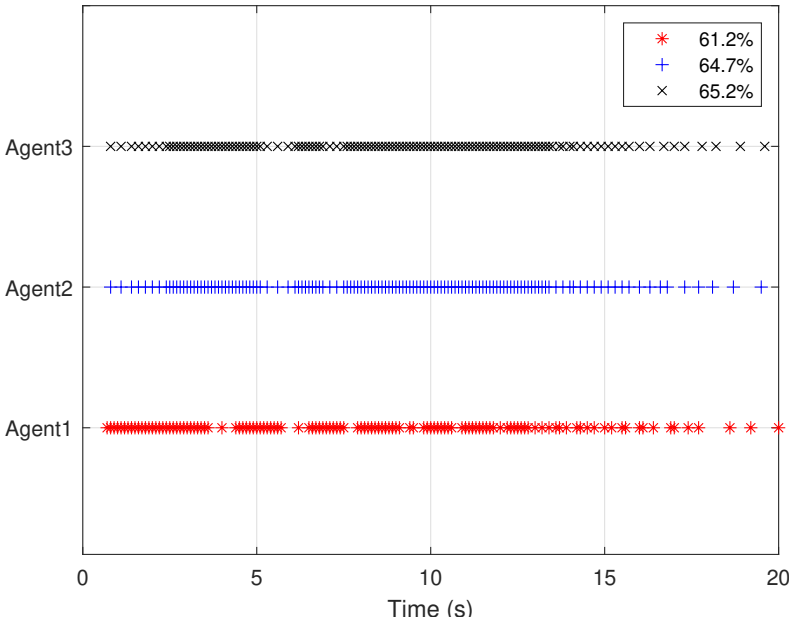

Figure 4.12: Experimental results of triggering instants

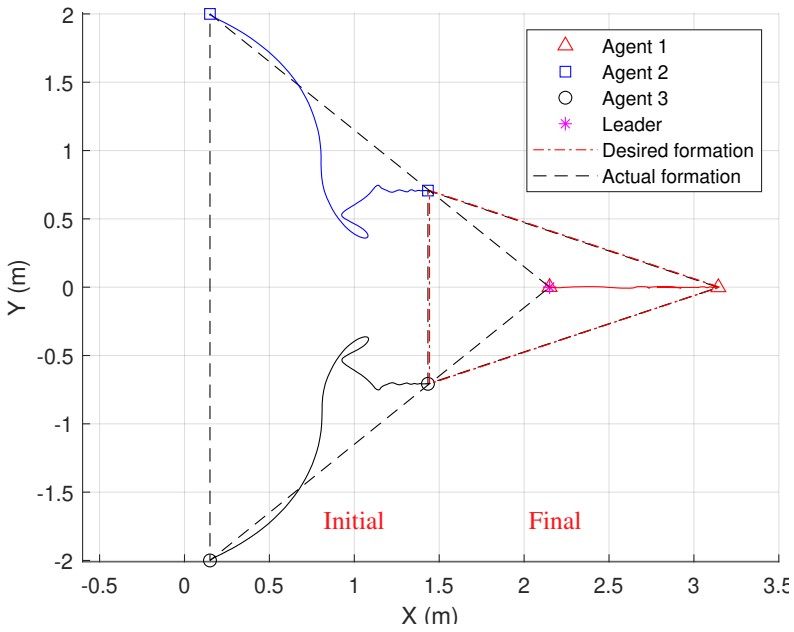

Figure 4.13: Experimental results of the evolution of the team under PCM

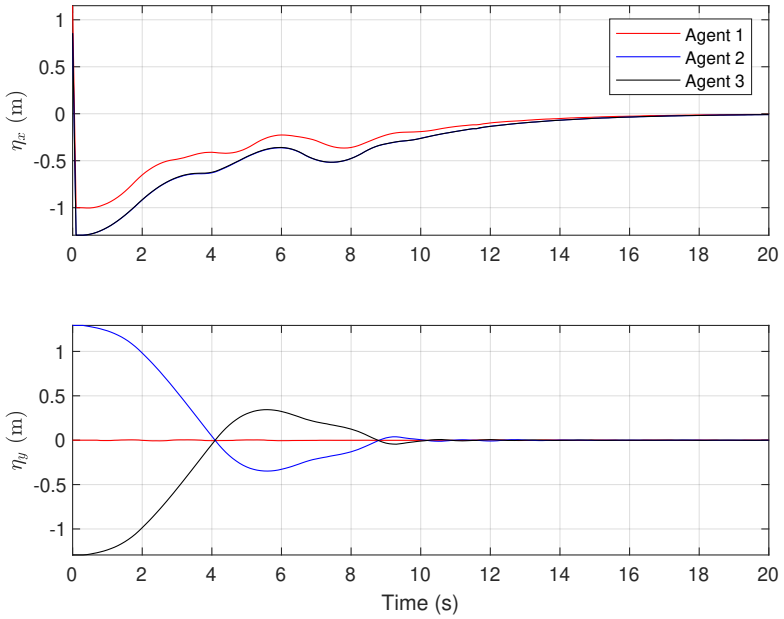

Figure 4.14: Experimental results of formation error profile under PCM

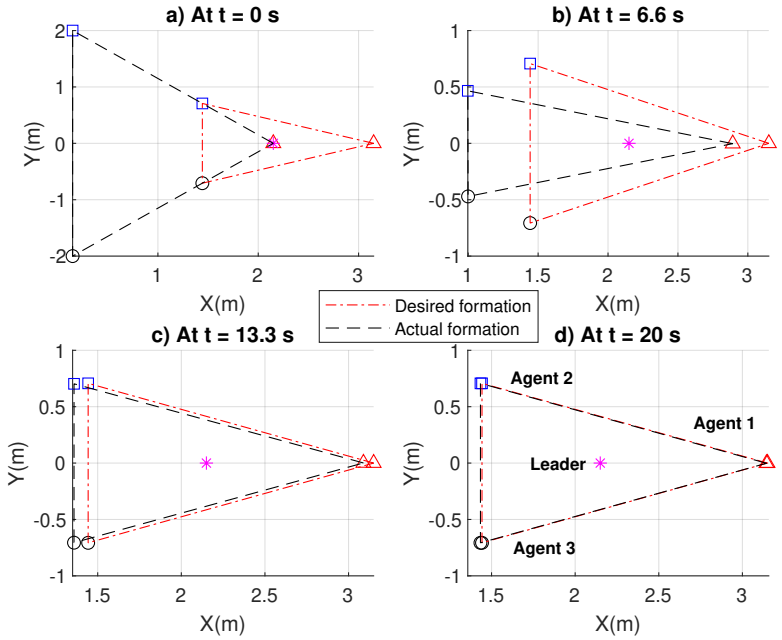

Figure 4.15: Experimental results of snapshots under PCM in the X-Y plane at: a) t=0 *sec*, b) t=6.6 *sec*, c) t=13.3 *sec*, d) t=20 *sec*

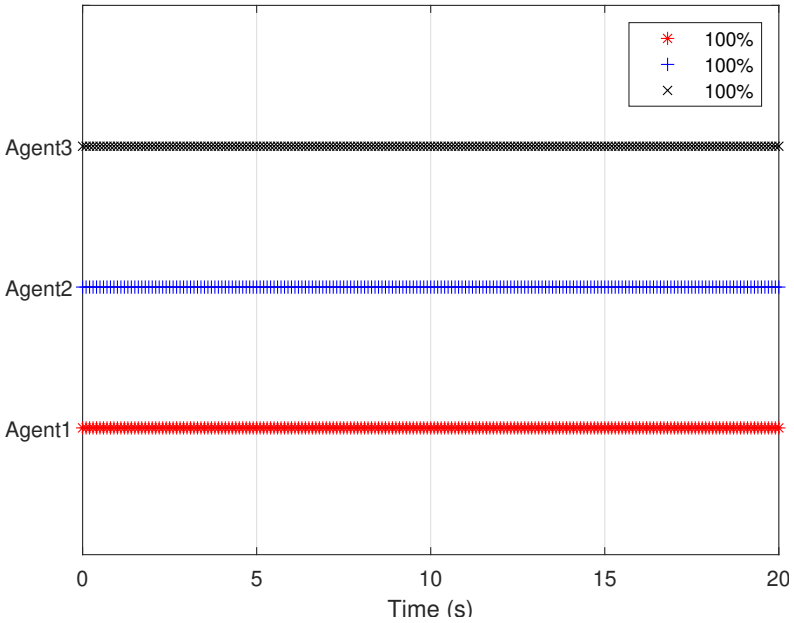

Figure 4.16: Experimental results of triggering instants under PCM

4.4 Conclusion

This chapter proposed a novel distributed formation tracking controller for general linear MASs consisting of one autonomous leader and multiple homogeneous followers. First, a new locally-computable state-estimate-based event-triggering communication condition was proposed for each agent. Then, the formation tracking problem was formulated as a stability analysis, controller gain and event-generator gain design problem of the closed-loop formation error dynamics. Sufficient conditions that guarantee the co-existence of a valid formation controller and an ECM were derived using a Lyapunov-based method and LMI techniques. In addition, equivalent low (agent-sized) dimensional sufficient conditions were obtained to reduce the computational complexity. The proposed method was validated in simulations and experiments using a group of unicycle-type mobile robots with linearized dynamics.

Chapter 5

Event-Triggered Formation Control with a Non-autonomous Leader

This Chapter is dedicated to solving Research Problem 2.2 as described in the problem formulation section of Chapter 2. Compared with an autonomous leader, a non-autonomous leader in a MAS described by (5.1) can vastly increase group functionalities.

$$\begin{cases} \dot{\mathbf{x}}_i &= A\mathbf{x}_i + B\mathbf{u}_i,\ i = 1, \cdots, N, \\ \dot{\mathbf{x}}_0 &= A\mathbf{x}_0 + Bu_0. \end{cases} \tag{5.1}$$

For instance, a human operator can remotely control a large group of robots by only directly controlling the leader. Therefore, this chapter extends the results from Chapter 4 to enable event-triggered formation control with a non-autonomous leader and develops a new ECM for regulating data transmission. A new distributed formation controller will also be proposed based on the regulated information. In addition, the controller and event generator gains will be co-designed based on the formulated sufficient LMI conditions that ensure the ultimate boundedness of the closed-loop formation error dynamics. Numerical simulations as well as experimental implementations for multiple mobile robots are then conducted to demonstrate the effectiveness and advantages of the proposed formation control method.

5.1 Distributed Event-Triggered Formation Control Strategy

In this section, a distributed formation controller along with a node-based communication-triggering mechanism will be developed to solve Research Problem 2.2.

5.1.1 Controller Design

For $t \in [vh, (v+1)h)$, a locally-computable formation control input for follower agent i can be proposed as

$$\begin{aligned}\mathbf{u}_i(t) = \frac{K}{|\mathcal{N}_i|}\big[\sum_{j=1}^{N} a_{ij}(\hat{\mathbf{x}}_i(vh) - \hat{\mathbf{x}}_j(vh) - f_i + f_j) + a_{i0}(\hat{\mathbf{x}}_i(vh) - f_i - \mathbf{x}_0)\big] \\ + \frac{\sum_{j=1}^{N} a_{ij}}{|\mathcal{N}_i|}\mathbf{u}_j(t^j_{k'}h) + \frac{a_{i0}}{|\mathcal{N}_i|}\mathbf{u}_0(vh) - \frac{\mu_i}{|\mathcal{N}_i|},\ i = 1, \cdots, N, \end{aligned} \tag{5.2}$$

where μ_i is the formation compensation input to be determined, $\hat{\mathbf{x}}_i(vh)$ and $\hat{\mathbf{x}}_j(vh)$ are the estimated states of agents i and j at the latest sampling instant vh. For Follower agents $i = 1, \cdots, N$, the state estimators follow the dynamics $\dot{\hat{x}}_i = A\hat{x}_i + B\mathbf{u}_i(t^i_{\tilde{k}}h)$, $t \in \left[t^i_{\tilde{k}}h, (t^i_{\tilde{k}}+1)h\right)$ and $\hat{x}_i(t^i_{\tilde{k}}h) = x_i(t^i_{\tilde{k}}h)$, where $t^i_{\tilde{k}}h$ and $(t^i_{\tilde{k}}+1)h$ represent the latest released and next triggering (available to their neighbors) sampling instants for agents i, respectively. K is a static gain matrix that will be designed based on the sufficient conditions that ensure the system stability. Moreover, from Lemma 2.3 there exists a matrix $\tilde{B}$ such that $\tilde{B}B = \mathbf{I}_m$ for a full column rank matrix B. μ_i can then be designed as $\tilde{B}A\sum_{j=0}^{N} a_{ij}(f_i - f_j)$.

Remark 5.1. *In addition to the formation tracking controller proposed in [93], the controller (5.2) also utilizes the control input information from neighboring agents. As a result, the final group formation error bound will be independent of the bound of leader's input.*

5.1.2 Closed-loop Dynamics

The networked closed-loop dynamics of agent i under the formation input (5.2) satisfies the following equation for $t \in [vh, (v+1)h)$

$$\begin{aligned}\sum_{j=0}^{N} a_{ij}B(\mathbf{u}_i(t) - \mathbf{u}_j(t)) = \sum_{j=0}^{N} a_{ij}BK(e_i(vh) - e_j(vh)) + \sum_{j=0}^{N} a_{ij}BK(\eta_i(vh) - \eta_j(vh)) \\ + \sum_{j=1}^{N} a_{ij}\bar{e}_j(vh) - B\mu_i, \end{aligned} \tag{5.3}$$

where $\mathbf{e}_i(vh) = \hat{\mathbf{x}}_i(vh) - \mathbf{x}_i(vh)$ and $\mathbf{e}_j(vh) = \hat{\mathbf{x}}_j(vh) - \mathbf{x}_j(vh)$ denote the state estimation error for agents i and j at the sampling instant vh, respectively. In addition, $\bar{e}_i(vh) = \mathbf{u}_i(t_k^i h) - \mathbf{u}_i(vh)$ denotes the self control input error at the sampling instant vh. Substitute the system dynamics (5.1) into (5.3) to obtain

$$\begin{aligned}\sum_{j=0}^{N} a_{ij}(\dot{x}_i(t) - \dot{x}_j(t)) = &\sum_{j=0}^{N} a_{ij}BK(e_i(vh) - e_j(vh)) + \sum_{j=0}^{N} a_{ij}BK(\eta_i(vh) - \eta_j(vh)) \\ &+ \sum_{j=1}^{N} a_{ij}\bar{e}_j(vh) + \sum_{j=0}^{N} a_{ij}(Ax_i(t) - Ax_j(t) - Af_i + Af_j) \\ &+ \sum_{j=0}^{N} a_{ij}(Af_i - Af_j) - B\mu_i. \end{aligned} \tag{5.4}$$

Note that f_i is constant for all $i = 1, \cdots, N$, we have $\dot{x}_i - \dot{x}_j = \dot{\eta}_i - \dot{\eta}_j$. Therefore, (5.4) can be rewritten as

$$\begin{aligned}\sum_{j=0}^{N} a_{ij}(\dot{\eta}_i(t) - \dot{\eta}_j(t)) = &\sum_{j=0}^{N} a_{ij}BK(e_i(vh) - e_j(vh)) + \sum_{j=0}^{N} a_{ij}BK(\eta_i(vh) - \eta_j(vh)) \\ &+ \sum_{j=1}^{N} a_{ij}\bar{e}_j(vh) + \sum_{j=0}^{N} a_{ij}A(\eta_i(t) - \eta_j(t)) \\ &+ \sum_{j=0}^{N} a_{ij}(Af_i - Af_j) - B\mu_i. \end{aligned} \tag{5.5}$$

We assume that Assumption 4.1 holds, and it can be verified that $Af_i = B\tilde{B}Af_i$ and the term $\sum_{j=0}^{N} a_{ij}(Af_i - Af_j) - B\mu_i$ in (5.5) is nullified. Therefore, (5.5) is reduced to

$$\begin{aligned}\sum_{j=0}^{N} a_{ij}(\dot{\eta}_i(t) - \dot{\eta}_j(t)) = &\sum_{j=0}^{N} a_{ij}BK(e_i(vh) - e_j(vh)) + \sum_{j=0}^{N} a_{ij}BK(\eta_i(vh) - \eta_j(vh)) \\ &+ \sum_{j=1}^{N} a_{ij}\bar{e}_j(vh) + \sum_{j=0}^{N} a_{ij}A(\eta_i(t) - \eta_j(t)). \end{aligned} \tag{5.6}$$

The augmented overall system dynamics are then given as

$$\begin{aligned}(L_{ff} \otimes \mathbf{I}_n)\dot{\eta}(t) = &(L_{ff} \otimes A)\eta(t) + (L_{ff} \otimes BK)\mathbf{e}(vh) + (L_{ff} \otimes BK)\eta(vh) \\ &+ (\mathcal{A}_f \otimes B)\bar{\mathbf{e}}(vh), \end{aligned} \tag{5.7}$$

where $\mathcal{A}_f$ denotes the Adjacency matrix among the follower agents, and $\dot{\eta}(t)$, $\eta(t)$, $\eta(vh)$, $\mathbf{e}(vh)$, and $\bar{\mathbf{e}}(vh)$ are the stacked form of $\dot{\eta}_i(t)$, $\eta_i(t)$, $\eta_i(vh)$, $e_i(vh)$, and $\bar{e}_i(vh)$, respectively. Considering Assumption 2.1 and Lemma 2.1, $L_{ff} \otimes \mathbf{I}_n$ is nonsingular, and the overall formation error dynamics can be obtained as

$$\begin{aligned}\dot{\eta}(t) = (\mathbf{I}_N \otimes A)\eta(t) + (\mathbf{I}_N \otimes BK)\mathbf{e}(t-\tau) + (\mathbf{I}_N \otimes BK)\eta(t-\tau) \\ + (L_{ff}^{-1}\mathcal{A}_f \otimes B)\bar{\mathbf{e}}(t-\tau),\end{aligned} \tag{5.8}$$

where, $\eta(t-\tau)$, $\mathbf{e}(t-\tau)$, and $\bar{\mathbf{e}}(t-\tau)$ are the stacked form of $\eta_i(t-\tau)$, $e_i(t-\tau)$, and $\bar{e}_i(t-\tau)$, respectively.

5.1.3 Event Generator Design

We define the combined formation error for agent i as

$$\begin{aligned}q_i(vh) &= \sum_{j=1}^{N} a_{ij}(\hat{x}_i(vh) - \hat{x}_j(vh) - f_i + f_j) + a_{i0}(\hat{x}_i(vh) - f_i - x_0) \\ &= \sum_{j=0}^{N} a_{ij}(\eta_i(vh) + e_i(vh) - \eta_j(vh) - e_j(vh)).\end{aligned} \tag{5.9}$$

Then, a node-based triggering function for agent i at instant vh can be designed as

$$f_i(vh) = e_i(vh)^T\Psi_1 e_i(vh) + \bar{e}_i^T(vh)\Psi_2\bar{e}_i^T(vh) - q_i(vh)^T\Phi q_i(vh) - \epsilon^2, \tag{5.10}$$

where Ψ_1, Ψ_2 and Φ are positive definite matrices to be determined and ϵ is a small positive design parameter. The next event release instant for agent i can then be determined as follows

$$t_{k+1}^i h = inf\{vh > t_k h |\ f_i(vh) > 0\},\ i = 1, \cdots, N. \tag{5.11}$$

It should be noted that the state estimate error $e_i(vh)$ and control input error $\bar{e}_i(vh)$ are reset to zero whenever inter-agent communications are enabled, which happens when triggering rules (5.11) are activated. Therefore, $f_i(vh) \leq 0$ can be enforced for all agents at all sampling instants, which implies $\sum_{i=1}^{N} f_i(vh) \leq 0$ is always satisfied.

Note that,

$$\begin{aligned}\sum_{i=1}^{N} f_i(vh) &= \sum_{i=1}^{N}(e_i(vh)^T\Psi_1 e_i(vh) + \bar{e}_i^T(vh)\Psi_2\bar{e}_i^T(vh) - q_i(vh)^T\Phi q_i(vh) - \epsilon^2) \\ &= \sum_{i=1}^{N} e_i(vh)^T\Psi_1 e_i(vh) + \sum_{i=1}^{N}\bar{e}_i^T(vh)\Psi_2\bar{e}_i^T(vh) - N\epsilon^2 \\ &\quad - \sum_{i=1}^{N}\left[\sum_{j=0}^{N} a_{ij}(\eta_i(vh) + e_i(vh) - \eta_j(vh) - e_j(vh)^T)\right]\Phi \\ &\quad \left[\sum_{j=0}^{N} a_{ij}(\eta_i(vh) + e_i(vh) - \eta_j(vh) - e_j(vh))\right]. \quad (5.12)\end{aligned}$$

Therefore, $\sum_{i=1}^{N} f_i(vh) \leq 0$ can be rewritten in the following matrix form

$$\begin{bmatrix}\mathbf{e}(vh)\\ \eta(vh)\\ \bar{\mathbf{e}}(vh)\end{bmatrix}^T \begin{bmatrix}\mathbf{I}_N\otimes\Psi_1 - L_{ff}^T L_{ff}\otimes\Phi & * & *\\ -L_{ff}^T L_{ff}\otimes\Phi & -L_{ff}^T L_{ff}\otimes\Phi & *\\ 0 & 0 & \mathbf{I}_N\otimes\Psi_2\end{bmatrix}\begin{bmatrix}\mathbf{e}(vh)\\ \eta(vh)\\ \bar{\mathbf{e}}(vh)\end{bmatrix} \leq N\epsilon^2, \quad (5.13)$$

By using the notation $vh = t - \tau$ from Definition 4.2, we have

$$\begin{bmatrix}\mathbf{e}(t-\tau)\\ \eta(t-\tau)\\ \bar{\mathbf{e}}(t-\tau)\end{bmatrix}^T \begin{bmatrix}\mathbf{I}_N\otimes\Psi_1 - L_{ff}^T L_{ff}\otimes\Phi & * & *\\ -L_{ff}^T L_{ff}\otimes\Phi & -L_{ff}^T L_{ff}\otimes\Phi & *\\ 0 & 0 & \mathbf{I}_N\otimes\Psi_2\end{bmatrix}\begin{bmatrix}\mathbf{e}(t-\tau)\\ \eta(t-\tau)\\ \bar{\mathbf{e}}(t-\tau)\end{bmatrix} \leq N\epsilon^2. \quad (5.14)$$

Remark 5.2. *State errors have been commonly used in triggering condition design in the literature [59], [64]. However, state-error-based event generators tend to produce frequent communication instants in the presence of a dynamic leader in formation control even when the desired formation has been achieved. An estimate-error-based event generator is developed in this section with the aim to reduce triggering instants while still guaranteeing comparable formation performance. It is observed in the simulations of formation control with a dynamic leader that the estimate error based triggering conditions generally introduce less triggering instants than the state error based ones while still guaranteeing comparable formation performances.*

5.1.4 Main Results

The following Theorem provides sufficient conditions for the event generator and formation controller design for Research Problem 2.2.

Theorem 5.1. *Under the control law (5.2) and the communication regulation condition (5.11), the system (5.1) achieves formation with bounded error if, for given positive scalars ρ, β, there exist symmetric positive definite matrices $\tilde{\Phi}$, $\tilde{\Psi}_1$, $\tilde{\Psi}_2$, $\tilde{P}$, $\tilde{Q}$, $\tilde{R} \in \mathbb{R}^{n\times n}$, as well as arbitrary matrices $\tilde{S} \in \mathbb{R}^{n\times n}$ and $Y \in \mathbb{R}^{m\times n}$, such that*

$$\begin{bmatrix} \tilde{R} & * \\ \tilde{S}^T & \tilde{R} \end{bmatrix} \geq 0,\ \hat{H}_i < 0,\ i \in 1, \cdots, N, \tag{5.15}$$

where

$$\begin{bmatrix} H_{11} & * & * & * & * & * & * \\ H_{21} & H_{22} & * & * & * & * & * \\ H_{31} & H_{32} & H_{33} & * & * & * & * \\ H_{41} & H_{42} & 0_{Nn} & H_{44} & * & * & * \\ H_{51} & 0_{Nn} & 0_{Nn} & 0_{Nn} & H_{55} & * & * \\ H_{61} & H_{62} & 0_{Nn} & H_{64} & 0_{Nn} & H_{66} & * \\ H_{71} & 0_{Nn} & 0_{Nn} & 0_{Nn} & 0_{Nn} & 0_{Nn} & H_{77} \end{bmatrix},$$

with

$$\begin{aligned} H_{11} &= \mathbf{I}_N \otimes (\tilde{P}A^T + A\tilde{P} + \tilde{Q} - \tilde{R}) \\ H_{21} &= \mathbf{I}_N \otimes (Y^T B^T + \tilde{R} - \tilde{S}^T) \\ H_{22} &= \mathbf{I}_N \otimes (-2\tilde{R} + \tilde{S} + \tilde{S}^T) + L_{ff}^T L_{ff} \otimes \tilde{\Phi} \end{aligned}$$

$$\begin{aligned} H_{31} &= \mathbf{I}_N \otimes \tilde{S}^T \\ H_{32} &= \mathbf{I}_N \otimes (\tilde{R} - \tilde{S}^T) \\ H_{33} &= -\mathbf{I}_N \otimes (\tilde{Q} + \tilde{R}) \\ H_{41} &= \mathbf{I}_N \otimes Y^T B^T \\ H_{42} &= L_{ff}^T L_{ff} \otimes \tilde{\Phi} \\ H_{44} &= -\mathbf{I}_N \otimes \tilde{\Psi}_1 + L_{ff}^T L_{ff} \otimes \tilde{\Phi} \\ H_{51} &= \mathcal{A}^T L_{ff}^{-T} \otimes \tilde{P} B^T \end{aligned}$$

$$\begin{aligned} H_{55} &= -\mathbf{I}_N \otimes \tilde{\Psi}_2 \\ H_{61} &= h(\mathbf{I}_N \otimes A\tilde{P}) \\ H_{62} &= h(\mathbf{I}_N \otimes BY) \\ H_{64} &= h(\mathbf{I}_N \otimes BY) \\ H_{65} &= h(L_{ff}^{-1}\mathcal{A} \otimes B\tilde{P}) \\ H_{66} &= \rho^2(\mathbf{I}_N \otimes \tilde{R}) - 2\rho(\mathbf{I}_N \otimes \tilde{P}) \\ H_{71} &= \mathbf{I}_N \otimes \tilde{P} \\ H_{77} &= -\frac{1}{\beta}\mathbf{I}_{Nn}. \end{aligned}$$

Then, the controller gain matrix K can be computed as $Y\tilde{P}^{-1}$, and the matrices Φ, Ψ_1 and Ψ_2 in the triggering conditions are obtained as $\tilde{P}^{-1}\tilde{\Phi}\tilde{P}^{-1}$, $\tilde{P}^{-1}\tilde{\Psi}_1\tilde{P}^{-1}$, and $\tilde{P}^{-1}\tilde{\Psi}_2\tilde{P}^{-1}$ respectively. In addition, the formation error is ultimately bounded as

$$\lim_{t\to\infty} \|\eta\| \leq \sqrt{\frac{N}{\beta}}\epsilon. \tag{5.16}$$

Proof. Consider the following continuous Lyapunov functional candidate on the interval $t \in [vh, (v+1)h)$ as

$$V(t) = V_1(t) + V_2(t) + V_3(t), \tag{5.17}$$

where

$$V_1(t) = \eta(t)^T(\mathbf{I}_N \otimes P)\eta(t), \tag{5.18}$$

$$V_2(t) = \int_{t-h}^{t} \eta^T(s)(\mathbf{I}_N \otimes Q)\eta(s)ds, \tag{5.19}$$

$$V_3(t) = h\int_{t-h}^{t}\int_{s}^{t} \dot{\eta}^T(\upsilon)(\mathbf{I}_N \otimes R)\dot{\eta}(\upsilon)d\upsilon ds, \tag{5.20}$$

and $P, Q, R \in R^{n\times n}$ are symmetric positive definite matrices. Taking the time derivative of the Lyapunov functional candidate along the augmented formation error dynamics (5.8) yields,

$$\begin{aligned}\dot{V}_1 &= \dot{\eta}(t)^T(\mathbf{I}_N \otimes P)\eta(t) + \eta(t)^T(\mathbf{I}_N \otimes P)\dot{\eta}(t)\\ &= \eta(t)^T(\mathbf{I}_N \otimes (A^TP + PA))\eta(t) + 2\eta(t-\tau)^T(\mathbf{I}_N \otimes K^TB^TP)\eta(t)\\ &\quad + 2\mathbf{e}(t-\tau)^T(\mathbf{I}_N \otimes K^TB^TP)\eta(t) + 2\bar{\mathbf{e}}(t-\tau)^T(\mathcal{A}_f^TL_{ff}^{-1} \otimes B^TP)\eta(t)\end{aligned}$$

$$\dot{V}_2 = \eta^T(t)(\mathbf{I}_N \otimes Q)\eta(t) - \eta^T(t-h)(\mathbf{I}_N \otimes Q)\eta(t-h),$$

$$\dot{V}_3 = -h\int_{t-h}^{t} \dot{\eta}^T(\upsilon)(\mathbf{I}_N \otimes R)\dot{\eta}(\upsilon)d\upsilon + h^2\dot{\eta}^T(t)(\mathbf{I}_N \otimes R)\dot{\eta}(t).$$

Then, from Lemma 4.1 we have

$$\begin{aligned}\dot{V}_3 \leq &-\phi_1^T(\mathbf{I}_N \otimes R)\phi_1 - \phi_2^T(\mathbf{I}_N \otimes R)\phi_2 - \phi_1^T(\mathbf{I}_N \otimes S)\phi_2\\ &- \phi_2^T(\mathbf{I}_N \otimes S^T)\phi_1 + h^2\dot{\eta}^T(t)(\mathbf{I}_N \otimes R)\dot{\eta}(t).\end{aligned}$$

Define $\xi(t)$ and ζ as

$$\xi(t) = \begin{bmatrix} \eta(t)^T & \eta(t-\tau)^T & \eta(t-h)^T & \mathbf{e}(t-\tau)^T & \bar{\mathbf{e}}(t-\tau)^T \end{bmatrix}^T,$$
$$\zeta = \begin{bmatrix} \mathbf{I}_N \otimes A & \mathbf{I}_N \otimes BK & 0 & \mathbf{I}_N \otimes BK & L_{ff}^{-1}\mathcal{A}_f \otimes B \end{bmatrix}.$$

Then, the closed-loop dynamics (5.8) can be expressed as $\dot{\eta}(t) = \zeta\xi(t)$, and $\dot{V}_3$ is upper bounded by

$$\dot{V}_3 \leq -\phi_1^T(\mathbf{I}_N \otimes R)\phi_1 - \phi_2^T(\mathbf{I}_N \otimes R)\phi_2 - \phi_1^T(\mathbf{I}_N \otimes S)\phi_2 - \phi_2^T(\mathbf{I}_N \otimes S^T)\phi_1 + h^2\xi(t)^T(\zeta^T(\mathbf{I}_N \otimes R)\zeta)\xi(t).$$

Combining results from $\dot{V}_1, \dot{V}_2, \dot{V}_3$, we have

$$\dot{V} \leq \xi^T(t)\Omega\xi(t) + h^2\xi(t)^T(\zeta^T(\mathbf{I}_N \otimes R)\zeta)\xi(t), \tag{5.21}$$

where

$$\Omega = \begin{bmatrix} \Omega_{11} & * & * & * & * \\ \Omega_{21} & \Omega_{22} & * & * & * \\ \Omega_{31} & \Omega_{32} & \Omega_{33} & * & * \\ \Omega_{41} & 0 & 0 & 0 & * \\ \Omega_{51} & 0 & 0 & 0 & 0 \end{bmatrix}, \tag{5.22}$$

with

$$\begin{aligned} \Omega_{11} &= \mathbf{I}_N \otimes (A^T P + PA + Q - R), \\ \Omega_{21} &= L_{ff}^T \otimes K^T B^T P + \mathbf{I}_N \otimes (R - S^T), \\ \Omega_{22} &= \mathbf{I}_N \otimes (-2R + S + S^T), \\ \Omega_{31} &= \mathbf{I}_N \otimes S^T, \\ \Omega_{32} &= \mathbf{I}_N \otimes (R - S^T), \\ \Omega_{33} &= -\mathbf{I}_N \otimes (Q + R), \\ \Omega_{41} &= \mathbf{I}_N \otimes K^T B^T P, \\ \Omega_{51} &= \mathcal{A}_f^T L_{ff}^{-T} \otimes B^T P. \end{aligned}$$

In addition, the matrix inequality (5.14) can be rewritten as

$$\xi^T(t)\bar{\Omega}\xi(t) \leq N\epsilon^2, \tag{5.23}$$

where

$$\bar{\Omega} = \begin{bmatrix} 0 & * & * & * & * \\ 0 & \bar{\Omega}_{22} & * & * & * \\ 0 & 0 & 0 & * & * \\ 0 & \bar{\Omega}_{42} & 0 & \bar{\Omega}_{44} & * \\ 0 & 0 & 0 & 0 & \bar{\Omega}_{55} \end{bmatrix}, \tag{5.24}$$

with

$$\begin{aligned} \bar{\Omega}_{22} &= -L_{ff}^T L_{ff} \otimes \Phi, \\ \bar{\Omega}_{42} &= -L_{ff}^T L_{ff} \otimes \Phi, \\ \bar{\Omega}_{44} &= \mathbf{I}_N \otimes \Psi_1 - L_{ff}^T L_{ff} \otimes \Phi, \\ \bar{\Omega}_{55} &= \mathbf{I}_N \otimes \Psi_2. \end{aligned}$$

Then, using (5.23), $\dot{V}$ in (5.21) can be enlarged and rewritten as

$$\dot{V} \leq \xi(t)^T \Xi \xi(t) - \beta\eta^T\eta + N\epsilon^2 \tag{5.25}$$

where β is a positive constant and

$$\Xi = \Omega - \bar{\Omega} + h^2\zeta^T(\mathbf{I}_N \otimes R)\zeta + \beta E_1^T E_1 \tag{5.26}$$

with $E_1 = \begin{bmatrix} \mathbf{I}_{Nn} & 0_{Nn} & 0_{Nn} & 0_{Nn} & 0_{Nn} \end{bmatrix}$. It can be shown that the formation error η will be ultimately bounded as (5.16) if $\Xi \leq 0$, is by repeatedly using Lemma 2.4 which is equivalent to

$$\begin{bmatrix} \Omega - \bar{\Omega} & * & * \\ h(\mathbf{I}_N \otimes R)\zeta & -\mathbf{I}_N \otimes R & * \\ E_1 & 0 & -\frac{1}{\beta}\mathbf{I}_{Nn} \end{bmatrix} < 0. \tag{5.27}$$

We pre- and post-multiply the inequality (5.27) by $diag\{\mathbf{I}_N \otimes \tilde{P}, \mathbf{I}_N \otimes \tilde{P}, \mathbf{I}_N \otimes \tilde{P}, \mathbf{I}_N \otimes$

$\tilde{P}, \mathbf{I}_N \otimes \tilde{P}, \mathbf{I}_N \otimes R^{-1}, \mathbf{I}_{Nn}\}$, where $\tilde{P} = P^{-1}$. In addition, define $\tilde{Q} = \tilde{P}Q\tilde{P}$. $\tilde{R}, \tilde{S}, \tilde{\Psi}_1, \tilde{\Psi}_2$, $\tilde{\Phi}, \tilde{M}$ are defined analogously. Then, by applying Lemma 2.4 again, the inequality in (5.27) is equivalent to

$$\begin{bmatrix} \tilde{\Omega} & * & * \\ h\zeta(\mathbf{I}_N \otimes \tilde{P}) & -\mathbf{I}_N \otimes R^{-1} & * \\ E_1(\mathbf{I}_N \otimes \tilde{P}) & 0 & -\frac{1}{\beta}\mathbf{I}_{Nn} \end{bmatrix} < 0, \tag{5.28}$$

where

$$\begin{aligned} \tilde{\Omega}_{11} &= \mathbf{I}_N \otimes (\tilde{P}A^T + A\tilde{P} + \tilde{Q} - \tilde{R}), \\ \tilde{\Omega}_{21} &= \mathbf{I}_N \otimes \tilde{P}K^T B^T + \mathbf{I}_N \otimes (\tilde{R} - \tilde{S}^T), \\ \tilde{\Omega}_{22} &= \mathbf{I}_N \otimes (-2\tilde{R} + \tilde{S} + \tilde{S}^T) + (L_{ff}^T L_{ff} \otimes \tilde{\Phi}), \end{aligned}$$

$$\begin{aligned} \tilde{\Omega}_{31} &= \mathbf{I}_N \otimes \tilde{S}^T, & \tilde{\Omega}_{42} &= L_{ff}^T L_{ff} \otimes \tilde{\Phi} \\ \tilde{\Omega}_{32} &= \mathbf{I}_N \otimes (\tilde{R} - \tilde{S}^T), & \tilde{\Omega}_{44} &= -\mathbf{I}_N \otimes \tilde{\Psi}_1 + L_{ff}^T L_{ff} \otimes \tilde{\Phi}, \\ \tilde{\Omega}_{33} &= -\mathbf{I}_N \otimes (\tilde{Q} + \tilde{R}), & \tilde{\Omega}_{51} &= \mathcal{A}_f^T L_{ff}^{-T} \otimes \tilde{P}B^T, \\ \tilde{\Omega}_{41} &= \mathbf{I}_N \otimes \tilde{P}K^T B^T, & \tilde{\Omega}_{55} &= -\mathbf{I}_N \otimes \tilde{\Psi}_2. \end{aligned}$$

Furthermore, we have $-\mathbf{I}_N \otimes R^{-1} \leq \rho^2 \mathbf{I}_N \otimes \tilde{R} - 2\rho(\mathbf{I}_N \otimes \tilde{P})$ for any positive constant $\rho > 0$ from Lemma 2.5. Therefore, it is sufficient to ensure the inequality in (5.28) if

$$H = \begin{bmatrix} \tilde{\Omega} & * & * \\ h\zeta(\mathbf{I}_N \otimes \tilde{P}) & \rho^2 \mathbf{I}_N \otimes \tilde{R} - 2\rho(\mathbf{I}_N \otimes \tilde{P}) & * \\ E_1(\mathbf{I}_N \otimes \tilde{P}) & 0 & -\frac{1}{\beta}\mathbf{I}_{Nn} \end{bmatrix} < 0, \tag{5.29}$$

is satisfied. In addition, the terms in H are defined in as (5.15). □

5.2 Simulation Results

Numerical simulations are carried out on a group of three follower mobile robots and a leader defined by (5.1) under the same communication topology as in Fig. 4.2 to validate the proposed formation tracking algorithm. The formation vectors are chosen as $f_1 = \begin{bmatrix} 1 & 0 \end{bmatrix}^T$, $f_2 = \begin{bmatrix} -0.7 & 0.7 \end{bmatrix}^T$, and $f_3 = \begin{bmatrix} -0.7 & -0.7 \end{bmatrix}^T$. The sampling

interval is $h = 0.1\ sec$ and the triggering threshold ϵ is empirically chosen as 0.0005. In a 14-sec simulation run, the virtual leader moves at a constant speed of $0.3\ m/s$ in the X-direction from the origin, and all followers are initially distributed near the origin. The LMI parameters are optimized using the method described in Section 4.2 as $\rho = 1.5198$, and $\beta = 1.0657$. The control gain matrix K and event generator gain matrices Φ_1, Φ_2 and Ψ can then be computed as

$$K = \begin{bmatrix} -1.0347 & 0 \\ 0 & -1.0347 \end{bmatrix}, \Phi = \begin{bmatrix} 0.0011 & 0 \\ 0 & 0.0011 \end{bmatrix},$$

$$\Psi_1 = \begin{bmatrix} 0.4087 & 0 \\ 0 & 0.4087 \end{bmatrix}, \Psi_2 = \begin{bmatrix} 1.8022 & 0 \\ 0 & 1.8022 \end{bmatrix},$$

from evaluating the feasibility of inequality (5.15).

Fig. 5.1 shows the simulated evolution of all agents under the proposed estimate-based controller (5.2) and event generator (5.11). Fig. 5.2 illustrates the formation error profiles of all agents in the X- and Y-directions, which clearly shows that a solution to Research Problem 2.2 has been achieved. Fig. 5.3 demonstrates the snapshots of the group formation in the X-Y plane at t = 0 sec, 4.6 sec, 9.3 sec, and 14 sec, respectively. The triggered communication events for all agents are depicted in Fig. 5.4, which shows that the communication events are relatively sparsely distributed as the system approaches the desired formation. In addition, the average communication triggering percentage on agents 1-3 are 41%, 74%, and 74%, respectively.

5.2.1 Effect of Communication Mechanisms

To compare with other communication mechanisms and to show the advantage of the proposed estimate-error-based ECM ($e_i(vh) = \hat{\mathbf{x}}_i(vh) - \mathbf{x}_i(t_k^i h)$, where $\hat{\mathbf{x}}_i$ is defined below (5.2)), similar simulations are also conducted using the state-error-based ECM ($e_i(vh) = \mathbf{x}_i(vh) - \mathbf{x}_i(t_k^i h)$) and a 10 Hz PCM. The l_2 norms of the formation errors of each follower agent under these different communication mechanisms are summarized in Table 5.1. It can be observed that the state-error-based ECM generally produces the largest l_2 norms (thus the worst performance) under similar simulation conditions. In addition, Table 5.2 summarizes the communication triggering percentage on

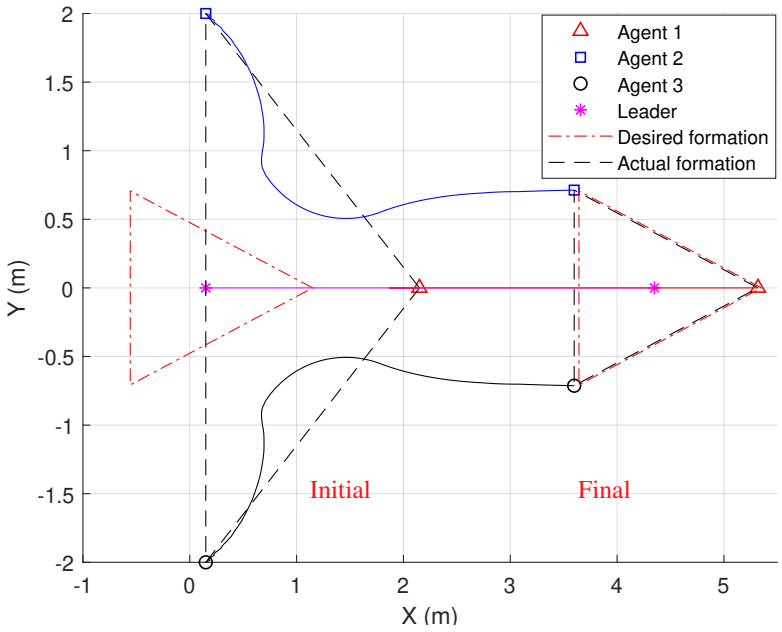

Figure 5.1: Simulation results of the formation evolution (5.1) with $\epsilon = 0.0005$

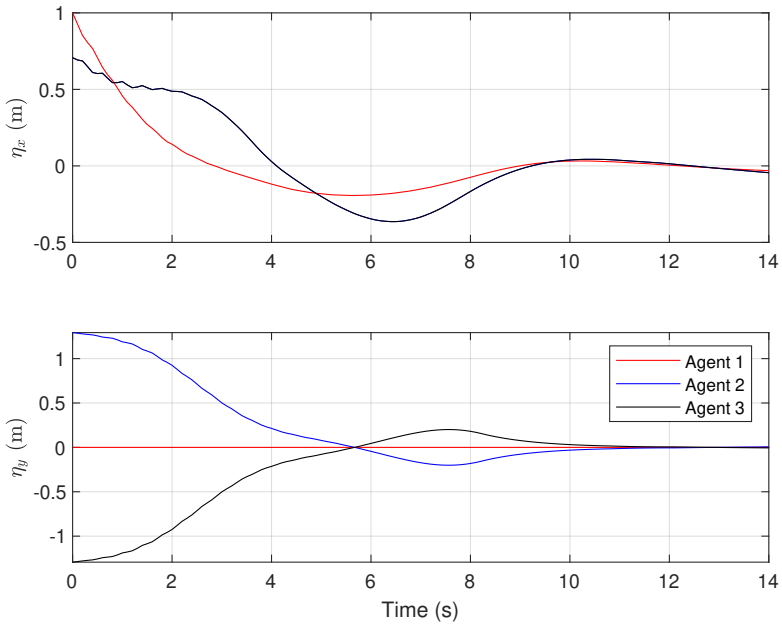

Figure 5.2: Simulation results of formation error profile

each agent under different communication mechanisms and shows that the proposed estimate-error-based ECM entails the least amount of communication resources.

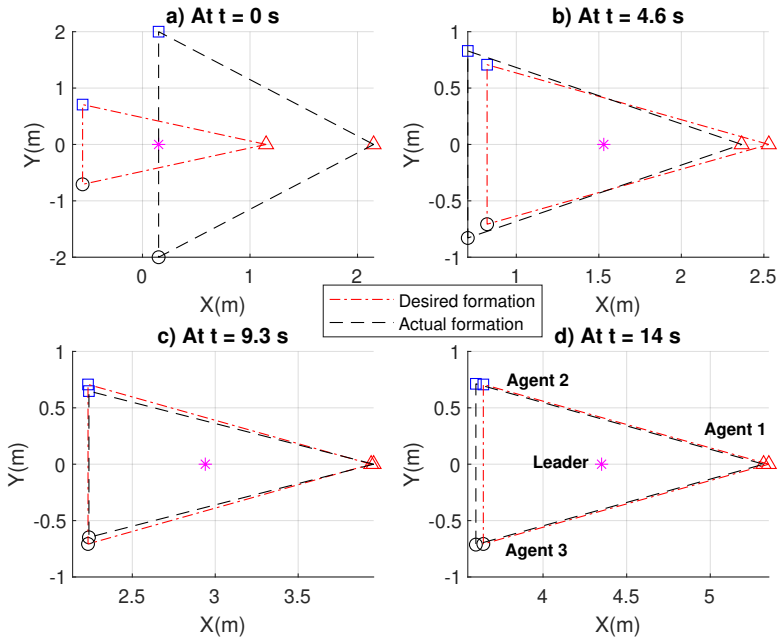

Figure 5.3: Simulation results of snapshots in the X-Y plane at: a) t=0 *sec*, b) t=4.6 *sec*, c) t=9.3 *sec*, d) t=14 *sec*

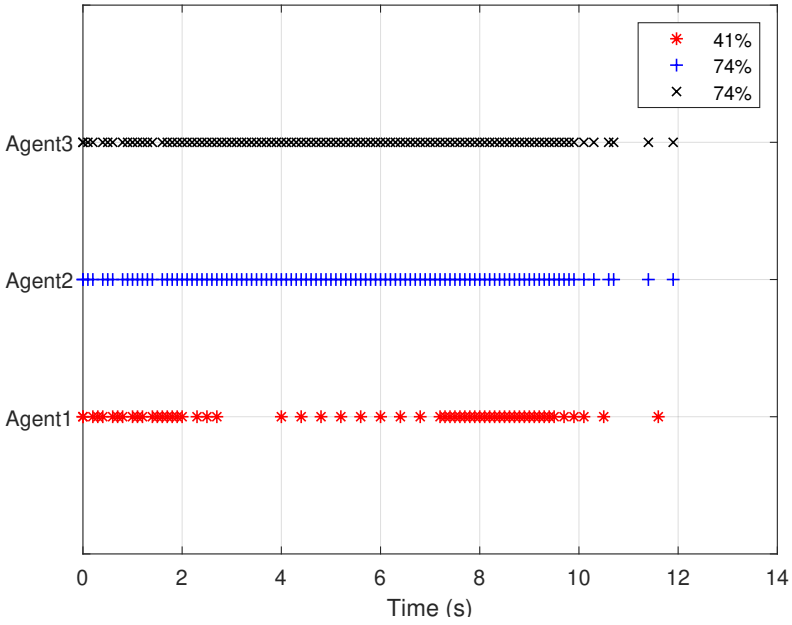

Figure 5.4: Simulation results of triggering instants

Table 5.1: Simulation results of l_2 norm (m) of formation error

Mechanisms	Agent 1	Agent 2	Agent 3
Estimate-error-based ECM	0.89	2.18	2.18
State-error-based ECM	0.90	2.32	2.32
PCM	0.88	2.17	2.17

Table 5.2: Simulation results of triggering percentage (%)

Mechanisms	Agent 1	Agent 2	Agent 3
Estimate-error-based ECM	41	74	74
State-error-based ECM	69	72	72
PCM	100	100	100

5.2.2 Effect of Triggering Threshold ϵ

The average communication frequency results for both state-error-based ECM and estimate-error-based ECM under the same simulation conditions with respect to different threshold values are summarized in Table 5.3. It can be observed that using a larger threshold in both communication mechanisms generally results in a smaller average communication triggering frequency; however, as shown in Table 5.4, a larger triggering threshold can generally induce a large l_2 norm of the formation error. In addition, a smaller l_2 norm of the system formation error can be obtained under the estimate-error-based ECM in comparison with the state-error-based ECM for all triggering thresholds in Table 5.4.

Table 5.3: Simulation results of average communication frequency (Hz) of all agents in the team under 10 Hz sampling frequency with different triggering thresholds

Mechanisms	For threshold ϵ=				
	0.0005	0.001	0.01	0.1	1
Estimate-error-based ECM	5.1	4.4	2.6	2	2.1
State-error-based ECM	7.5	5.1	3.6	1.6	0.93

Table 5.4: Simulation results of l_2 norm (m) of formation error in the team under different triggering thresholds

Mechanisms	For threshold ϵ=				
	0.0005	0.001	0.01	0.1	1
Estimate-error-based ECM	3.22	3.20	3.32	4.45	5.59
State-error-based ECM	3.40	3.41	3.61	3.82	10.15
PCM	3.32	3.32	3.32	3.32	3.32

5.3 Experimental Results

The experimental validation was conducted using the same setup as in Section 4.3. Fig. 5.5 shows the system evolution of the Pioneer robots in a 14 *sec* experiment under the newly-developed formation controller (5.2) and communication triggering rule (5.11). Fig. 5.6 illustrates the formation error evolution for each agent in the X and Y directions. Fig. 5.7 depicts the snapshots of the Pioneer group formation at $t = 0$ *sec*, $t = 4.6$ *sec*, $t = 9.3$ *sec* and $t = 14$ *sec*, respectively. The communication instants on each Pioneer robot are given in Fig. 5.8, which clearly shows that the communication events are sparsely distributed as the system approaches the desired formation. The system evolution, formation error profile, group formation snapshots, and triggering instants for the Pioneer robot system under the state-error-based ECM and PCM are shown in Figs. 5.9 to 5.12, and Figs. 5.13 to 5.16, respectively.

Note that, different from the triggering instants shown in Fig. 5.8, the communication instants under the conventional state-error-based ECM in Fig. 5.12 and PCM in Fig. 5.16 were still densely gathered (corresponding to unnecessary communication) when the desired group formation was approached. In addition, the experimental results of the l_2 norm of formation errors and communication triggering percentage of all Pioneer agents under the three communication mechanisms are summarized in Table 5.5 and Table 5.6. The results show that the experimental results follow the same trends as the simulation results—with the proposed estimate-error-based ECM able to produce comparable performance while requiring the least amount of communication resources.

Table 5.5: Experimental results of l_2 norm of formation error (m)

Mechanisms	Agent 1	Agent 2	Agent 3
Estimate-error-based ECM	1.01	2.08	2.08
State-error-based ECM	1.12	2.37	2.40
PCM	1.01	2.04	2.05

Table 5.6: Experimental results of triggering percentage (%)

Mechanisms	Agent 1	Agent 2	Agent 3
Estimate-error-based ECM	30	54	57
State-error-based ECM	80	70	70
PCM	100	100	100

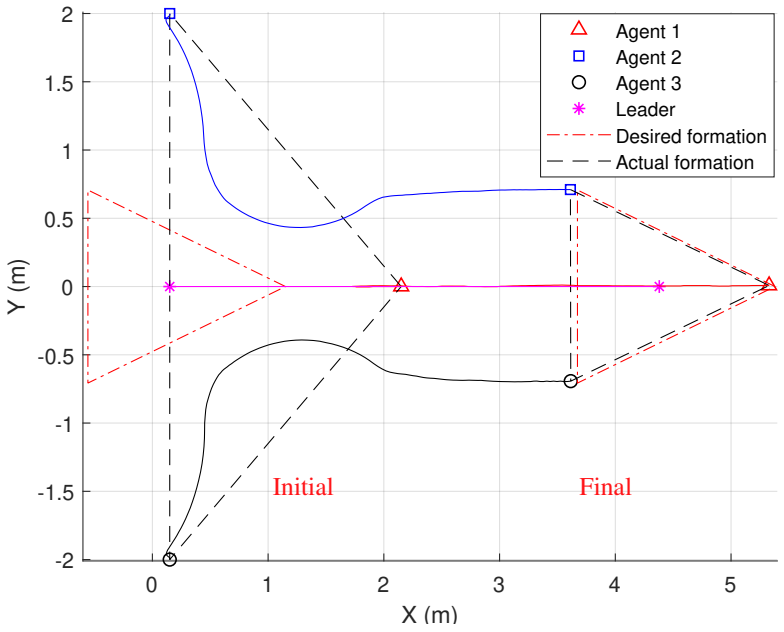

Figure 5.5: Experimental results of the formation evolution under estimate-error-based ECM

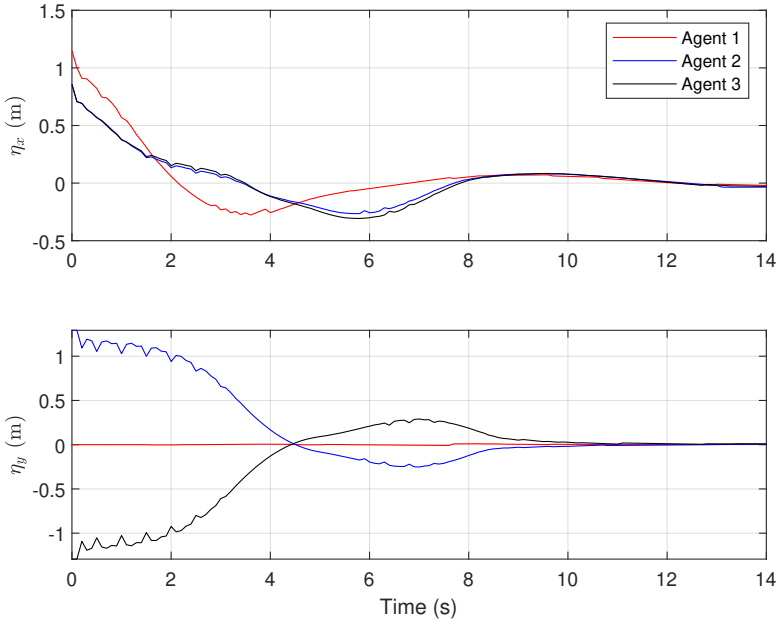

Figure 5.6: Experimental results of the formation error under estimate-error-based ECM

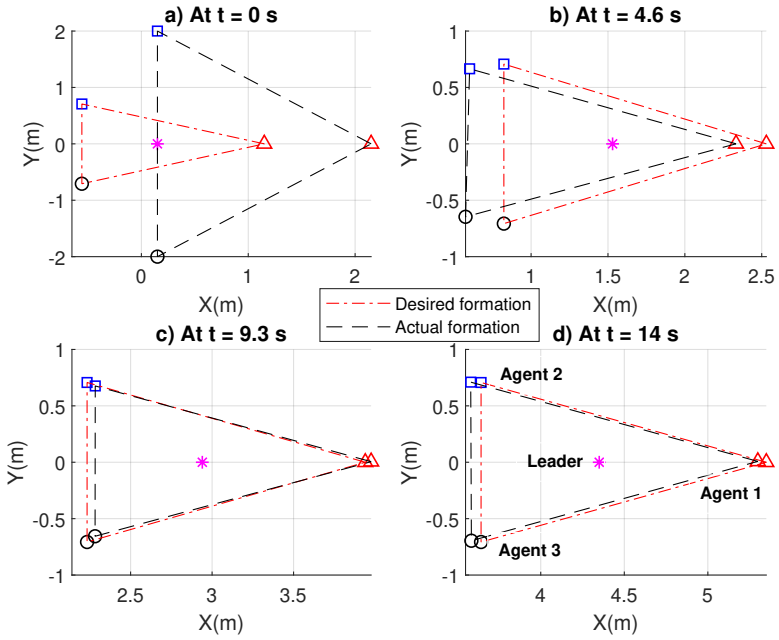

Figure 5.7: Experimental results of snapshots under estimate-error-based ECM in the X-Y plane at: a) t=0 *sec*, b) t=4.6 *sec*, c) t=9.3 *sec*, d) t=14 *sec*

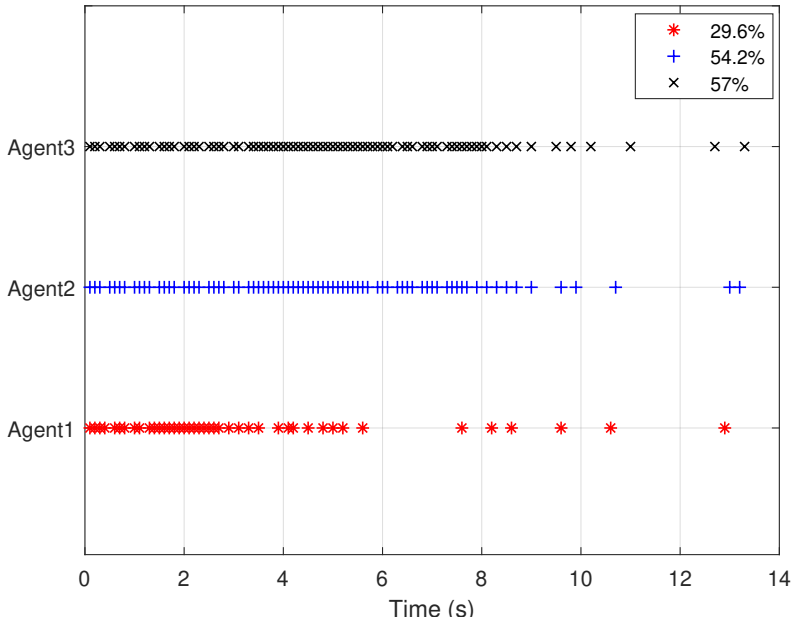

Figure 5.8: Experimental results of triggering instants under estimate-error-based ECM

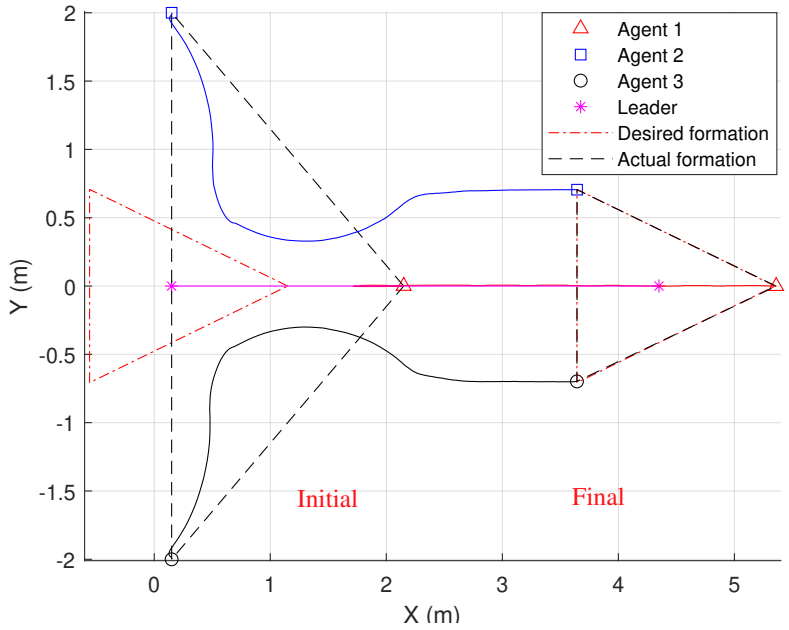

Figure 5.9: Experimental results of the formation evolution under state-error-based ECM

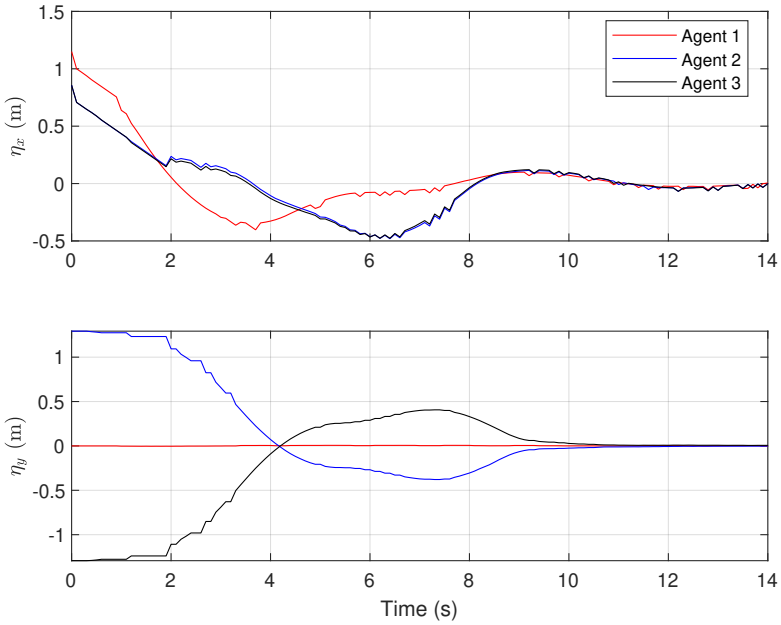

Figure 5.10: Experimental results of the formation error under state-error-based ECM

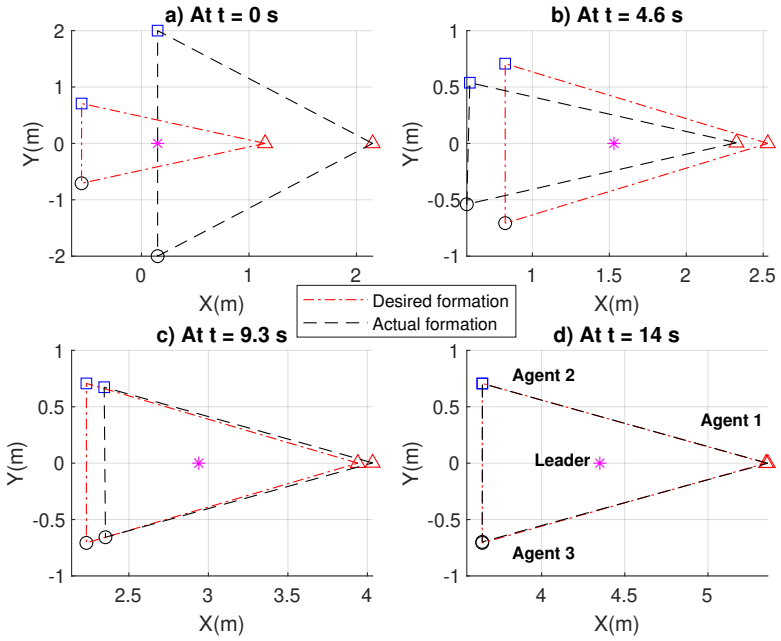

Figure 5.11: Experimental results of snapshots under state-error-based ECM in the X-Y plane at: a) t=0 *sec*, b) t=4.6 *sec*, c) t=9.3 *sec*, d) t=14 *sec*

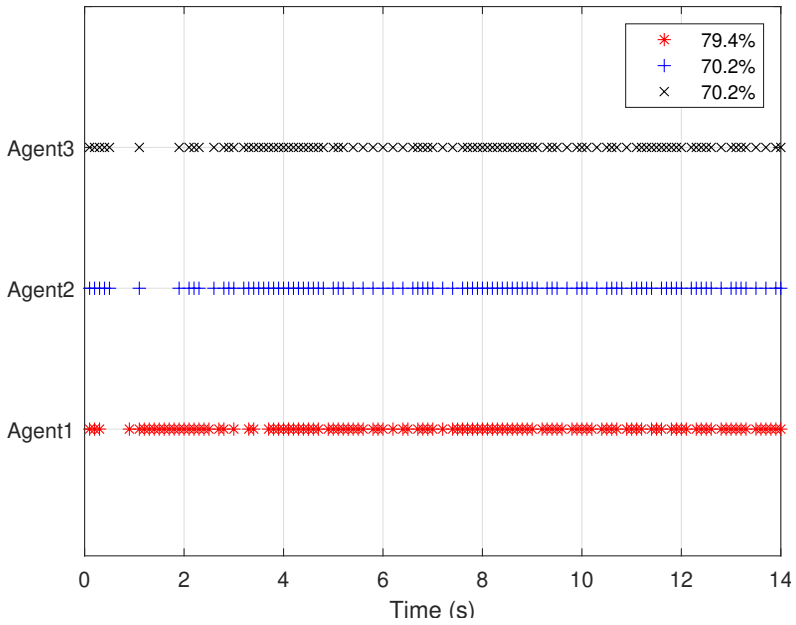

Figure 5.12: Experimental results of triggering instants under state-error-based ECM

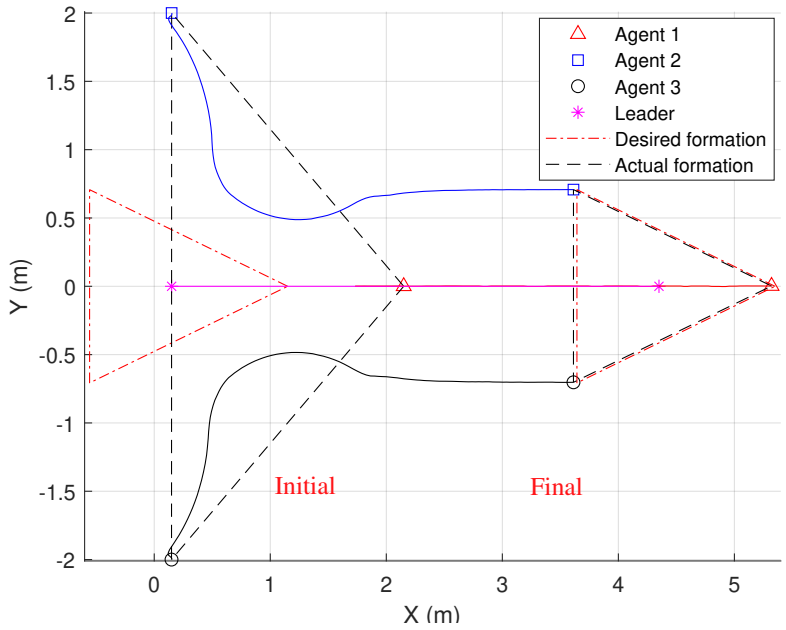

Figure 5.13: Experimental results of the formation evolution under PCM

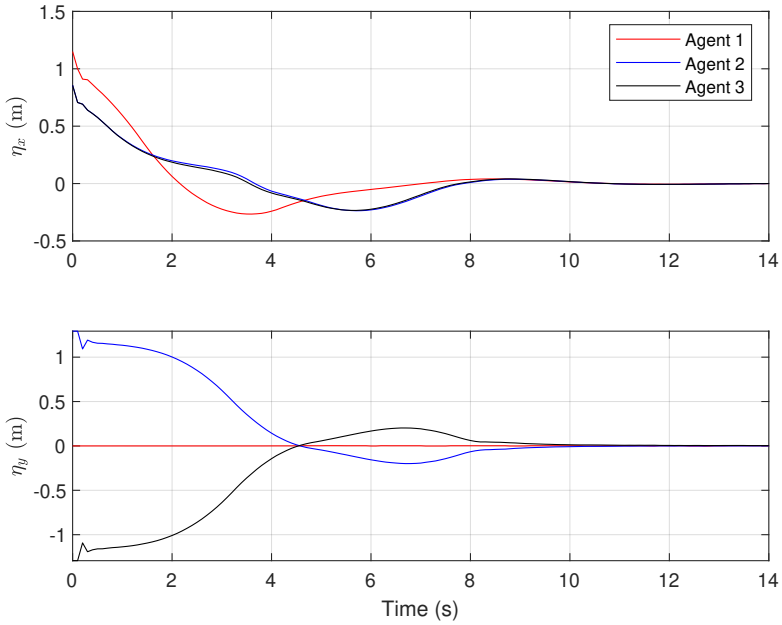

Figure 5.14: Experimental results of the formation error under PCM

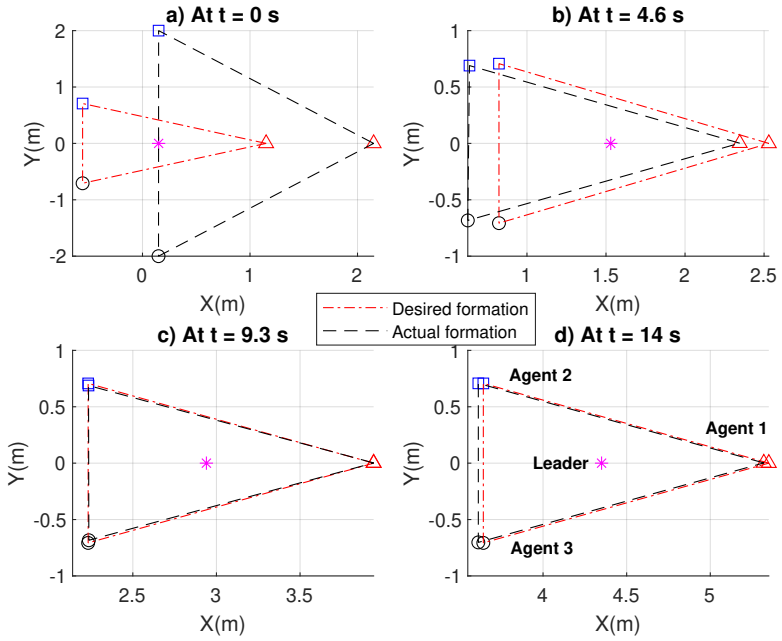

Figure 5.15: Experimental results of snapshots under PCM in the X-Y plane at: a) t=0 *sec*, b) t=4.6 *sec*, c) t=9.3 *sec*, d) t=14 *sec*

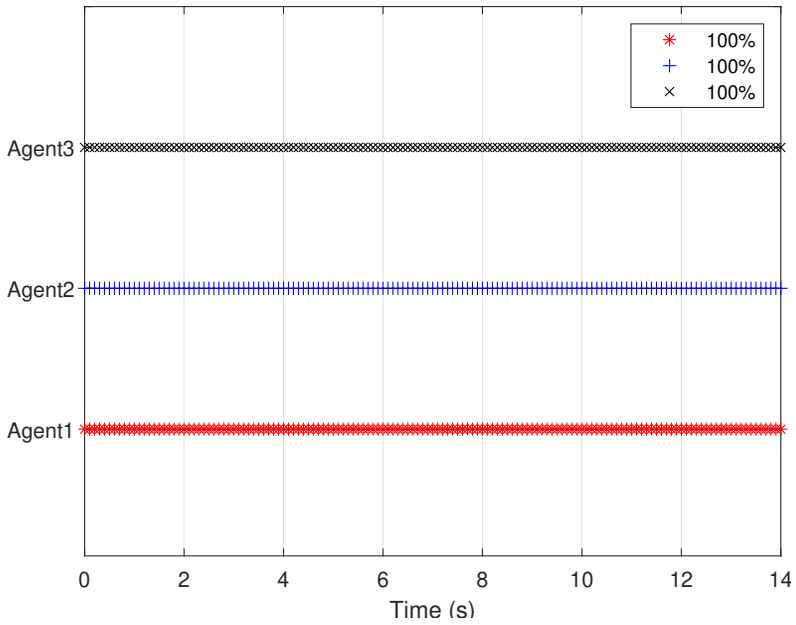

Figure 5.16: Experimental results of triggering instants under PCM

5.4 Conclusion

This chapter studied the leader-follower formation tracking control problem for linear MASs with a non-autonomous leader. A new estimate-error-based ECM was developed to account for the heterogeneity introduced by the leader's control input. The formation tracking controller was then designed based on the event-generator regulated state information and the neighboring control input information. Sufficient LMI conditions that guarantee an asymptotic convergence to the neighborhood of the of the desired formation were derived. Simulation and experiment show that the proposed ECM generally requires less communication resource than the state-error-based ECM and PCM while maintaining comparable performance.

Chapter 6

Edge-Triggered Formation Control

This Chapter addresses Research Problem 2.2 as described in the problem formulation section of Chapter 2 using a novel edge-based ECM. Recall that the ECMs developed in Chapter 4 and Chapter 5 are all node-based, where a triggering function is designed for each agent (node) and agents broadcast their state and control information to all of their neighbors when the triggering rules are activated. However, in the edge-based ECM developed in this Chapter, the triggering functions are designed for communication edges, where an agent transmits its sampled information to a specific neighboring agent that is connected to a specific edge when an edge triggering rule is activated. Therefore, systems under edge-based ECM can potentially maintain comparable performance while consuming reduced communication resources compared with node-based ECMs. Fig. 6.1 illustrates a node-triggered and an edge-triggered scheme. In addition to the LMI conditions for an asymptotic system convergence rate, conditions that guarantee an exponential convergence rate are derived by utilizing an extended Wirtinger's inequality [94]. Moreover, the exponential convergence rate is explicitly expressed in the derived conditions and can be tuned based on design requirements. Numerical simulations and hardware implementations are carried out to validate the proposed method. The exponential form of the extended Wirtinger inequality is summarized in the following lemma.

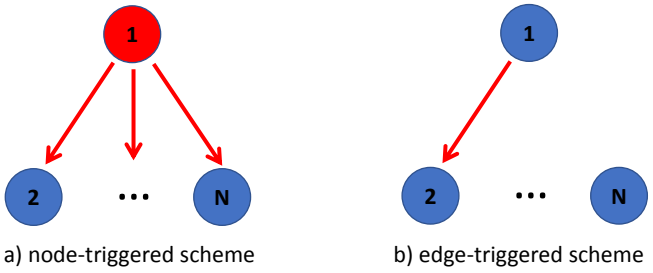

Figure 6.1: Node and edge triggered schemes (red arrow denotes a communication edge is enabled)

Lemma 6.1. [95] *Let $\eta : [a, b] \to R^n$ be an absolutely continuous function with a square integrable first order derivative and $\eta(a) = 0$, or $\eta(b) = 0$. Then, for any positive constant α and positive definite matrix $W \in \mathcal{R}^{n\times n}$, the following inequality holds:*

$$e^{2\alpha(b-a)}(b-a)^2 \int_a^b e^{2\alpha s}\dot{\eta}^T(s)W\dot{\eta}(s)ds - \frac{\pi^2}{4}\int_a^b e^{2\alpha s}\eta^T(s)W\eta(s)ds \geq 0. \tag{6.1}$$

6.1 Edge-Triggered Formation Control Strategy

An edge-based ECM along with a distributed formation controller utilizing the edge-triggered state are proposed in this section.

6.1.1 Edge-states-based Formation Controller Design

For $t \in [vh, (v+1)h)$, an edge-state-estimate-based control input for follower agent i is proposed as

$$\begin{aligned}\mathbf{u}_i(t) = &\frac{1}{\sum_{j=0}^N a_{ij}}\big[K\sum_{j=1}^N a_{ij}(\hat{\mathbf{x}}_{ji}(vh) - \hat{\mathbf{x}}_{ij}(vh) - f_i + f_j) + \sum_{j=1}^N a_{ij}\mathbf{u}_{ij}(t_{k'}^{ij}h)\big] \\ &+ \frac{1}{\sum_{j=0}^N a_{ij}}\big[a_{i0}\mathbf{u}_0(vh) - \mu_i + a_{i0}K(\frac{\sum_{j=1}^N a_{ji}\hat{\mathbf{x}}_{ji}(vh)}{\sum_{j=1}^N a_{ji}} - f_i - \mathbf{x}_0(vh))\big], \\ &\qquad\qquad i = 1, \cdots, N,\end{aligned} \tag{6.2}$$

where μ_i is the formation compensation input which is the same as the one designed in Section 5.1.1, $\hat{\mathbf{x}}_{ij}(vh)$ and $\hat{\mathbf{x}}_{ji}(vh)$ are the estimated states of agents j and i on edges $\mathcal{E}_{ij} \in \mathcal{E}$ and $\mathcal{E}_{ji} \in \mathcal{E}$. In addition, the state estimates $\hat{\mathbf{x}}_{ij}(vh)$ for all $\mathcal{E}_{ij} \in \mathcal{E}$ follow the dynamics $\dot{\hat{\mathbf{x}}}_{ij} = A\hat{\mathbf{x}}_{ij} + B\mathbf{u}_j(t_{\tilde{k}}^{ij}h)$, $t \in \left[t_{\tilde{k}}^{ij}h, (t_{\tilde{k}}^{ij}+1)h\right)$, where $t_{\tilde{k}}^{ij}h$ and $(t_{\tilde{k}}^{ij}+1)h$ are the latest released and next releasing communication events for the edge $\mathcal{E}_{ij}$, respectively. K is a static gain matrix to be determined.

6.1.2 Closed-loop Formation Error Dynamics

The closed-loop system dynamics under the controller (6.2) satisfies the following equation for $t \in [vh, (v+1)h)$

$$\begin{aligned}\sum_{j=0}^{N} a_{ij} B\mathbf{u}_i(t) = BK \sum_{j=1}^{N} a_{ij}(\mathbf{e}_{ji}(vh) - \mathbf{e}_{ij}(vh) - f_i + f_j + \mathbf{x}_i(vh) - \mathbf{x}_j(vh)) \\ + \sum_{j=1}^{N} a_{ij} B(\bar{\mathbf{e}}_{ij}(vh) + \mathbf{u}_j(vh)) + a_{i0} B\mathbf{u}_0(vh) - B\mu_i \\ + a_{i0} BK(\frac{\sum_{j=1}^{N} a_{ji}(\mathbf{e}_{ji}(vh) + \mathbf{x}_i(vh))}{\sum_{j=1}^{N} a_{ji}} - f_i - \mathbf{x}_0(vh)), \qquad (6.3)\end{aligned}$$

where $\mathbf{e}_{ij}(vh) = \hat{\mathbf{x}}_{ij}(vh) - \mathbf{x}_j(vh)$ and $\mathbf{e}_{ji}(vh) = \hat{\mathbf{x}}_{ji}(vh) - \mathbf{x}_i(vh)$ denote the state estimation error for agents j and i on edges $\mathcal{E}_{ij}$ and $\mathcal{E}_{ij}$ at sampling instant vh, respectively. In addition, $\bar{\mathbf{e}}_{ij}(vh) = \mathbf{u}_{ij}(t_k^{ij} h) - \mathbf{u}_j(vh)$ denotes the control input error at sampling instant vh. Note that (6.3) can be rearranged as

$$\begin{aligned}\sum_{j=0}^{N} a_{ij} B\mathbf{u}_i(t) - a_{i0} B\mathbf{u}_0(vh) - \sum_{j=1}^{N} a_{ij} B\mathbf{u}_j(vh) - \sum_{j=1}^{N} a_{ij} B(\bar{\mathbf{e}}_{ij}(vh)) \\ = BK \sum_{j=1}^{N} a_{ij}(\mathbf{e}_{ji}(vh) - \mathbf{e}_{ij}(vh) - f_i + f_j + \mathbf{x}_i(vh) - \mathbf{x}_j(vh)) \\ + a_{i0} BK(\frac{\sum_{j=1}^{N} a_{ji}(\mathbf{e}_{ji}(vh) + \mathbf{x}_i(vh))}{\sum_{j=1}^{N} a_{ji}} - f_i - \mathbf{x}_0(vh)) - B\mu_i \qquad (6.4)\end{aligned}$$

Since a sampled-data setting is adopted in this study, we assume that the control inputs are held constant for each sampling interval. Therefore, we have $\mathbf{u}_0(vh) = \mathbf{u}_0(t)$, and $\mathbf{u}_j(vh) = \mathbf{u}_j(t)$ for $t \in [vh, (v+1)h)$, and (6.4) can be rewritten as

$$\begin{aligned}\sum_{j=0}^{N} a_{ij} B(\mathbf{u}_i(t) - \mathbf{u}_j(t)) = BK \sum_{j=1}^{N} a_{ij}(\mathbf{e}_{ji}(vh) - \mathbf{e}_{ij}(vh)) + a_{i0} BK \frac{\sum_{j=1}^{N} a_{ji}\mathbf{e}_{ji}(vh)}{\sum_{j=1}^{N} a_{ji}} \\ + BK \sum_{j=0}^{N} a_{ij}(\eta_i(vh) - \eta_j(vh)) + B \sum_{j=1}^{N} a_{ij} \bar{\mathbf{e}}_{ij}(vh) - B\mu_i. \qquad (6.5)\end{aligned}$$

Substituting system dynamics (5.1) into (6.5), we can obtain

$$\begin{aligned}
&\sum_{j=0}^{N} a_{ij}(\dot{\mathbf{x}}_i(t) - \dot{\mathbf{x}}_j(t)) - \sum_{j=0}^{N} a_{ij}(A\eta_i(t) - A\eta_j(t)) \\
&\quad = BK\sum_{j=1}^{N} a_{ij}(\mathbf{e}_{ji}(vh) - \mathbf{e}_{ij}(vh)) + BK\sum_{j=0}^{N} a_{ij}(\eta_i(vh) - \eta_j(vh)) - B\mu_i \\
&\qquad + B\sum_{j=1}^{N} a_{ij}\bar{\mathbf{e}}_{ij}(vh) + a_{i0}BK\frac{\sum_{j=1}^{N} a_{ji}\mathbf{e}_{ji}(vh)}{\sum_{j=1}^{N} a_{ji}} + \sum_{j=0}^{N} a_{ij}(Af_i - Af_j). \qquad (6.6)
\end{aligned}$$

Note that the formation compensation input μ_i is designed such that the term $B\mu_i - \sum_{j=0}^{N} a_{ij}(Af_i - Af_j)$ is nullified. In addition, from the definition of formation error, we have $\dot{\mathbf{x}}_i(t) - \dot{\mathbf{x}}_j(t) = \dot{\eta}_i(t) - \dot{\eta}_j(t)$. Therefore, (6.6) can be rewritten as

$$\begin{aligned}
&\sum_{j=0}^{N} a_{ij}(\dot{\eta}_i(t) - \dot{\eta}_j(t)) - \sum_{j=0}^{N} a_{ij}(A\eta_i(t) - A\eta_j(t)) \\
&\quad = BK\sum_{j=1}^{N} a_{ij}(\mathbf{e}_{ji}(vh) - \mathbf{e}_{ij}(vh)) + BK\sum_{j=0}^{N} a_{ij}(\eta_i(vh) - \eta_j(vh)) \\
&\qquad + B\sum_{j=1}^{N} a_{ij}\bar{\mathbf{e}}_{ij}(vh) + a_{i0}BK\frac{\sum_{j=1}^{N} a_{ji}\mathbf{e}_{ji}(vh)}{\sum_{j=1}^{N} a_{ji}}. \qquad (6.7)
\end{aligned}$$

Now, we define $\dot{\eta}(t)$, $\eta(t)$, $\eta(vh)$, $\mathbf{e}(vh)$, and $\bar{\mathbf{e}}(vh)$ as the stacked form of $\dot{\eta}_i(t)$, $\eta_i(t)$, $\eta_i(vh)$, $e_{ij}(vh)$, and $\bar{e}_{ij}(vh)$, respectively. Then (6.7) can be compactly written as

$$\begin{aligned}
&(L_{ff}(i,:) \otimes \mathbf{I}_n)\dot{\eta}(t) - (L_{ff}(i,:) \otimes A)\eta(t) \\
&\quad = (L_{ff}(i,:) \otimes BK)\eta(vh) + (\mathbf{I}_H(i,:)^T \otimes BK)\mathbf{e}(vh) \\
&\qquad + (\mathbf{I}_H(i,:)^T \otimes B)\bar{\mathbf{e}}(vh) + \frac{a_{i0}}{\sum_{j=1}^{N} a_{ji}}(\mathbf{I}_T(i,:)^T \otimes BK)\mathbf{e}(vh) \\
&\qquad\quad - (\mathbf{I}_T(i,:)^T \otimes BK)\mathbf{e}(vh), \qquad (6.8)
\end{aligned}$$

where $L_{ff}(i,:)$ represents the i^{th} row of the matrix L_{ff}, with $\mathbf{I}_H(i,:)$ and $\mathbf{I}_T(i,:)$ defined analogously. The augmented overall closed-loop dynamics are then given as

$$\begin{aligned}
&(L_{ff}\otimes \mathbf{I}_n)\dot{\eta}(t) - (L_{ff}\otimes A)\eta(t)\\
&\quad = (L_{ff}\otimes BK)\eta(vh) + (\mathbf{I}_H^T\otimes BK)\mathbf{e}(vh) - (\mathbf{I}_T^T\otimes BK)\mathbf{e}(vh)\\
&\qquad + (\mathbf{I}_H^T\otimes B)\bar{\mathbf{e}}(vh) + \left(\begin{bmatrix} \frac{a_{10}}{\sum_{j=1}^{N} a_{j1}} & & \\ & \ddots & \\ & & \frac{a_{N0}}{\sum_{j=1}^{N} a_{jN}} \end{bmatrix}\mathbf{I}_T^T\otimes BK\right)\mathbf{e}(vh), \qquad (6.9)
\end{aligned}$$

which can be more compactly written as

$$\begin{aligned}
(L_{ff}\otimes \mathbf{I}_n)\dot{\eta}(t) = (L_{ff}\otimes A)\eta(t) + (L_{ff}\otimes BK)\mathbf{e}(vh) + (\tilde{\mathbf{I}}\otimes BK)\eta(vh)\\
+ (\mathbf{I}_H^T\otimes B)\bar{\mathbf{e}}(vh), \qquad (6.10)
\end{aligned}$$

where $\tilde{\mathbf{I}} = \mathbf{I}_{inc}^T + diag\{a_{10},\cdots,a_{N0}\}\mathcal{D}^{-1}\mathbf{I}_T^T$. In addition, considering Definition 4.2 together with Lemma 2.1, we conclude that $(L_{ff}\otimes \mathbf{I}_n)$ is invertible and the overall formation error dynamics for $t\in[vh,(v+1)h)$ can be obtained as

$$\begin{aligned}
\dot{\eta}(t) = (\mathbf{I}_N\otimes A)\eta(t) + (\mathbf{I}_N\otimes BK)\mathbf{e}(t-\tau) + (L_{ff}^{-1}\tilde{\mathbf{I}}\otimes BK)\eta(t-\tau)\\
+ (L_{ff}^{-1}\mathbf{I}_H^T\otimes B)\bar{\mathbf{e}}(t-\tau), \qquad (6.11)
\end{aligned}$$

where, $\eta(t-\tau)$, $\mathbf{e}(t-\tau)$, and $\bar{\mathbf{e}}(t-\tau)$ are the stacked form of $\eta_i(t-\tau)$, $e_i(t-\tau)$, and $\bar{e}_i(t-\tau)$, respectively.

6.2 Edge Event Generator Design

A novel asynchronous edge-based event-triggered communication mechanism will be designed in this section. In essence, when an edge-event is detected, only the node that is incident to the edge will update the corresponding state-estimate using the triggered states. Inspired by the edge-triggering function designed for continuous systems [48], we propose an edge-triggering function for the edge $\mathcal{E}_{ij}\in\mathcal{E}$ as

$$f_{ij}(vh) = \mathbf{e}_{ij}^T(vh)\Phi_1\mathbf{e}_{ij}(vh) + \bar{\mathbf{e}}_{ij}^T(vh)\Phi_2\bar{\mathbf{e}}_{ij}(vh) - \tilde{\eta}_{ij}(vh)^T\Psi\tilde{\eta}_{ij}(vh), \qquad (6.12)$$

where $\tilde{\eta}_{ij}(vh) = \hat{\mathbf{x}}_{ij}(vh) - \hat{\mathbf{x}}_{ji}(vh) - f_j + f_i$, and Φ_1, Φ_2, and Ψ are positive definite matrices to be designed. From the definition of $\mathbf{e}_{ij}(vh)$ and $\mathbf{e}_{ji}(vh)$, $\tilde{\eta}_{ij}(vh)$ can be expressed as $\mathbf{e}_{ij}(vh) - \mathbf{e}_{ji}(vh) + \eta_j(vh) - \eta_i(vh)$ and (6.12) can be rewritten as

$$\begin{aligned} f_{ij}(vh) =& \mathbf{e}_{ij}^T(vh)\Phi_1\mathbf{e}_{ij}(vh) - (\mathbf{e}_{ij}(vh) - \mathbf{e}_{ji}(vh) + \eta_j(vh) - \eta_i(vh))^T \\ & \Psi(\mathbf{e}_{ij}(vh) - \mathbf{e}_{ji}(vh) + \eta_j(vh) - \eta_i(vh)) + \bar{\mathbf{e}}_{ij}^T(vh)\Phi_2\bar{\mathbf{e}}_{ij}(vh). \end{aligned} \tag{6.13}$$

Note that from the Lemma 2.6, we have

$$\begin{aligned} &-(\mathbf{e}_{ij}(vh) - \mathbf{e}_{ji}(vh) + \eta_j(vh) - \eta_i(vh))^T\Psi(\mathbf{e}_{ij}(vh) - \mathbf{e}_{ji}(vh) + \eta_j(vh) - \eta_i(vh)) \\ &\quad = -(\mathbf{e}_{ij}(vh) - \mathbf{e}_{ji}(vh))^T\Psi(\mathbf{e}_{ij}(vh) - \mathbf{e}_{ji}(vh)) - (\eta_j(vh) - \eta_i(vh))^T \\ &\qquad \Psi(\eta_j(vh) - \eta_i(vh)) - 2(\mathbf{e}_{ij}(vh) - \mathbf{e}_{ji}(vh))^T\Psi(\eta_j(vh) - \eta_i(vh)) \\ &\quad \geq -2(\mathbf{e}_{ij}(vh) - \mathbf{e}_{ji}(vh))^T\Psi(\mathbf{e}_{ij}(vh) - \mathbf{e}_{ji}(vh)) \\ &\qquad - 2(\eta_j(vh) - \eta_i(vh))^T\Psi(\eta_j(vh) - \eta_i(vh)). \end{aligned} \tag{6.14}$$

Apply Lemma 2.6 again, we obtain

$$\begin{aligned} -2(\mathbf{e}_{ij}(vh) &- \mathbf{e}_{ji}(vh))^T\Psi(\mathbf{e}_{ij}(vh) - \mathbf{e}_{ji}(vh)) \\ &= -2\mathbf{e}_{ij}(vh)\Psi\mathbf{e}_{ij}(vh) - 2\mathbf{e}_{ji}(vh)\Psi\mathbf{e}_{ji}(vh) + 4\mathbf{e}_{ij}(vh)\Psi\mathbf{e}_{ji}(vh) \\ &\geq -2\mathbf{e}_{ij}(vh)\Psi\mathbf{e}_{ij}(vh) - 2\mathbf{e}_{ji}(vh)\Psi\mathbf{e}_{ji}(vh) \\ &\quad - 2\mathbf{e}_{ij}(vh)\Psi\mathbf{e}_{ij}(vh) - 2\mathbf{e}_{ji}(vh)\Psi\mathbf{e}_{ji}(vh) \\ &= -4\mathbf{e}_{ij}(vh)\Psi\mathbf{e}_{ij}(vh) - 4\mathbf{e}_{ji}(vh)\Psi\mathbf{e}_{ji}(vh). \end{aligned} \tag{6.15}$$

Since our communication is bi-directional, we have

$$\sum_{\mathcal{E}_{ij}\in\mathcal{E}} -4\mathbf{e}_{ij}(vh)\Psi\mathbf{e}_{ij}(vh) - 4\mathbf{e}_{ji}(vh)\Psi\mathbf{e}_{ji}(vh) = -8\mathbf{e}^T(vh)(\mathbf{I}_M \otimes \Psi)\mathbf{e}(vh). \tag{6.16}$$

In addition,

$$\begin{aligned} -2(\eta_j(vh) - \eta_i(vh))^T&\Psi(\eta_j(vh) - \eta_i(vh)) \\ &= -2\eta(vh)^T\big(\mathbf{I}_{inc}(i,:)^T \otimes \mathbf{I}_n\big)\Psi\big(\mathbf{I}_{inc}(i,:) \otimes \mathbf{I}_n\big)\eta(vh), \end{aligned} \tag{6.17}$$

and

$$\begin{aligned}
&\sum_{\mathcal{E}_{ij}\in\mathcal{E}} -2(\eta_j(vh)-\eta_i(vh))^T\Psi(\eta_j(vh)-\eta_i(vh)) \\
&\qquad = -2\eta(vh)^T\Big(\sum_{i=1}^{M}\big(\mathbf{I}_{inc}(i,:)^T\otimes\mathbf{I}_n\big)\Psi\big(\mathbf{I}_{inc}(i,:)\otimes\mathbf{I}_n\big)\Big)\eta(vh) \\
&\qquad = -2\eta(vh)^T\Big(\sum_{i=1}^{M}\big(\mathbf{I}_{inc}(i,:)^T\mathbf{I}_{inc}(i,:)\otimes\mathbf{I}_n\big)\big(\mathbf{I}_N\otimes\Psi\big)\Big)\eta(vh) \\
&\qquad = -2\eta(vh)^T\big(\mathbf{I}_{inc}^T\mathbf{I}_{inc}\otimes\mathbf{I}_n\big)\big(\mathbf{I}_N\otimes\Psi\big)\eta(vh) \\
&\qquad = -2\eta(vh)^T\big(\mathbf{I}_{inc}^T\mathbf{I}_{inc}\otimes\Psi\big)\eta(vh). \qquad (6.18)
\end{aligned}$$

Therefore, by combining (6.13)-(6.18) we have

$$\begin{aligned}
\sum_{\mathcal{E}_{ij}\in\mathcal{E}} f_{ij}(vh) \geq& \mathbf{e}^T(vh)(\mathbf{I}_M\otimes\Phi_1)\mathbf{e}(vh)+\bar{\mathbf{e}}^T(vh)(\mathbf{I}_M\otimes\Phi_2)\bar{\mathbf{e}}(vh) \\
&-8\mathbf{e}^T(vh)(\mathbf{I}_M\otimes\Psi)\mathbf{e}(vh)-2\eta(vh)^T\big(\mathbf{I}_{inc}^T\mathbf{I}_{inc}\otimes\Psi\big)\eta(vh). \qquad (6.19)
\end{aligned}$$

The next event release instant for edge $\mathcal{E}_{ij}\in\mathcal{E}$ can then be determined as follows

$$t_{k+1}^{ij}h = inf\{vh > t_k^{ij}h|\ f_{ij}(vh)>0\}. \qquad (6.20)$$

Note that the state estimate error $e_{ij}(vh)$ and control input error $\bar{e}_{ij}(vh)$ will be reset to zero whenever the communication on the edge $\mathcal{E}_{ij}$ is triggered. For this reason, $f_{ij}(vh)\leq 0$ can be enforced for all edges at all sampling instants, which implies that $\sum_{\mathcal{E}_{ij}\in\mathcal{E}} f_{ij}(vh)\leq 0$ is always satisfied. Therefore, under the triggering rule (6.20), the inequality (6.19) can be enlarged as

$$\begin{aligned}
0\geq\sum_{\mathcal{E}_{ij}\in\mathcal{E}} f_{ij}(vh) \geq& \mathbf{e}^T(vh)(\mathbf{I}_M\otimes\Phi_1)\mathbf{e}(vh)+\bar{\mathbf{e}}^T(vh)(\mathbf{I}_M\otimes\Phi_2)\bar{\mathbf{e}}(vh) \\
&-8\mathbf{e}^T(vh)(\mathbf{I}_M\otimes\Psi)\mathbf{e}(vh)-2\eta(vh)^T\big(\mathbf{I}_{inc}^T\mathbf{I}_{inc}\otimes\Psi\big)\eta(vh), \qquad (6.21)
\end{aligned}$$

which can be rearranged as

$$\begin{aligned}
&-\mathbf{e}^T(vh)(\mathbf{I}_M\otimes\Phi_1)\mathbf{e}(vh)-\bar{\mathbf{e}}^T(vh)(\mathbf{I}_M\otimes\Phi_2)\bar{\mathbf{e}}(vh) \\
&+8\mathbf{e}^T(vh)(\mathbf{I}_M\otimes\Psi)\mathbf{e}(vh)+2\eta(vh)^T\big(\mathbf{I}_{inc}^T\mathbf{I}_{inc}\otimes\Psi\big)\eta(vh)\geq 0, \qquad (6.22)
\end{aligned}$$

Therefore, $\sum_{i=1}^{N} f_i(vh) \leq 0$ can be compactly rewritten in the following matrix form

$$\begin{bmatrix} \eta(vh) \\ \mathbf{e}(vh) \\ \bar{\mathbf{e}}(vh) \end{bmatrix}^T \begin{bmatrix} 2(\mathbf{I}_{inc}^T \mathbf{I}_{inc} \otimes \Psi) & * & * \\ 0_{Mn \times Nn} & 8(\mathbf{I}_M \otimes \Psi) - (\mathbf{I}_M \otimes \Phi_1) & * \\ 0_{Mm \times Nn} & 0_{Mm \times Mn} & -\mathbf{I}_M \otimes \Psi_2 \end{bmatrix} \begin{bmatrix} \eta(vh) \\ \mathbf{e}(vh) \\ \bar{\mathbf{e}}(vh) \end{bmatrix} \geq 0, \tag{6.23}$$

Using the notation $vh = t - \tau$ from Definition 4.2, we have

$$\begin{bmatrix} \eta(t-\tau) \\ \mathbf{e}(t-\tau) \\ \bar{\mathbf{e}}(t-\tau) \end{bmatrix}^T \begin{bmatrix} 2(\mathbf{I}_{inc}^T \mathbf{I}_{inc} \otimes \Psi) & * & * \\ 0_{Mn \times Nn} & 8(\mathbf{I}_M \otimes \Psi) - (\mathbf{I}_M \otimes \Phi_1) & * \\ 0_{Mm \times Nn} & 0_{Mm \times Mn} & -\mathbf{I}_M \otimes \Psi_2 \end{bmatrix} \begin{bmatrix} \eta(t-\tau) \\ \mathbf{e}(t-\tau) \\ \bar{\mathbf{e}}(t-\tau) \end{bmatrix} \geq 0. \tag{6.24}$$

6.3 Main Results

The following Theorems present sufficient LMI conditions for co-designing event generator and controller gains that provide asymptotic and exponential convergence to the desired formation, respectively.

Theorem 6.1. *Under the control law (6.2) and the edge-based communication regulation condition (6.12), the system (5.1) achieves formation asymptotically if, for given positive scalars ρ, there exist symmetric positive definite matrices $\tilde{\Phi}$, $\tilde{\Psi}_1$, $\tilde{\Psi}_2$, $\tilde{P}$, $\tilde{Q}$, $\tilde{R} \in \mathbb{R}^{n \times n}$, as well as arbitrary matrices $\tilde{S} \in \mathbb{R}^{n \times n}$ and $Y \in \mathbb{R}^{m \times n}$, such that*

$$\begin{bmatrix} \tilde{R} & * \\ \tilde{S}^T & \tilde{R} \end{bmatrix} \geq 0, \; H < 0, \tag{6.25}$$

where

$$H = \begin{bmatrix} H_{11} & * & * & * & * & * \\ H_{21} & H_{22} & * & * & * & * \\ H_{31} & H_{32} & H_{33} & * & * & * \\ H_{41} & 0 & 0 & H_{44} & * & * \\ H_{51} & 0 & 0 & 0 & H_{55} & * \\ H_{61} & H_{62} & 0 & H_{64} & H_{65} & H_{66} \end{bmatrix},$$

with

$$H_{11} = \mathbf{I}_N \otimes (\tilde{P}A^T + A\tilde{P} + \tilde{Q} - \tilde{R})$$
$$H_{21} = \mathbf{I}_N \otimes (Y^T B^T + \tilde{R} - \tilde{S}^T)$$
$$H_{22} = \mathbf{I}_N \otimes (-2\tilde{R} + \tilde{S} + \tilde{S}^T) + 2(\mathbf{I}_{inc}^T \mathbf{I}_{inc} \otimes \tilde{\Phi})$$
$$H_{31} = \mathbf{I}_N \otimes \tilde{S}^T$$
$$H_{32} = \mathbf{I}_N \otimes (\tilde{R} - \tilde{S}^T)$$
$$H_{33} = -\mathbf{I}_N \otimes (\tilde{Q} + \tilde{R})$$
$$H_{41} = (\tilde{\mathbf{I}}^T L_{ff}^{-T}) \otimes Y^T B^T$$
$$H_{44} = -\mathbf{I}_M \otimes \tilde{\Psi}_1 + 8(\mathbf{I}_M \otimes \tilde{\Phi}),$$
$$H_{51} = (\mathbf{I}_H L_{ff}^{-T}) \otimes \tilde{P}B^T$$
$$H_{55} = -\mathbf{I}_M \otimes \tilde{\Psi}_2$$
$$H_{61} = h(\mathbf{I}_N \otimes A\tilde{P})$$
$$H_{62} = h(\mathbf{I}_N \otimes BY)$$
$$H_{64} = h(L_{ff}^{-T}\tilde{\mathbf{I}} \otimes BY)$$
$$H_{65} = h(L_{ff}^{-1}\mathbf{I}_H^T \otimes B\tilde{P})$$
$$H_{66} = \rho^2(\mathbf{I}_N \otimes \tilde{R}) - 2\rho(\mathbf{I}_N \otimes \tilde{P}).$$

Then, the controller gain matrix K can be computed as $Y\tilde{P}^{-1}$, and the matrices Φ, Ψ_1 and Ψ_2 in the triggering conditions are obtained as $\tilde{P}^{-1}\tilde{\Phi}\tilde{P}^{-1}$, $\tilde{P}^{-1}\tilde{\Psi}_1\tilde{P}^{-1}$, and $\tilde{P}^{-1}\tilde{\Psi}_2\tilde{P}^{-1}$, respectively.

Proof. Rewrite the closed-loop dynamics (6.11) as $\dot{\eta}(t) = \zeta\xi$, where

$$\xi(t) = \begin{bmatrix} \eta(t)^T & \eta(t-\tau)^T & \eta(t-h)^T & \mathbf{e}(t-\tau)^T & \bar{\mathbf{e}}(t-\tau)^T \end{bmatrix}^T, \tag{6.26}$$
$$\zeta = \begin{bmatrix} \mathbf{I}_N \otimes A & \mathbf{I}_N \otimes BK & 0 & L_{ff}^{-1}\tilde{\mathbf{I}} \otimes BK & L_{ff}^{-1}\mathbf{I}_H^T \otimes B \end{bmatrix}. \tag{6.27}$$

The proof can then be completed by utilizing the Lyapunov functional candidate (5.17) and following the same procedures as in the proof of Theorem 5.1. □

Theorem 6.2. *Under the control law (6.2) and the edge-based communication regulation condition (6.12), the system (5.1) achieves formation exponentially with a convergence rate of α if, for given positive scalars ρ_1, ρ_2, and α, there exist symmetric positive definite matrices $\tilde{\Phi}$, $\tilde{\Psi}_1$, $\tilde{\Psi}_2$, $\tilde{W}$, $\tilde{P}$, $\tilde{Q}$, $\tilde{R} \in \mathbb{R}^{n\times n}$, as well as arbitrary matrices $\tilde{S} \in \mathbb{R}^{n\times n}$ and $Y \in \mathbb{R}^{m\times n}$, such that*

$$\begin{bmatrix} \tilde{R} & * \\ \tilde{S}^T & \tilde{R} \end{bmatrix} \geq 0,\ H < 0, \tag{6.28}$$

where

$$H = \begin{bmatrix} H_{11} & * & * & * & * & * & * & * \\ H_{21} & H_{22} & * & * & * & * & * & * \\ H_{31} & H_{32} & H_{33} & * & * & * & * & * \\ H_{41} & 0 & 0 & H_{44} & * & * & * & * \\ H_{51} & 0 & 0 & 0 & H_{55} & * & * & * \\ 0 & 0 & 0 & 0 & 0 & H_{66} & * & * \\ H_{71} & H_{72} & 0 & H_{74} & H_{75} & 0 & H_{77} & * \\ H_{81} & H_{82} & 0 & H_{84} & H_{85} & 0 & 0 & H_{88} \end{bmatrix},$$

with

$$\begin{aligned} H_{11} &= \mathbf{I}_N \otimes (\tilde{P}A^T + A\tilde{P} + \tilde{Q} - \tilde{R} + 2\alpha\tilde{P} - e^{-2\alpha h}\tilde{R}) \\ H_{21} &= \mathbf{I}_N \otimes (Y^T B^T + e^{-2\alpha h}(\tilde{R} - \tilde{S}^T)) \\ H_{22} &= \mathbf{I}_N \otimes \left(e^{-2\alpha h}(-2\tilde{R} + \tilde{S} + \tilde{S}^T)\right) + 2(\mathbf{I}_{inc}^T \mathbf{I}_{inc} \otimes \tilde{\Phi}), \end{aligned}$$

$$\begin{aligned} H_{31} &= e^{-2\alpha h}(\mathbf{I}_N \otimes \tilde{S}^T) \\ H_{32} &= \mathbf{I}_N \otimes \left(e^{-2\alpha h}(\tilde{R} - \tilde{S}^T)\right) \\ H_{33} &= -\mathbf{I}_N \otimes \left(e^{-2\alpha h}(\tilde{Q} + \tilde{R})\right) \\ H_{41} &= (\tilde{\mathbf{I}}^T L_{ff}^{-T}) \otimes Y^T B^T \\ H_{44} &= -\mathbf{I}_M \otimes \tilde{\Psi}_1 + 8(\mathbf{I}_M \otimes \tilde{\Phi}) \\ H_{51} &= (\mathbf{I}_H L_{ff}^{-T}) \otimes \tilde{P} B^T \\ H_{55} &= -\mathbf{I}_M \otimes \tilde{\Psi}_2 \\ H_{66} &= -\frac{\pi^2}{4}(\mathbf{I}_N \otimes \tilde{W}) \\ H_{71} &= h(\mathbf{I}_N \otimes A\tilde{P}), \end{aligned}$$

$$\begin{aligned} H_{72} &= h(\mathbf{I}_N \otimes BY) \\ H_{74} &= h(L_{ff}^{-T}\tilde{\mathbf{I}} \otimes BY) \\ H_{75} &= h(L_{ff}^{-1}\mathbf{I}_H^T \otimes B\tilde{P}) \\ H_{77} &= \rho_1^2(\mathbf{I}_N \otimes \tilde{R}) - 2\rho_1(\mathbf{I}_N \otimes \tilde{P}) \\ H_{81} &= h(\mathbf{I}_N \otimes A\tilde{P}) \\ H_{82} &= h(\mathbf{I}_N \otimes BY) \\ H_{84} &= h(L_{ff}^{-T}\tilde{\mathbf{I}} \otimes BY) \\ H_{85} &= h(L_{ff}^{-1}\mathbf{I}_H^T \otimes B\tilde{P}) \\ H_{88} &= e^{-2\alpha h}\rho_2^2(\mathbf{I}_N \otimes \tilde{W}) \\ &\quad - 2e^{-2\alpha h}\rho_2(\mathbf{I}_N \otimes \tilde{P}). \end{aligned}$$

Then, the controller gain matrix K can be computed as $Y\tilde{P}^{-1}$, and the matrices Φ, Ψ_1 and Ψ_2 in the triggering conditions are obtained as $\tilde{P}^{-1}\tilde{\Phi}\tilde{P}^{-1}$, $\tilde{P}^{-1}\tilde{\Psi}_1\tilde{P}^{-1}$, and $\tilde{P}^{-1}\tilde{\Psi}_2\tilde{P}^{-1}$ respectively.

Proof. Consider the following Lyapunov functional candidate on the interval $t \in$

$[vh, (v+1)h)$

$$V(t) = V_1(t) + V_2(t) + V_3(t) + V_4(t, vh), \tag{6.29}$$

where

$$\begin{aligned}
V_1(t) &= \eta(t)^T(\mathbf{I}_N \otimes P)\eta(t), \\
V_2(t) &= \int_{t-h}^{t} e^{2\alpha(s-t)}\eta^T(s)(\mathbf{I}_N \otimes Q)\eta(s)ds, \\
V_3(t) &= h\int_{t-h}^{t}\int_{s}^{t} e^{2\alpha(v-t)}\dot{\eta}^T(v)(\mathbf{I}_N \otimes R)\dot{\eta}(v)dvds, \\
V_4(t, vh) &= h^2e^{2\alpha h}\int_{vh}^{t} e^{2\alpha(s-t)}\dot{\eta}^T(s)(\mathbf{I}_N \otimes W)\dot{\eta}(s)ds \\
&\qquad - \frac{\pi^2}{4}\int_{vh}^{t} e^{2\alpha(s-t)}\eta^T(s)(\mathbf{I}_N \otimes W)\eta(s)ds,
\end{aligned}$$

and $P, Q, R, W \in R^{n\times n}$ are symmetric positive definite matrices, and α is positive constant. Taking the time derivative of the Lyapunov functional candidate along the formation error dynamics (6.11) yields,

$$\begin{aligned}
\dot{V}_1 + 2\alpha V_1 &= \dot{\eta}^T(t)(\mathbf{I}_N \otimes P)\eta(t) + \eta(t)^T(\mathbf{I}_N \otimes P)\dot{\eta}(t) + 2\alpha\eta^T(t)(\mathbf{I}_N \otimes P)\eta(t) \\
&= \xi^T(t)\zeta^T(\mathbf{I}_N \otimes P)\eta(t) + \eta(t)^T(\mathbf{I}_N \otimes P)\eta\xi(t) + 2\alpha\eta^T(t)(\mathbf{I}_N \otimes P)\eta(t),
\end{aligned} \tag{6.30}$$

$$\begin{aligned}
\dot{V}_2 + 2\alpha V_2 &= \eta^T(t)(\mathbf{I}_N \otimes Q)\eta(t) - 2\alpha\int_{t-h}^{t} e^{2\alpha(s-t)}\eta^T(s)(\mathbf{I}_N \otimes Q)\eta(s)ds \\
&\quad - e^{-2\alpha h}\eta^T(t-h)(\mathbf{I}_N \otimes Q)\eta(t-h) + 2\alpha\int_{t-h}^{t} e^{2\alpha(s-t)}\eta^T(s)(\mathbf{I}_N \otimes Q)\eta(s)ds \\
&= \eta^T(t)(\mathbf{I}_N \otimes Q)\eta(t) - e^{-2\alpha h}\eta^T(t-h)(\mathbf{I}_N \otimes Q)\eta(t-h),
\end{aligned} \tag{6.31}$$

$$\begin{aligned}
\dot{V}_3 + 2\alpha V_3 &= -h\int_{t-h}^{t} e^{2\alpha(v-t)}\dot{\eta}^T(v)(\mathbf{I}_N \otimes R)\dot{\eta}(v)dv + h^2\dot{\eta}^T(t)(\mathbf{I}_N \otimes R)\dot{\eta}(t) \\
&\quad + \int_{t-h}^{t}\int_{s}^{t} \dot{\eta}^T(v)(\mathbf{I}_N \otimes R)\dot{\eta}(v)e^{2\alpha(v-t)}(-2\alpha)dvds \\
&\quad + 2\alpha\int_{t-h}^{t}\int_{s}^{t} \dot{\eta}^T(v)(\mathbf{I}_N \otimes R)\dot{\eta}(v)e^{2\alpha(v-t)}dvds \\
&= -h\int_{t-h}^{t} e^{2\alpha(v-t)}\dot{\eta}^T(v)(\mathbf{I}_N \otimes R)\dot{\eta}(v)dv + h^2\dot{\eta}^T(t)(\mathbf{I}_N \otimes R)\dot{\eta}(t),
\end{aligned} \tag{6.32}$$

$$\begin{aligned}\dot{V}_4 + 2\alpha V_4 = &-h^2 e^{2\alpha h}\int_{vh}^{t} 2\alpha e^{2\alpha(s-t)}\dot{\eta}^T(s)(\mathbf{I}_N \otimes W)\dot{\eta}(s)ds \\ &+ 2\alpha h^2 e^{2\alpha h}\int_{vh}^{t} e^{2\alpha(s-t)}\dot{\eta}^T(s)(\mathbf{I}_N \otimes W)\dot{\eta}(s)ds \\ &+ \frac{\pi^2}{4}\int_{vh}^{t} 2\alpha e^{2\alpha(s-t)}\bar{\eta}^T(s)(\mathbf{I}_N \otimes W)\bar{\eta}(s) + h^2 e^{2\alpha h}\dot{\eta}^T(t)(\mathbf{I}_N \otimes W)\dot{\eta}(t) \\ &- 2\alpha\frac{\pi^2}{4}\int_{vh}^{t} e^{2\alpha(s-t)}\bar{\eta}^T(s)(\mathbf{I}_N \otimes W)\bar{\eta}(s)ds - \frac{\pi^2}{4}\bar{\eta}^T(t)(\mathbf{I}_N \otimes W)\bar{\eta}(t) \\ = &\, h^2 e^{2\alpha h}\dot{\eta}^T(t)(\mathbf{I}_N \otimes W)\dot{\eta}(t) - \frac{\pi^2}{4}\bar{\eta}^T(t)(\mathbf{I}_N \otimes W)\bar{\eta}(t), \end{aligned} \tag{6.33}$$

where $\bar{\eta}(t) = \eta(t) - \eta(vh)$ and $\bar{\eta}(s) = \eta(s) - \eta(vh)$. Note that $e^{2\alpha(v-t)} \geq e^{2\alpha(t-h-t)} = e^{-2\alpha h}$, for $v \in [t-h, t]$, and by combining the results from Lemma 4.1, (6.32) can be enlarged as

$$\begin{aligned}\dot{V}_3 + 2\alpha V_3 &\leq -he^{-2\alpha h}\int_{t-h}^{t}\dot{\eta}^T(\upsilon)(\mathbf{I}_N \otimes R)\dot{\eta}(\upsilon)d\upsilon + h^2\dot{\eta}^T(t)(\mathbf{I}_N \otimes R)\dot{\eta}(t) \\ &\leq -he^{-2\alpha h}\big(- \phi_1^T(\mathbf{I}_N \otimes R)\phi_1 - \phi_2^T(\mathbf{I}_N \otimes R)\phi_2 - \phi_1^T(\mathbf{I}_N \otimes S)\phi_2 \\ &\quad - \phi_2^T(\mathbf{I}_N \otimes S^T)\phi_1\big) + h^2\dot{\eta}^T(t)(\mathbf{I}_N \otimes R)\dot{\eta}(t), \end{aligned} \tag{6.34}$$

given that $\phi_1 = \eta(t-\tau) - \eta(t)$, and $\phi_2 = \eta(t-h) - \eta(t-\tau)$ and there exists an arbitrary matrix S such that

$$\begin{bmatrix} R & * \\ S^T & R \end{bmatrix} \geq 0.$$

In addition, for $t \in [vh, (v+1)h)$ and from Lemma 6.1, we have

$$\begin{aligned} h^2 e^{2\alpha h}&\int_{vh}^{t} e^{2\alpha(s-t)}\dot{\eta}^T(s)(\mathbf{I}_N \otimes W)\dot{\eta}(s)ds \\ &\geq (t-vh)^2 e^{2\alpha(t-vh)}\int_{vh}^{t} e^{2\alpha(s-t)}\dot{\eta}^T(s)(\mathbf{I}_N \otimes W)\dot{\eta}(s)ds \\ &\geq \frac{\pi^2}{4}\int_{vh}^{t} e^{2\alpha(s-t)}\eta^T(s)(\mathbf{I}_N \otimes W)\eta(s)ds, \end{aligned}$$

which implies $V_4 \geq 0$, and therefore V is a valid Lyapunov candidate. Moreover, V_4 vanishes at each sampling instant, therefore $V_4(vh^-) \geq V_4(vh)$ and $V(vh^-) \geq V(vh)$.

Defining $\bar{\xi}$ and $\bar{\zeta}$ as

$$\bar{\xi}(t) = \begin{bmatrix} \eta(t)^T & \eta(t-\tau)^T & \eta(t-h)^T & \mathbf{e}(t-\tau)^T & \bar{\mathbf{e}}(t-\tau)^T & \bar{\eta}^T(t) \end{bmatrix}^T, \tag{6.35}$$

$$\bar{\zeta} = \begin{bmatrix} \mathbf{I}_N \otimes A & \mathbf{I}_N \otimes BK & 0 & L_{ff}^{-1}\tilde{\mathbf{I}} \otimes BK & L_{ff}^{-1}\mathbf{I}_H^T \otimes B & 0 \end{bmatrix}, \tag{6.36}$$

and combining the results from (6.30), (6.31), (6.33), and (6.34) yields

$$\dot{V} + 2\alpha V \leq \bar{\xi}^T(t)\big(\bar{\zeta}(\mathbf{I}_N \otimes R)\bar{\zeta} + h^2 e^{2\alpha h}\bar{\zeta}(\mathbf{I}_N \otimes W)\bar{\zeta}\big)\bar{\xi}(t) + \bar{\xi}^T(\Omega + \hat{\Omega} + \bar{\Omega} + \tilde{\Omega})\bar{\xi}, \tag{6.37}$$

where

$$\Omega = \begin{bmatrix} \mathbf{I}_N \otimes (PA + A^TP + 2\alpha P) & * & * & * & * & * \\ \mathbf{I}_N \otimes (K^TB^TP) & 0 & * & * & * & * \\ 0 & 0 & 0 & * & * & * \\ (\tilde{\mathbf{I}}^T L_{ff}^{-T}) \otimes (K^TB^TP) & 0 & 0 & 0 & * & * \\ (\mathbf{I}_H L_{ff}^{-T}) \otimes (B^TP) & 0 & 0 & 0 & 0 & * \\ 0 & 0 & 0 & 0 & 0 & 0 \end{bmatrix},$$

$$\hat{\Omega} = \begin{bmatrix} \mathbf{I}_N \otimes Q & * & * & * & * & * \\ 0 & 0 & * & * & * & * \\ 0 & 0 & -e^{-2\alpha h}(\mathbf{I}_N \otimes Q) & * & * & * \\ 0 & 0 & 0 & 0 & * & * \\ 0 & 0 & 0 & 0 & 0 & * \\ 0 & 0 & 0 & 0 & 0 & 0 \end{bmatrix},$$

$$\bar{\Omega} = \begin{bmatrix} -e^{2\alpha h}(\mathbf{I}_N \otimes R) & * & * & * & * & * \\ e^{-2\alpha h}\mathbf{I}_N \otimes (R - S^T) & e^{2\alpha h}\mathbf{I}_N \otimes (-2R + S + S^T) & * & * & * & * \\ e^{-2\alpha h}(\mathbf{I}_N \otimes S^T) & e^{-2\alpha h}\mathbf{I}_N \otimes (R - S^T) & -e^{-2\alpha h}(\mathbf{I}_N \otimes R) & * & * & * \\ 0 & 0 & 0 & 0 & * & * \\ 0 & 0 & 0 & 0 & 0 & * \\ 0 & 0 & 0 & 0 & 0 & 0 \end{bmatrix},$$

and

$$\tilde{\Omega} = \begin{bmatrix} 0 & * & * & * & * & * \\ 0 & 2(\mathbf{I}_{inc}^T \mathbf{I}_{inc} \otimes \Phi) & * & * & * & * \\ 0 & 0 & 0 & * & * & * \\ 0 & 0 & 0 & -\mathbf{I}_M \otimes \Psi_1 + 8(\mathbf{I}_M \otimes \Phi) & * & * \\ 0 & 0 & 0 & 0 & -\mathbf{I}_M \otimes \Psi_2 & * \\ 0 & 0 & 0 & 0 & 0 & -\frac{\pi^2}{4}(\mathbf{I}_N \otimes W) \end{bmatrix}.$$

We now define

$$\Xi = h^2 \bar{\zeta}(\mathbf{I}_N \otimes R)\bar{\zeta} + h^2 e^{2\alpha h} \bar{\zeta}(\mathbf{I}_N \otimes W)\bar{\zeta} + \Omega + \hat{\Omega} + \bar{\Omega} + \tilde{\Omega}. \tag{6.38}$$

It is clear that when $\Xi < 0$, we have $\dot{V} + 2\alpha V \leq 0$ for $t \in [vh, (v+1)h)$, where v is a non-negative integer. In addition, since V_1, V_2, V_3 are continuous and the discontinuous term V_4 does not grow at each sampling instant (in fact, V_4 vanishes), the Lyapunov functional candidate V does not grow at sampling instants, that is $\lim_{t \to vh^-} V(t) \geq V(vh)$. Therefore, by the Comparison Lemma [96],

$$V(t) \leq V(vh) e^{-2\alpha(t-vh)}, \; \forall t \in [vh, (v+1)h)\,. \tag{6.39}$$

By repeatedly applying (6.39), we have

$$\begin{aligned} V(t) &\leq V(vh) e^{-2\alpha(t-vh)} \leq V(vh^-) e^{-2\alpha(t-vh)} \\ &\leq V((v-1)h) e^{-2\alpha(vh-(v-1)h)} e^{-2\alpha(t-vh)} \\ &\leq V((v-1)h^-) e^{-2\alpha(vh-(v-1)h)} e^{-2\alpha(t-vh)} \leq \cdots \leq V(0) e^{-2\alpha t}. \end{aligned} \tag{6.40}$$

A schematic illustration of the steps used to obtain (6.40) is given in Fig. 6.2. From the definition of the Lyapunov functional candidate (6.29), we have

$$\|\eta(t)\| \leq \frac{e^{-\alpha t}}{\lambda_{min}(P)} \sqrt{V(0)}, \tag{6.41}$$

where $\lambda_{min}(\cdot)$ denotes the minimum eigenvalue of a matrix. If we further assume that the formation error function $\eta(t)$ is bounded and its first order derivatives are

square integrable on the interval $[-h, 0)$, then it can be shown that $\sqrt{V(0)}$ is finite. Therefore, $\|\eta(t)\|$ converges to the origin (system converges to the desired formation) at an exponential convergence rate of α.

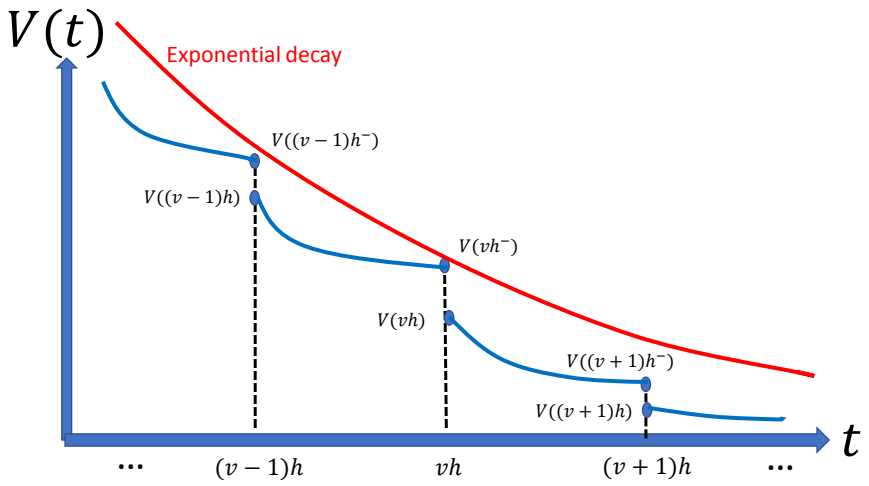

Figure 6.2: A schematic illustration of the steps in (6.40)

It remains to show that (6.28) implies $\Xi < 0$. To proceed, it can be shown by repeatedly applying Lemma 2.4 that $\Xi < 0$ is equivalent to

$$\begin{bmatrix} \Omega + \hat{\Omega} + \bar{\Omega} + \tilde{\Omega} & * & * \\ h(\mathbf{I}_N \otimes R)\bar{\zeta} & -\mathbf{I}_N \otimes R & * \\ h(\mathbf{I}_N \otimes W)\bar{\zeta} & 0 & -e^{-2\alpha h}(\mathbf{I}_N \otimes W) \end{bmatrix} < 0. \tag{6.42}$$

We pre- and post-multiply the inequality (6.42) by the non-singular matrix $diag\{\mathbf{I}_N \otimes \tilde{P}, \mathbf{I}_N \otimes \tilde{P}, \mathbf{I}_N \otimes \tilde{P}, \mathbf{I}_M \otimes \tilde{P}, \mathbf{I}_M \otimes \tilde{P}, \mathbf{I}_N \otimes \tilde{P}, \mathbf{I}_N \otimes R^{-1}, \mathbf{I}_N \otimes W^{-1}\}$, where $\tilde{P} = P^{-1}$. In addition, define $\tilde{Q} = \tilde{P}Q\tilde{P}$. $\tilde{R}, \tilde{S}, \tilde{\Psi}_1, \tilde{\Psi}_2, \tilde{\Phi}, \tilde{W}$ are defined analogously. Then, the inequality (6.42) is equivalent to

$$\begin{bmatrix} \breve{\Omega} & * & * \\ h\bar{\zeta}(\mathbf{I}_N \otimes \tilde{P}) & -(\mathbf{I}_N \otimes R)^{-1} & * \\ h\bar{\zeta}(\mathbf{I}_N \otimes \tilde{P}) & 0 & -e^{-2\alpha h}(\mathbf{I}_N \otimes W)^{-1} \end{bmatrix} < 0, \tag{6.43}$$

where

$$
\begin{aligned}
\breve{\Omega}_{11} &= \mathbf{I}_N \otimes (\tilde{P}A^T + A\tilde{P} + \tilde{Q} - \tilde{R} + 2\alpha\tilde{P} - e^{-2\alpha h}\tilde{R}) \\
\breve{\Omega}_{21} &= \mathbf{I}_N \otimes (\tilde{P}K^T B^T + e^{-2\alpha h}(\tilde{R} - \tilde{S}^T)) \\
\breve{\Omega}_{22} &= \mathbf{I}_N \otimes \left(e^{-2\alpha h}(-2\tilde{R} + \tilde{S} + \tilde{S}^T)\right) + 2(\mathbf{I}_{inc}^T \mathbf{I}_{inc} \otimes \tilde{\Phi}) \\
\breve{\Omega}_{31} &= e^{-2\alpha h}(\mathbf{I}_N \otimes \tilde{S}^T) \\
\breve{\Omega}_{32} &= \mathbf{I}_N \otimes \left(e^{-2\alpha h}(\tilde{R} - \tilde{S}^T)\right) \\
\breve{\Omega}_{33} &= -\mathbf{I}_N \otimes \left(e^{-2\alpha h}(\tilde{Q} + \tilde{R})\right) \\
\breve{\Omega}_{41} &= (\tilde{\mathbf{I}}^T L_{ff}^{-T}) \otimes \tilde{P}K^T B^T \\
\breve{\Omega}_{44} &= -\mathbf{I}_M \otimes \tilde{\Psi}_1 + 8(\mathbf{I}_M \otimes \tilde{\Phi}) \\
\breve{\Omega}_{51} &= (\mathbf{I}_H L_{ff}^{-T}) \otimes \tilde{P}B^T \\
\breve{\Omega}_{55} &= -\mathbf{I}_M \otimes \tilde{\Psi}_2 \\
\breve{\Omega}_{66} &= -\frac{\pi^2}{4}(\mathbf{I}_N \otimes \tilde{W}),
\end{aligned}
$$

and $\breve{\Omega}_{ij} = 0$ if not specified. Moreover, from Lemma 2.5 we have

$$
\begin{aligned}
-\mathbf{I}_N \otimes R^{-1} &\leq \rho_1^2 \mathbf{I}_N \otimes \tilde{R} - 2\rho_1(\mathbf{I}_N \otimes \tilde{P}), \\
-\mathbf{I}_N \otimes W^{-1} &\leq \rho_2^2 \mathbf{I}_N \otimes \tilde{W} - 2\rho_2(\mathbf{I}_N \otimes \tilde{P}),
\end{aligned}
$$

for any positive constants ρ_1, and ρ_2. Therefore, it is sufficient to ensure $\Xi < 0$ if

$$
\begin{bmatrix}
\breve{\Omega} & * & * \\
h\bar{\zeta}(\mathbf{I}_N \otimes \tilde{P}) & \rho_1^2 \mathbf{I}_N \otimes \tilde{R} - 2\rho_1(\mathbf{I}_N \otimes \tilde{P}) & * \\
h\bar{\zeta}(\mathbf{I}_N \otimes \tilde{P}) & 0 & e^{-2\alpha h}\rho_2^2(\mathbf{I}_N \otimes \tilde{W} - 2\rho_2(\mathbf{I}_N \otimes \tilde{P}))
\end{bmatrix} < 0. \tag{6.44}
$$

Clearly, (6.44) is equivalent to (6.28) by denoting $Y = K\tilde{P}$. □

Remark 6.1. *Note that if we choose $\alpha = 0$ and exclude the Lapunov functional term V_4, the LMI conditions in Theorem 6.2 are equivalent to that in Theorem 6.1. Therefore, Theorem 6.2 is more general than Theorem 6.1. In addition, the inclusion of the positive constant α in Theorem 6.2 provides explicit knowledge about the convergence speed of the system.*

Remark 6.2. *Although more decision variables (increasing complexity) are introduced from the inclusion of the discontinuous Lyapunov functional V_4, less conservative conditions (allowing for larger sampling intervals) can often be derived [97], [98].*

Note that a small positive number ϵ^2 can usually be introduced in the triggering function to reduce the numbers of unnecessary triggers. In this case, the triggering function (6.12) can be modified as

$$f_{ij}(vh) = \mathbf{e}_{ij}^T(vh)\Phi_1\mathbf{e}_{ij}(vh) + \bar{\mathbf{e}}_{ij}^T(vh)\Phi_2\bar{\mathbf{e}}_{ij}(vh) - \tilde{\eta}_{ij}(vh)^T\Psi\tilde{\eta}_{ij}(vh) - \epsilon^2. \tag{6.45}$$

Theorem 6.3. *Under the control law (6.2) and the edge-triggered communication regulation condition (6.45), the system (5.1) exponentially converges to a neighborhood of the desired formation with a convergence rate of α if all the conditions stated in Theorem 6.2 are satisfied. In addition, the neighborhood is defined by $\{\eta \in \mathcal{R}^{Nn} | \|\eta\| \leq \sqrt{\frac{M}{2\alpha\lambda_{min}(P)}}\epsilon\}$.*

Proof. From the triggering function (6.45) and the triggering rule (6.20), we have

$$\begin{aligned} &2\eta(t-\tau)^T\big(\mathbf{I}_{inc}^T\mathbf{I}_{inc}\otimes\Psi\big)\eta(t-\tau) - \mathbf{e}^T(t-\tau)(\mathbf{I}_M\otimes\Phi_1)\mathbf{e}(t-\tau) \\ &\quad - \bar{\mathbf{e}}^T(t-\tau)(\mathbf{I}_M\otimes\Phi_2)\bar{\mathbf{e}}(t-\tau) + 8\mathbf{e}^T(t-\tau)(\mathbf{I}_M\otimes\Psi)\mathbf{e}(t-\tau) + M\epsilon^2 \geq 0. \end{aligned} \tag{6.46}$$

We propose the same Lyapunov function as in (6.29) and follow the proof of Theorem 6.2. It can be verified that if the LMI conditions in (6.28) are satisfied, we have

$$\dot{V}(t) + 2\alpha V(t) \leq M\epsilon^2, \ \ \forall t \in [vh, (v+1)h)\,. \tag{6.47}$$

By the Comparison Lemma [96], for $t \in [vh, (v+1)h)$

$$\begin{aligned} V(t) &\leq (V(vh) - \frac{M\epsilon^2}{2\alpha})e^{-2\alpha(t-vh)} + \frac{M\epsilon^2}{2\alpha} \\ &\leq V(vh^-)e^{-2\alpha(t-vh)} - \frac{M\epsilon^2}{2\alpha}e^{-2\alpha(t-vh)} + \frac{M\epsilon^2}{2\alpha}. \end{aligned} \tag{6.48}$$

Then by applying (6.47) on the interval $[(v-1)h, vh^-]$, we have

$$V(vh^-) \leq (V((v-1)h) - \frac{M\epsilon^2}{2\alpha})e^{-2\alpha(vh^- - (v-1)h)} + \frac{M\epsilon^2}{2\alpha}. \tag{6.49}$$

Substitute (6.49) into (6.48) to obtain,

$$\begin{aligned} V(t) &\leq V((v-1)h)e^{-2\alpha(vh^- -(v-1)h)}e^{-2\alpha(t-vh)} - \frac{M\epsilon^2}{2\alpha}e^{-2\alpha(vh^- -(v-1)h)}e^{-2\alpha(t-vh)} \\ &\quad + \frac{M\epsilon^2}{2\alpha}e^{-2\alpha(t-vh)} - \frac{M\epsilon^2}{2\alpha}e^{-2\alpha(t-vh)} + \frac{M\epsilon^2}{2\alpha} \\ &= V((v-1)h)e^{-2\alpha(t-(v-1)h)} - \frac{M\epsilon^2}{2\alpha}e^{-2\alpha(t-(v-1)h)} + \frac{M\epsilon^2}{2\alpha} \\ &\leq V((v-1)h^-)e^{-2\alpha(t-(v-1)h)} - \frac{M\epsilon^2}{2\alpha}e^{-2\alpha(t-(v-1)h)} + \frac{M\epsilon^2}{2\alpha}. \end{aligned} \tag{6.50}$$

Again, from applying (6.47) on the interval $[(v-2)h, (v-1)h^-]$, we have

$$V((v-1)h^-) \leq (V((v-2)h) - \frac{M\epsilon^2}{2\alpha})e^{-2\alpha((v-1)h^- -(v-2)h)} + \frac{M\epsilon^2}{2\alpha}. \tag{6.51}$$

We then substitute (6.51) into (6.50) to obtain

$$V(t) \leq V((v-2)h^-)e^{-2\alpha(t-(v-2)h)} - \frac{M\epsilon^2}{2\alpha}e^{-2\alpha(t-(v-2)h)} + \frac{M\epsilon^2}{2\alpha}. \tag{6.52}$$

Then, by repeating the same procedures from above for intervals $[(v-3)h, (v-2)h^-]$, $[(v-4)h, (v-3)h^-]$, $\cdots$, $[0, h^-]$, we can conclude that

$$V(t) \leq V(0)e^{-2\alpha t} - \frac{M\epsilon^2}{2\alpha}e^{-2\alpha t} + \frac{M\epsilon^2}{2\alpha}. \tag{6.53}$$

Follow the discussions below (6.41), we have a finite $V(0)$. In addition, since $V(t) \geq \lambda_{min}(P)\|\eta(t)\|^2$, thus

$$\lambda_{min}(P)\|\eta(t)\|^2 \leq V(0)e^{-2\alpha t} - \frac{M\epsilon^2}{2\alpha}e^{-2\alpha t} + \frac{M\epsilon^2}{2\alpha}, \tag{6.54}$$

which reveals that $\|\eta(t)\|$ is ultimately bounded with an ultimate bound of $\sqrt{\frac{M}{2\lambda_{min}(P)\alpha}}\epsilon$. □

Remark 6.3. *Large α gives a faster convergence rate and implies a smaller neighborhood of the desired formation; however, it introduces more positive definiteness to the term H_{11} in the LMI conditions (6.28), which can potentially render the LMI conditions infeasible (so that no feasible controllers can be obtained). Therefore, there is a trade-off between choosing large α values (better performance) and guaranteeing*

the existence of feasible controllers.

6.4 Simulation Results

In this section, the proposed edge-state-based controller (6.2) and event generator (6.20) with the gains computed from evaluating (6.28) are applied in numerical simulations to a group of four networked (one leader and three followers) linearized mobile robots under the topology shown in Fig. 6.3. The formation vectors are chosen as $f_1 = \begin{bmatrix} 1 & 0 \end{bmatrix}^T$, $f_2 = \begin{bmatrix} -0.7 & 0.7 \end{bmatrix}^T$, and $f_3 = \begin{bmatrix} -0.7 & -0.7 \end{bmatrix}^T$. In all simulations, the sampling frequency is 10 Hz and the triggering threshold ϵ is selected as 0.0005, and the virtual leader moves at a constant speed of 0.3 m/s in the X-direction from the origin. The parameters ρ_1, ρ_2, and α in (6.28) are optimized using the methods discussed in Section 4.2 as $\rho_1 = 0.7348$, $\rho_2 = 0.0094$, and $\alpha = 0.1541$. The control gain matrix K and edge event generator gain matrices Φ_1, Φ_2 and Ψ are then computed as

$$K = \begin{bmatrix} -0.9121 & 0 \\ 0 & -0.9121 \end{bmatrix}, \Phi = \begin{bmatrix} 0.0002 & 0 \\ 0 & 0.0002 \end{bmatrix},$$

$$\Psi_1 = \begin{bmatrix} 0.2391 & 0 \\ 0 & 0.2391 \end{bmatrix}, \Psi_2 = \begin{bmatrix} 0.4645 & 0 \\ 0 & 0.4645 \end{bmatrix}.$$

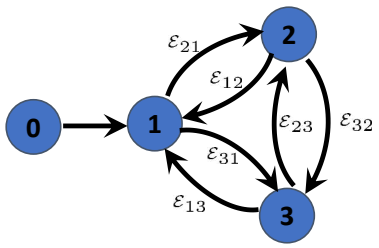

Figure 6.3: A leader-follower communication topology with edges labeled

In a 20 *sec* simulation run, Fig. 6.4 shows the simulated evolution of all agents. Fig. 6.5 illustrates the formation error profiles of all agents in the X- and Y-directions, which clearly shows that a solution to Research Problem 2.2 has been achieved using the newly-proposed edge-state based formation controller and event generator. The snapshots of the group formation in the X-Y plane at t = 0 sec, 6.6 sec, 13.3 sec,

and 20 sec are depicted in Fig. 6.6, which also demonstrates the achievement of the desired group formation. Fig. 6.7 demonstrates the communication instants of each communication edge over the span of the simulation. It can be observed that all the edges tend to trigger less frequently (with less communication events after $t = 10\,sec$) as the system approaches the desired group formation. In addition, the average communication triggering percentage on edges $\mathcal{E}_{12}$, $\mathcal{E}_{13}$, $\mathcal{E}_{21}$, $\mathcal{E}_{23}$, $\mathcal{E}_{31}$, $\mathcal{E}_{32}$ are computed as 56%, 56%, 14%, 14%, 56%, and 56%, respectively.

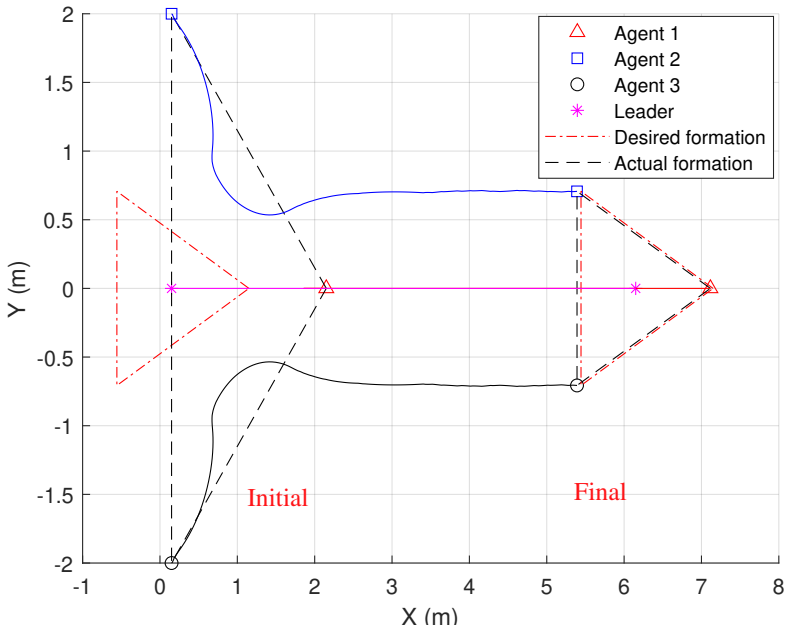

Figure 6.4: Simulation results of the formation evolution of the system (5.1) under edge-triggered ECM

6.4.1 Feasibility Region Analysis

As discussed in Remark 6.3, a large α (fast convergence) can potentially cause the LMI condition in (6.28) to be infeasible (so that no controller and event generator exist). Therefore, the author investigated the feasible regions spanned by the parameters ρ_1, ρ_2, and α. In the following, the conditions in (6.28) are tested for the region specified by $\rho_1, \rho_2, \alpha \in [0, 2]$ with a resolution of 0.1 in all directions. Fig. 6.8 shows the 3-D feasibility region (yellow region) over the specified testing region. It can be observed that the LMI conditions in (6.28) tend to be less feasible (blue region) as α grows larger regardless of the values in ρ_1 and ρ_2. Fig. 6.9 shows the feasible region over ρ_1

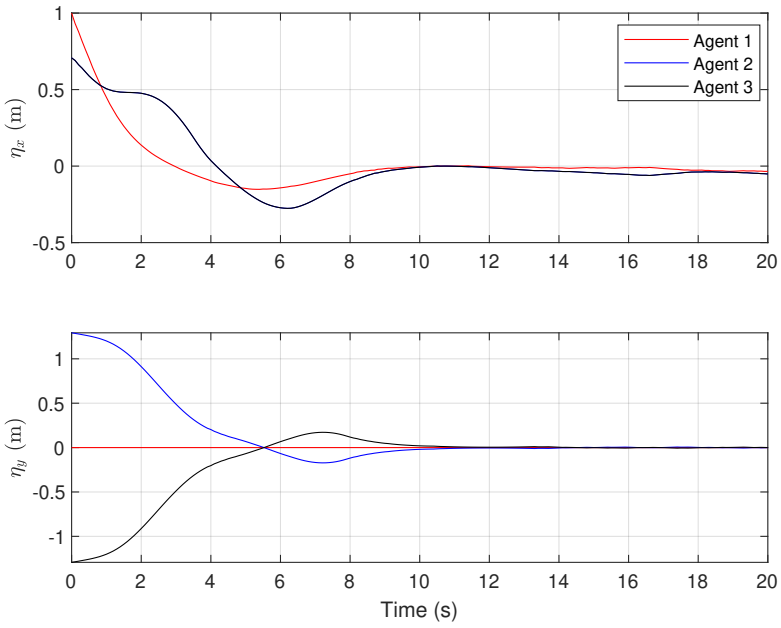

Figure 6.5: Simulation results of the formation error profile of the system (5.1) under edge-triggered ECM

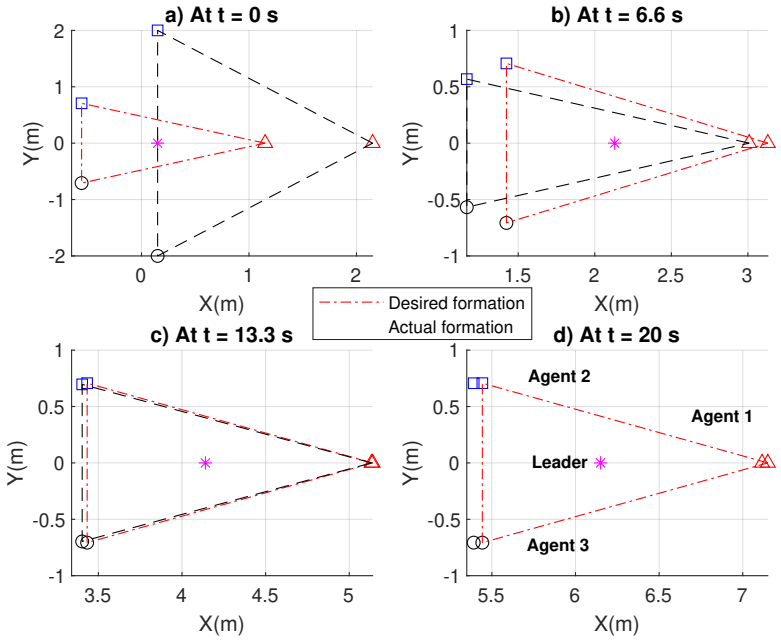

Figure 6.6: Simulation results of snapshots of the system (5.1) under edge-triggered ECM in the X-Y plane at: a) t=0 *sec*, b) t=4.6 *sec*, c) t=9.3 *sec*, d) t=14 *sec*

and ρ_2 when α is fixed at 1. It is tempting to conclude that (6.28) is feasible for any $\rho_2 > 0$ given that $\alpha = 1$ and $\rho_1 > 0.9$. Nevertheless, supplementary tests reveal that

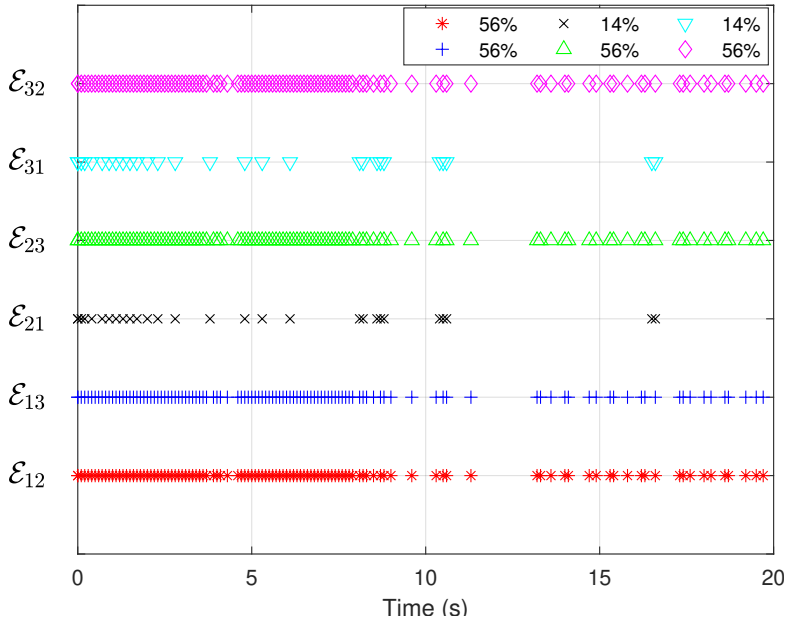

Figure 6.7: Simulation results of triggering instants of the system (5.1) under edge-triggered ECM

(6.28) can become infeasible with either large ρ_1 or large ρ_2.

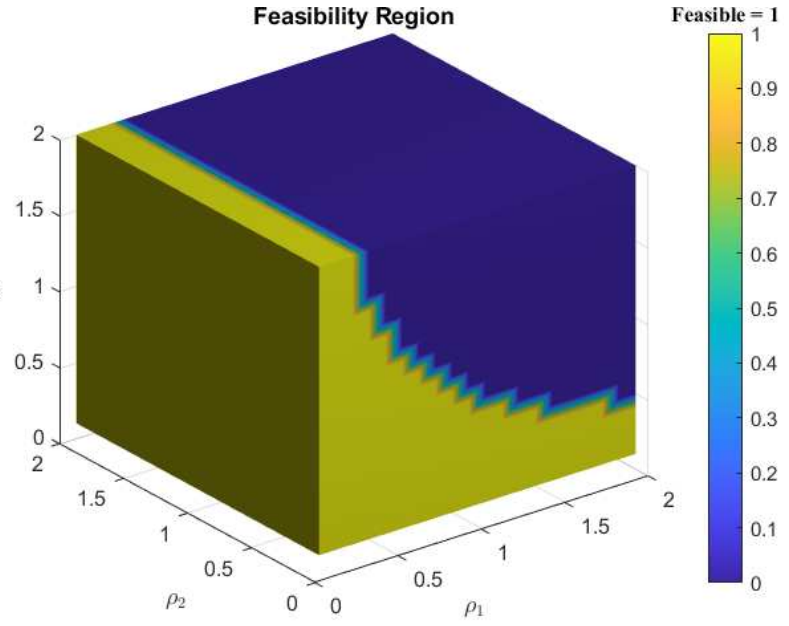

Figure 6.8: Feasibility region of (6.28) over $\rho_1, \rho_2, \alpha \in [0, 2]$

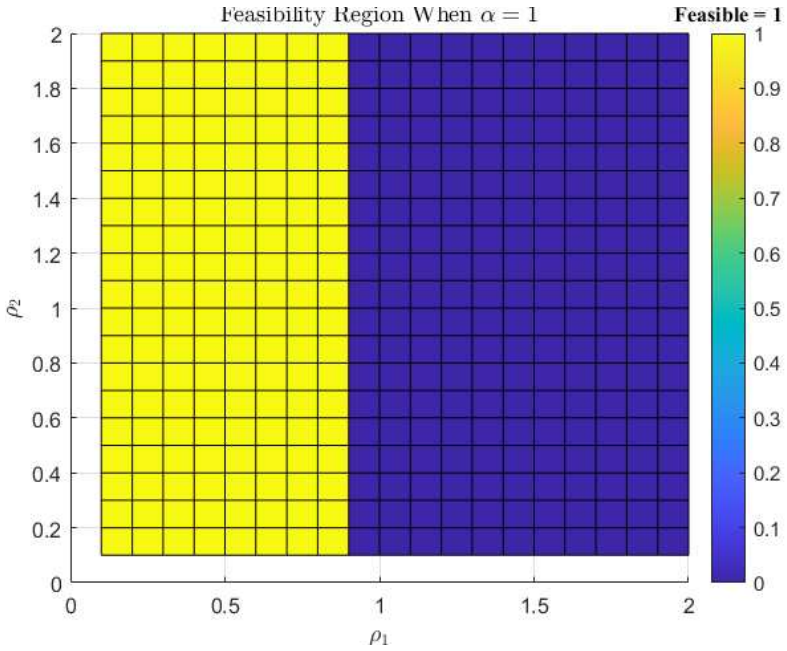

Figure 6.9: Feasibility region of (6.28) over $\rho_1, \rho_2 \in [0, 2]$ when $\alpha = 1$

6.4.2 Effect of Communication Mechanisms

Extensive simulations were carried out by the author to study the effect of different communication mechanisms. Table 6.1 summarizes the simulation results of triggering percentages of all communication edges in Fig. 6.3 under estimate-error-based ECM, state-error-based ECM, and PCM, while Table 6.2 summarizes the corresponding formation error l_2 norms. It is evident that, among these three ECMs, the proposed edge-triggered estimated-error-based ECM demands the least amount of triggering on all edges while still being able to produce comparable formation performance.

Table 6.1: Simulation results of triggering percentage (%) of edges in Fig. 6.3 under three ECMs

Mechanisms	$\mathcal{E}_{12}$	$\mathcal{E}_{13}$	$\mathcal{E}_{21}$	$\mathcal{E}_{23}$	$\mathcal{E}_{31}$	$\mathcal{E}_{32}$
Estimate-error-based ECM	56	56	14	56	14	56
State-error-based ECM	62	62	58	60	58	60
PCM	100	100	100	100	100	100

Table 6.2: Simulation results of l_2 norm (m) of formation error of system (5.1) under three ECMs

Mechanisms	Agent 1	Agent 2	Agent 3
Estimate-error-based ECM	0.86	2.13	2.13
State-error-based ECM	0.82	2.10	2.10
PCM	0.82	2.11	2.11

6.4.3 Effect of Triggering Threshold ϵ

To study the effects of the triggering threshold and to compare with the node-triggered ECM from Chapter 5, the control and event generator from the node-triggered case has been applied to the simulations with edge-triggered ECMs for threshold values from 0.0005 to 1. To quantify the communication usages, we define a communication event as communication between any of two neighboring agents. For instance, one trigger on the edge $\mathcal{E}_{21}$ in Fig. 6.3 counts for one communication event, whereas one trigger on the node 1 counts for two communication events (since the communication event is broadcast to two neighbors). Table 6.3 summarizes the total communication events for system (5.1) under edge-triggered ECM and node-triggered ECM with respect to different triggering thresholds, and (6.4) summarizes the corresponding formation error l_2 norms. Simulation results show that large triggering thresholds can generally reduce the number of communication events at the cost of performance using both ECMs. In addition, it can be observed that, under the same simulation conditions, the proposed edge-based triggering algorithm generally generates fewer triggering events than the node-based triggering algorithms while maintaining comparable performances over the span of the simulation.

Table 6.3: Simulation results of total communication events in system (5.1) under edge-triggered ECM and node-triggered ECM with respect to different triggering thresholds

Mechanisms	For threshold ϵ=				
	0.0005	0.001	0.01	0.1	1
Edge-triggered ECM	412	398	272	192	222
Node-triggered ECM	608	524	316	244	256

Table 6.4: Simulation results of l_2 norm of formation error of system (5.1) under edge-triggered ECM and node-triggered ECM with respect to different triggering thresholds

Mechanisms	For threshold $\epsilon=$				
	0.0005	0.001	0.01	0.1	1
Edge-triggered ECM	3.14	3.17	3.23	3.41	6.53
Node-triggered ECM	3.22	3.20	3.32	4.45	5.59

6.5 Experimental Results

Experimental validation was conducted using the edge-triggered estimate-error-based ECM, the state-error-based ECM, and the PCM, on the same setup as in Section 4.3. The system evolution, formation error profile, group formation snapshots, and edge triggering instants for the Pioneer robot system under the edge-triggered estimate-error-based ECM, the state-error-based ECM, and the PCM are shown in Figs. 6.10 to 6.13, Figs. 6.14 to 6.17, and Figs. 6.18 to 6.21, respectively. It is observed that the solution to Research Problem 2.2 can be achieved under all three ECMs. Moreover, Table 6.5 summarizes the experimental results of the triggering percentages of all communication edges under these three ECMs, and Table 6.6 summarizes the corresponding experimental results of the formation error l_2 norms. It can be concluded from the experimental results that, with similar formation performances, the proposed edge-triggered ECM in this chapter demands the least amount of communication resources (matching the observations from simulations) among the three ECMs.

Table 6.5: Experimental results of triggering percentage (%) of edges in Fig. 6.3 under three ECMs

Mechanisms	$\mathcal{E}_{12}$	$\mathcal{E}_{13}$	$\mathcal{E}_{21}$	$\mathcal{E}_{23}$	$\mathcal{E}_{31}$	$\mathcal{E}_{32}$
Estimate-error-based ECM	43	45	16	43	16	41
State-error-based ECM	77	74	62	71	62	74
PCM	100	100	100	100	100	100

Table 6.6: Experimental results of l_2 norm (m) of the formation error of the system (5.1) under three ECMs

Mechanisms	Agent 1	Agent 2	Agent 3
Estimate-error-based ECM	1.01	2.19	2.21
State-error-based ECM	1.02	2.19	2.21
PCM	0.99	2.16	2.18

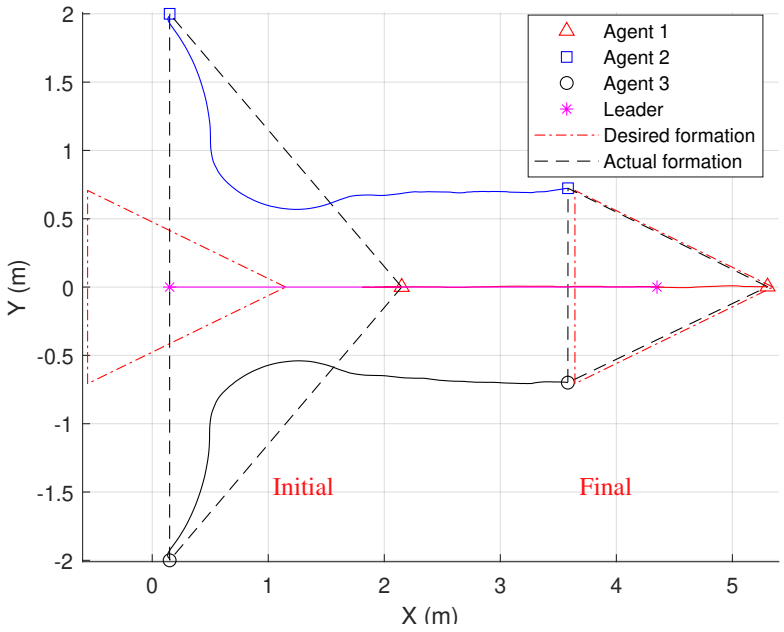

Figure 6.10: Experimental results of formation evolution of system (5.1) under the edge-triggered estimate-error-based ECM

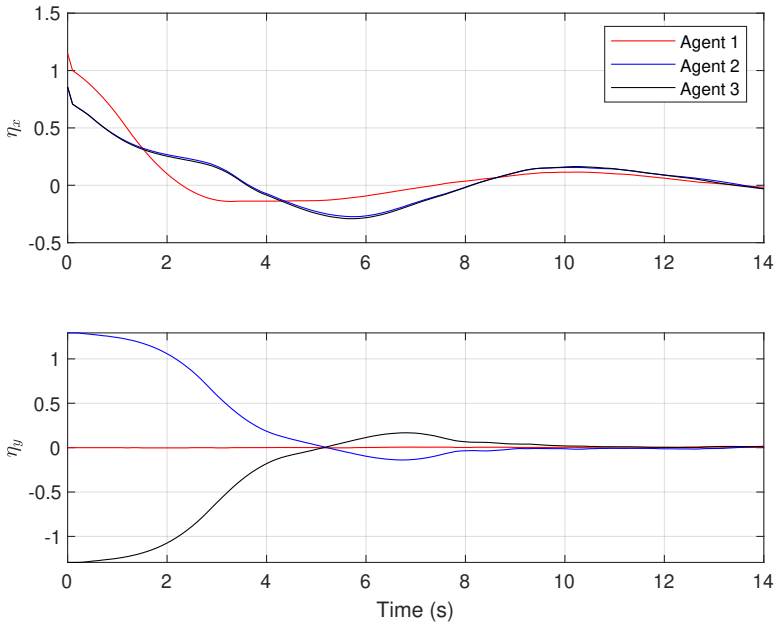

Figure 6.11: Experimental results of the formation error system (5.1) under the edge-triggered estimate-error-based ECM

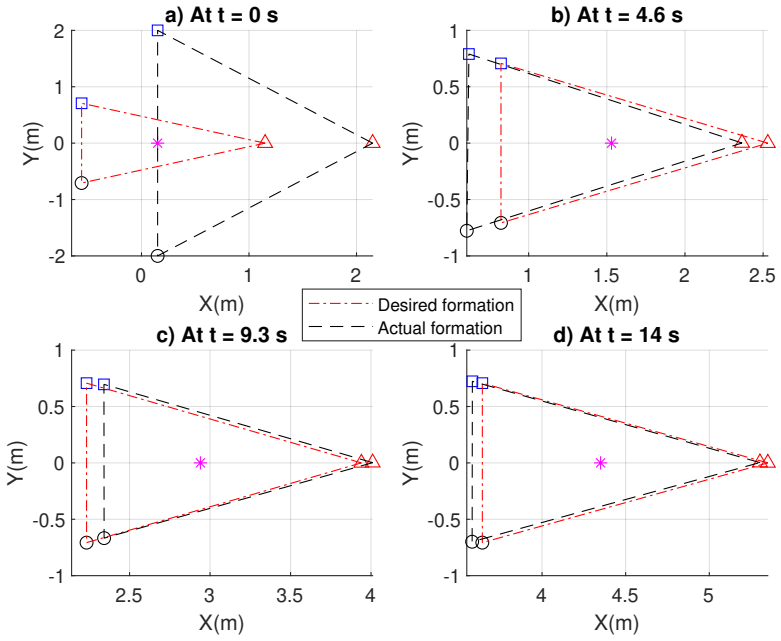

Figure 6.12: Experimental results of snapshots of the system (5.1) under edge-triggered estimate-error-based ECM in the X-Y plane at: a) t=0 *sec*, b) t=4.6 *sec*, c) t=9.3 *sec*, d) t=14 *sec*

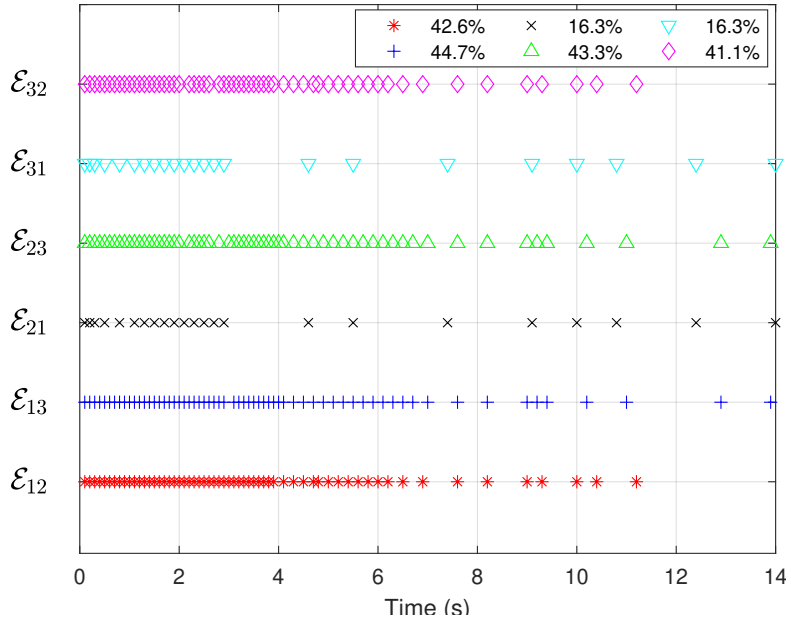

Figure 6.13: Experimental results of triggering instants of the system (5.1) under the edge-triggered estimate-error-based ECM

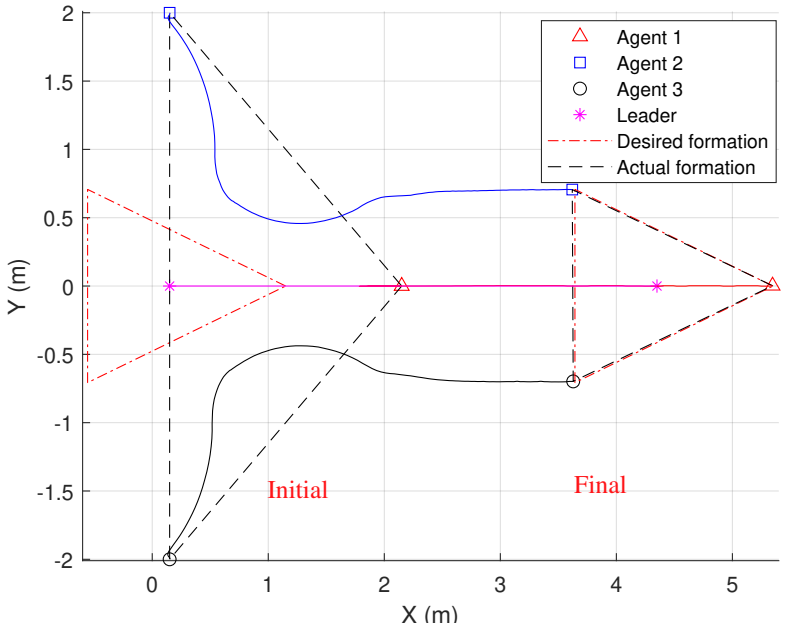

Figure 6.14: Experimental results of the formation evolution of the system (5.1) under the edge-triggered state-error-based ECM

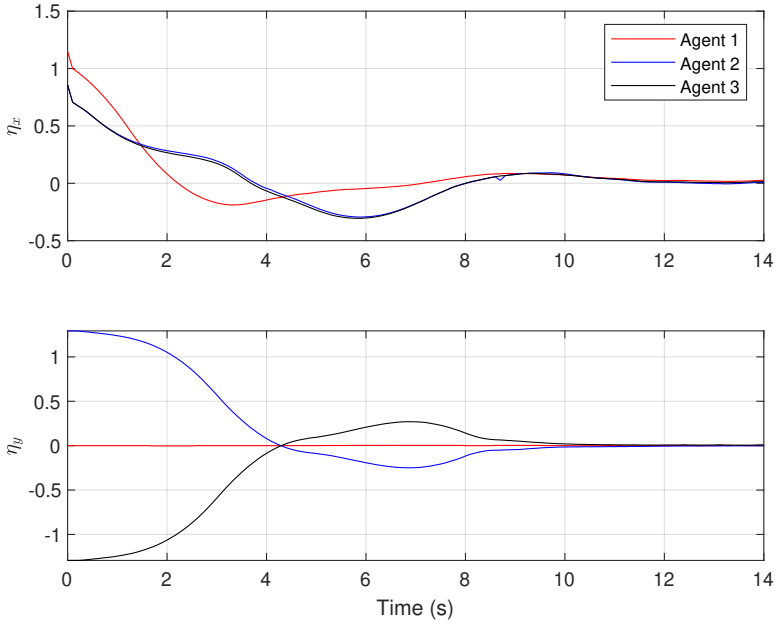

Figure 6.15: Experimental results of the formation error of the system (5.1) under the edge-triggered state-error-based ECM

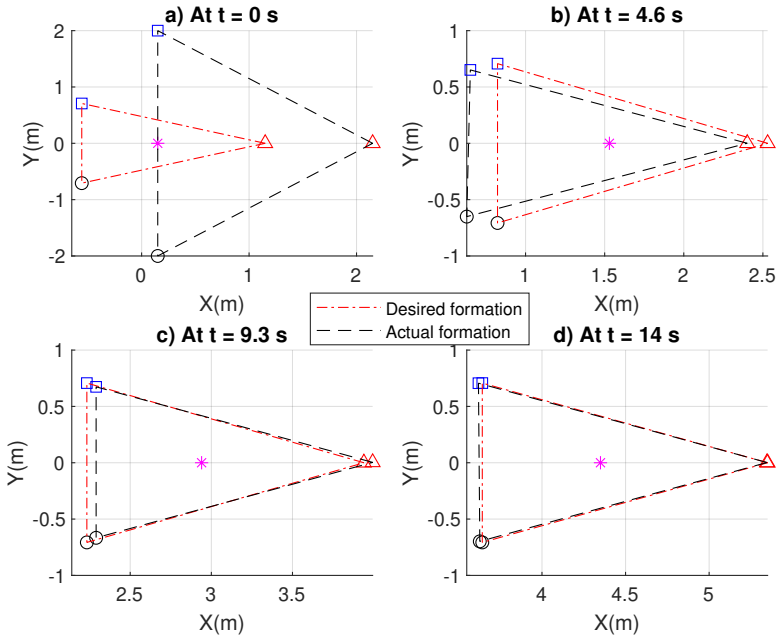

Figure 6.16: Experimental results of snapshots of the system (5.1) under the edge-triggered state-error-based ECM in the X-Y plane at: a) t=0 *sec*, b) t=4.6 *sec*, c) t=9.3 *sec*, d) t=14 *sec*

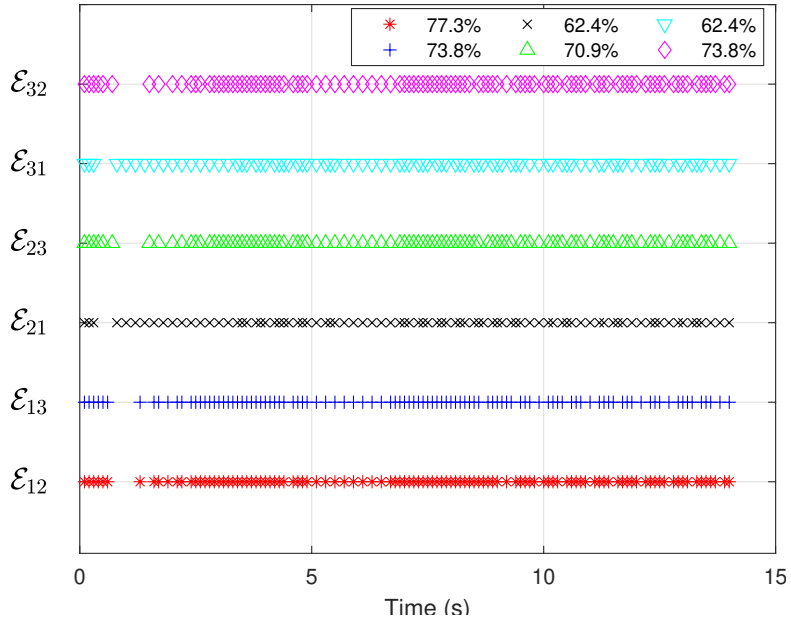

Figure 6.17: Experimental results of triggering instants of the system (5.1) under the edge-triggered state-error-based ECM

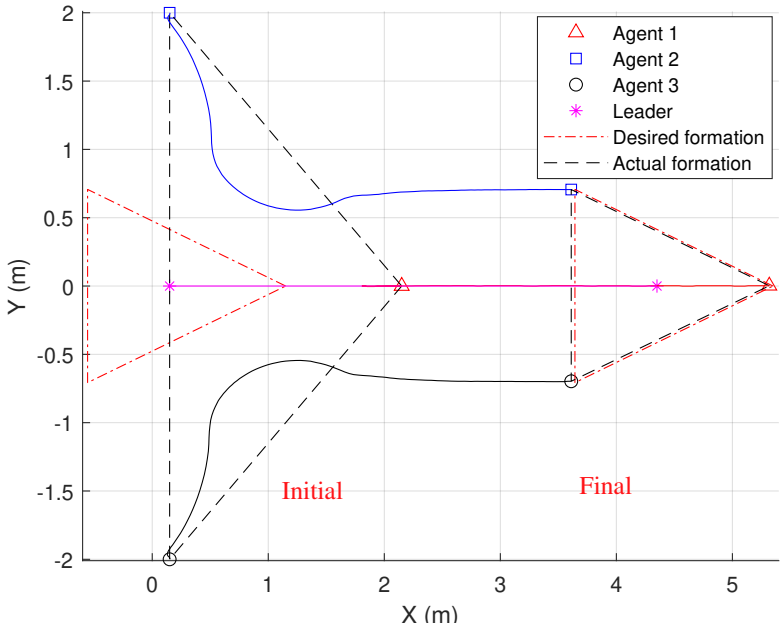

Figure 6.18: Experimental results of the formation evolution of the system (5.1) under the edge-based PCM

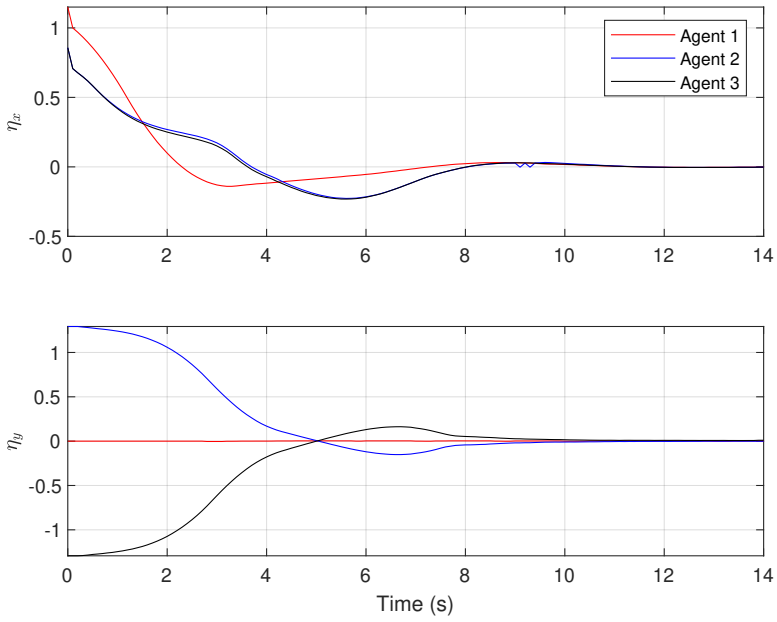

Figure 6.19: Experimental results of the formation error of the system (5.1) under the edge-based PCM

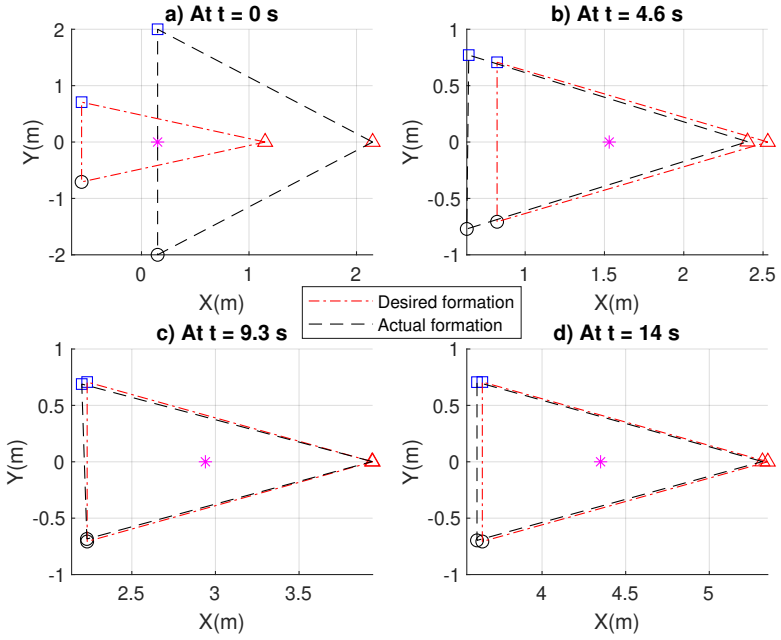

Figure 6.20: Experimental results of snapshots of the system (5.1) under the edge-based PCM in the X-Y plane at: a) t=0 *sec*, b) t=4.6 *sec*, c) t=9.3 *sec*, d) t=14 *sec*

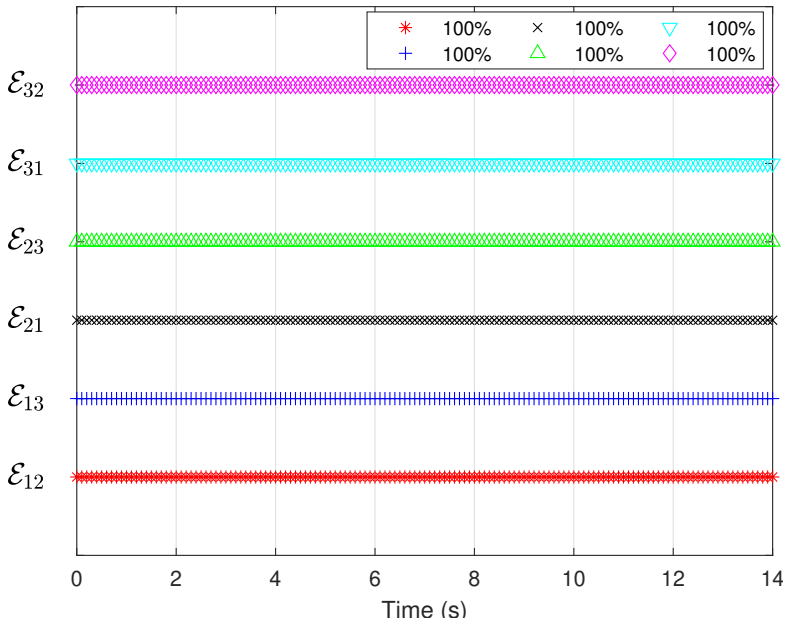

Figure 6.21: Experimental results of the triggering instants of the system (5.1) under the edge-based PCM

6.6 Conclusion

The leader-follower formation tracking control problem for a networked linear MAS consisting of one non-autonomous leader was investigated in this chapter. A novel locally-computable asynchronous edge-based ECM was proposed to regulate the inter-agent communication. A new distributed formation tracking controller was then designed based on the edge-event-generator-regulated information. Sufficient LMI conditions that ensure the formation error signals converge to a neighborhood near the origin asymptotically or exponentially were derived using Lyapunov-based methods. Simulation and experiment show that the developed edge-based ECM can generally generate less communication events than a node-based ECM while still providing a comparable performance.

Chapter 7

Affine Formation Control for Multiple Quadcopters

This Chapter investigates Research Problem 2.3 as described in the problem formulation section of Chapter 2. It is important to note that the desired formations in the previous chapters are specified by a set of pre-designed constant formation vectors (i.e. $f_1, \cdots, f_N$), and the developed formation control strategies are not adapted to changes in the environment (e.g. obstacle avoidance). In contrast, the desired group formation is a time-varying transformation (i.e. rotation, scaling, and shear) of a nominal formation in affine formation control designs, and the transformations are completely specified by a subset of agents (leaders). Therefore, the leaders (equipped with intelligent decision making programs and advanced sensors) can influence the followers (without advanced decision making abilities) to dynamically respond to the environment by properly designing the affine formation control strategies. In this chapter, we design affine formation controllers for a group of quadcopters with theoretical translational dynamics (7.1a) and experimentally identified attitude dynamics (7.1b) for the i^{th} agent as follows (note the translational dynamics and attitude dynamics are taken from Section 3.2)

$$\begin{bmatrix} \ddot{x}_i \\ \ddot{y}_i \\ \ddot{z}_i \end{bmatrix} = -g \begin{bmatrix} 0 \\ 0 \\ 1 \end{bmatrix} + \frac{T}{m} \begin{bmatrix} C_{\psi_i} S_{\theta_i} C_{\phi_i} + S_{\psi_i} S_{\phi_i} \\ S_{\psi_i} S_{\theta_i} C_{\phi_i} - C_{\psi_i} S_{\phi_i} \\ C_{\theta_i} C_{\phi_i} \end{bmatrix}, \tag{7.1a}$$

$$\begin{bmatrix} \dot{\phi}_i \\ \dot{\theta}_i \\ \dot{\psi}_i \end{bmatrix} = \begin{bmatrix} \frac{1}{\tau_{\phi_i}}(-\phi_i + k_{\phi_i}\phi_{ci}) \\ \frac{1}{\tau_{\theta_i}}(-\theta_i + k_{\theta_i}\theta_{ci}) \\ \psi_{ci} \end{bmatrix}. \tag{7.1b}$$

7.1 Affine Controller Design

Note that the Z-dynamics (7.1a) and yaw-dynamics (7.1b) are fully-actuated and controllers (e.g. PID controllers) can be designed to independently stabilize them. To simplify the affine formation control design, we only consider the coupled dynamics in the XY-plane as

$$\begin{bmatrix} \ddot{x}_i \\ \ddot{y}_i \end{bmatrix} = \frac{T}{m} \begin{bmatrix} C_{\psi_i} S_{\theta_i} C_{\phi_i} + S_{\psi_i} S_{\phi_i} \\ S_{\psi_i} S_{\theta_i} C_{\phi_i} - C_{\psi_i} S_{\phi_i} \end{bmatrix}, \tag{7.2a}$$

$$\begin{bmatrix} \dot{\phi}_i \\ \dot{\theta}_i \end{bmatrix} = \begin{bmatrix} \frac{1}{\tau_{\phi_i}}(-\phi_i + k_{\phi_i}\phi_{ci}) \\ \frac{1}{\tau_{\theta_i}}(-\theta_i + k_{\theta_i}\theta_{ci}) \end{bmatrix}. \tag{7.2b}$$

In the following development, we propose a two-layer (formation layer and local control layer) affine formation control design. In the formation layer, we define the virtual affine formation control input for (7.2a) as

$$\begin{bmatrix} U_{xi} \\ U_{yi} \end{bmatrix} = \frac{T}{m} \begin{bmatrix} C_{\psi_i} S_{\theta_i} C_{\phi_i} + S_{\psi_i} S_{\phi_i} \\ S_{\psi_i} S_{\theta_i} C_{\phi_i} - C_{\psi_i} S_{\phi_i} \end{bmatrix}. \tag{7.3}$$

Therefore, (7.2a) can be rewritten as a virtual double-integrator system

$$\begin{bmatrix} \ddot{x}_i \\ \ddot{y}_i \end{bmatrix} = \begin{bmatrix} U_{xi} \\ U_{yi} \end{bmatrix}. \tag{7.4}$$

We further define U_i, p_i, v_i and a_i for the i^{th} agent as

$$U_i = \begin{bmatrix} U_{xi} \\ U_{yi} \end{bmatrix}, p_i = \begin{bmatrix} x_i \\ y_i \end{bmatrix}, v_i = \begin{bmatrix} \dot{x}_i \\ \dot{y}_i \end{bmatrix}, a_i = \begin{bmatrix} \ddot{x}_i \\ \ddot{y}_i \end{bmatrix},$$

and propose an affine formation controller as

$$U_i = -\frac{1}{r_i} \sum_{j \in \mathcal{N}_i} \omega_{ij} \big[k_p(p_i - p_j) + k_v(v_i - v_j) - a_j \big], \tag{7.5}$$

where $r_i = [\Omega_{ii}]$ (Ω_{ii} is the diagonal term in a stress matrix), and k_p, k_v are positive gains. In addition, from Lemma 2.2, the matrix Ω_{ff} is positive definite and thus $r_i > 0$ ((7.5) is well-defined) for a group nominal formation $(\mathcal{G}, r)$ satisfying Assumption 2.2.

Then the augmented closed-loop system can be obtained as

$$\bar{\Omega}_{ff}\dot{v}_f + \bar{\Omega}_{fl}\dot{v}_l = -k_p\bar{\Omega}_{fl}p_l - k_p\bar{\Omega}_{ff}p_f - k_v\bar{\Omega}_{fl}v_l - k_v\bar{\Omega}_{ff}v_f, \tag{7.6}$$

where $\bar{\Omega}_{ll}$ is defined as $\Omega_{ll} \otimes \mathbf{I}_2$ with Ω_{ll} from (2.2). $\bar{\Omega}_{lf}$, $\bar{\Omega}_{fl}$, $\bar{\Omega}_{ff}$ are defined analogously. p_f/v_f denotes the stacked follower position/velocity vector and p_f/v_f denotes the stacked leader position/velocity vector. The dyanmics of the affine formation error in Definition 2.5 can then be represented using (7.6) as

$$\begin{bmatrix}\dot{\delta}_p \\ \dot{\delta}_v\end{bmatrix} = \begin{bmatrix}\delta_v \\ -k_p\delta_p - k_v\delta_v\end{bmatrix}, \tag{7.7}$$

which is stable for $k_p > 0$ and $k_v > 0$. Note that the desired pitch and roll angles induced by the virtual control inputs can be computed from (7.1a) as

$$\phi_{di} = \arcsin(\frac{m}{T}(U_{xi}S_{\psi_i} - U_{yi}C_{\psi_i})), \tag{7.8a}$$

$$\theta_{di} = \arctan(\frac{U_{xi}C_{\psi_i} + U_{yi}S_{\psi_i}}{U_{zi} + g}), \tag{7.8b}$$

where U_{zi} denotes the virtual control input in Z-direction. In addition, it can be verified that $U_{xi}^2 + U_{yi}^2 + (g + U_{zi})^2 = (\frac{T}{m})^2$. Therefore, ϕ_{di} and θ_{di} can be further simplified as

$$\phi_{di} = \arcsin\big(\frac{(U_{xi}S_{\psi_i} - U_{yi}C_{\psi_i}}{\sqrt{U_{xi}^2 + U_{yi}^2 + g^2}}\big), \tag{7.9a}$$

$$\theta_{di} = \arctan\big(\frac{U_{xi}C_{\psi_i} + U_{yi}S_{\psi_i}}{g}\big). \tag{7.9b}$$

Then, finite-time controllers will be proposed to track ϕ_{di} and θ_{di} in the local control layer. To proceed, we define the tracking error in the roll-direction as $e_{\phi_i} = \phi_{di} - \phi$ and propose the following Lyapunov function candidate

$$V_{\phi_i} = \frac{1}{2}e_{\phi_i}^2. \tag{7.10}$$

Take the time derivative of V_{ϕ_i} to obtain

$$\dot{V}_{\phi_i} = e_{\phi_i}(\dot{\phi}_{di} - \frac{1}{\tau_{\phi_i}}(e_{\phi_i} - \phi_{di} + k_{\phi_i}\phi_{ci})), \tag{7.11}$$

which is bounded as

$$\dot{V}_{\phi_i} \leq -(\sigma_{\phi_i} - |\dot{\phi}_{di}|)|e_{\phi_i}|, \tag{7.12}$$

by designing

$$\phi_{ci} = \frac{1}{k_{\phi_i}}(-e_{\phi_i} + \phi_{di} + \tau_\phi \sigma_{\phi_i} sign(e_{\phi_i})) \tag{7.13}$$

In addition, (7.12) can be rewritten as

$$\dot{V}_{\phi_i} + (\sigma_{\phi_i} - |\dot{\phi}_{di}|)\sqrt{2V_{\phi_i}} \leq 0. \tag{7.14}$$

It can be concluded that $V_{\phi_i} \to 0$ in finite time [99] if we choose $\sigma_{\phi_i} > \max|\dot{\phi}_{di}|$. A similar finite-time tracking controller can be designed for the pitch motion as

$$\theta_{ci} = \frac{1}{k_{\theta_i}}(-e_{\theta_i} + \theta_{di} + \tau_\theta \sigma_{\theta_i} sign(e_{\theta_i})), \tag{7.15}$$

where $\sigma_{\theta_i} \max|\dot{\theta}_{di}|$.

7.2 Simulation Results

In this section, we study the developed two-layer affine formation controller with a group of six quadcopter agents (three followers and three leaders) under a nominal formation configuration $(\mathcal{G}, r)$ shown in Fig. 7.1. Note that the affine formation controllers will only be applied to the XY-plane and each agent is independently controlled in Z- and yaw-directions using well-tuned PID controllers. In addition, three leaders are selected in the nominal formation in order to satisfy the affine-span-condition in Assumption 2.2 since at least three leaders are required to affinely span a 2-D space. It can be verified that the communication graph in Fig. 7.1 is universally rigid based on Definition 2.1. Therefore, all the conditions stated in Assumption 2.2 are satisfied and the resultant Ω_{ff} matrix is positive definite. The nominal configuration r is designed as

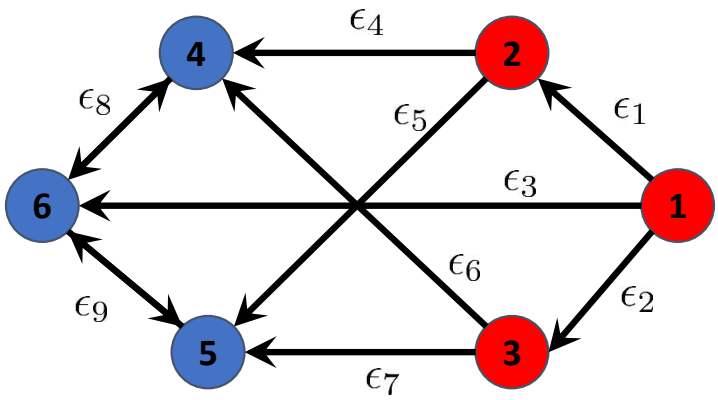

Figure 7.1: Nominal formation configuration with three leaders (in red) and three followers (in blue)

$$r_1 = \begin{bmatrix} 0.5 \\ 0 \end{bmatrix}, r_2 = \begin{bmatrix} 0 \\ 0.5 \end{bmatrix}, r_3 = \begin{bmatrix} 0 \\ -0.5 \end{bmatrix}, r_4 = \begin{bmatrix} -0.5 \\ 0.5 \end{bmatrix}, r_5 = \begin{bmatrix} -0.5 \\ -0.5 \end{bmatrix}, r_6 = \begin{bmatrix} -1 \\ 0 \end{bmatrix}.$$

The normalized equilibrium stress vector for edges $\epsilon_1, \cdots, \epsilon_9$ can then be computed based on the nominal configuration as

$$\omega = \begin{bmatrix} 0.3254 & 0.3254 & -0.2169 & 0.4881 & -0.1627 & -0.1627 & 0.4881 & 0.3254 & 0.3254 \end{bmatrix},$$

and the corresponding stress matrix is given as

$$\Omega = \begin{bmatrix} 0.4339 & -0.3254 & -0.3254 & 0 & 0 & 0.2169 \\ -0.3254 & 0.6508 & 0 & -0.4881 & 0.1627 & 0 \\ -0.3254 & 0 & 0.6508 & 0.1627 & -0.4881 & 0 \\ 0 & -0.4881 & 0.1627 & 0.6508 & 0 & -0.3254 \\ 0 & 0.1627 & -0.4881 & 0 & 0.6508 & -0.3254 \\ 0.2169 & 0 & 0 & -0.3254 & -0.3254 & 0.4339 \end{bmatrix}.$$

Moreover, in all simulations, the controller parameters are chosen as $k_p = 10$, $k_v = 7.05$, $\sigma_{\phi_i} = \sigma_{\theta_i} = 7.31$, and the *Sign* functions in (7.13) and (7.15) are replaced by a Sigmoid function to reduce the chattering effect that may occur.

Fig. 7.2 shows the simulated evolution of all agents under the proposed two-layer affine formation controller in the X-Y plane. The leaders' trajectories are planned in advance, and all leaders are initially moving at a constant speed in the X-direction and

then they try to scale down to a tighter formation in order to pass through a narrow passage. The leaders will then scale back to the nominal formation when successfully leaving the passage. Note that leaders may generate desired trajectories online based on the task requirements and surrounding conditions in real life applications. Fig. 7.3 depicts the system affine formation error over the duration of the simulation, which validates that a solution to Research Problem 2.3 has been accomplished in simulation. The snapshots of the group formation in the X-Y plane at t = 0 sec, 10 sec, 20 sec, and 30 sec are given in Fig. 7.4, and Fig. 7.5 demonstrates the group evolution in 3D.

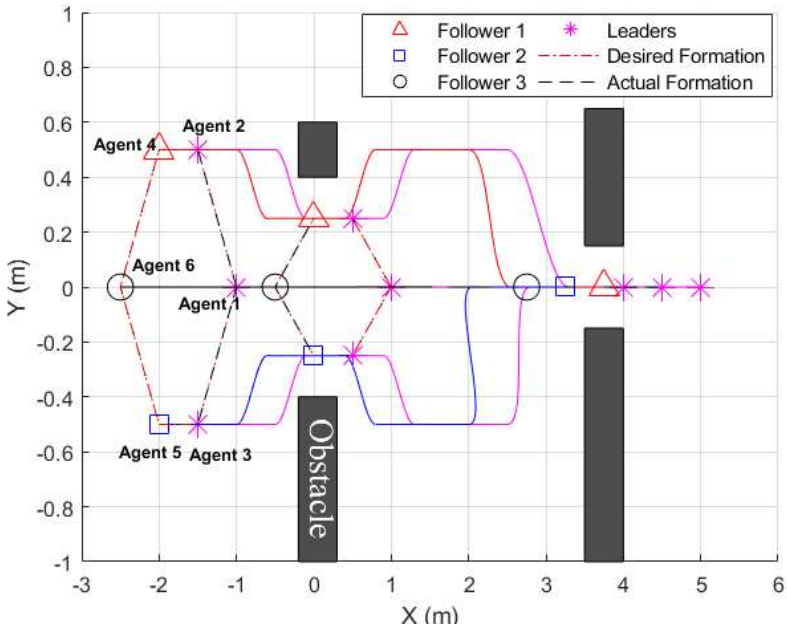

Figure 7.2: Simulation results of the formation evolution in X-Y plane

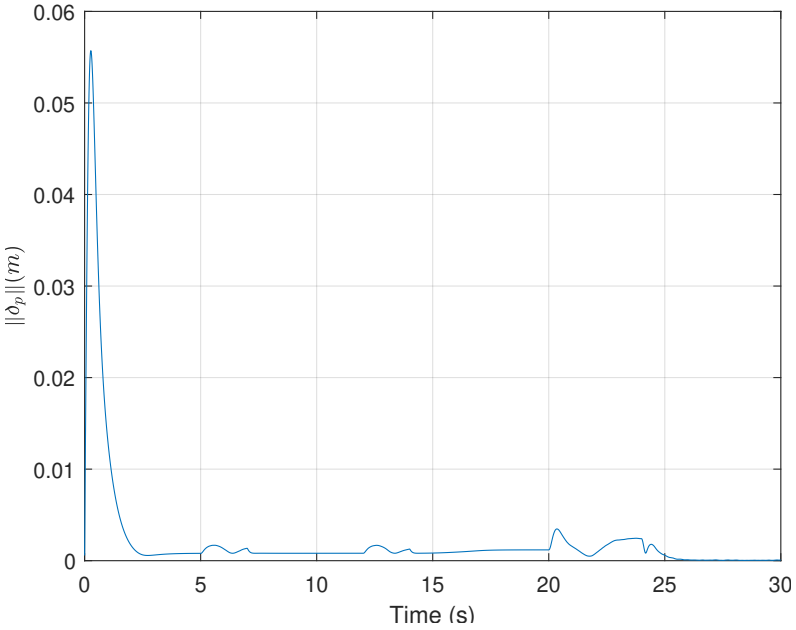

Figure 7.3: Simulation results of the affine formation error

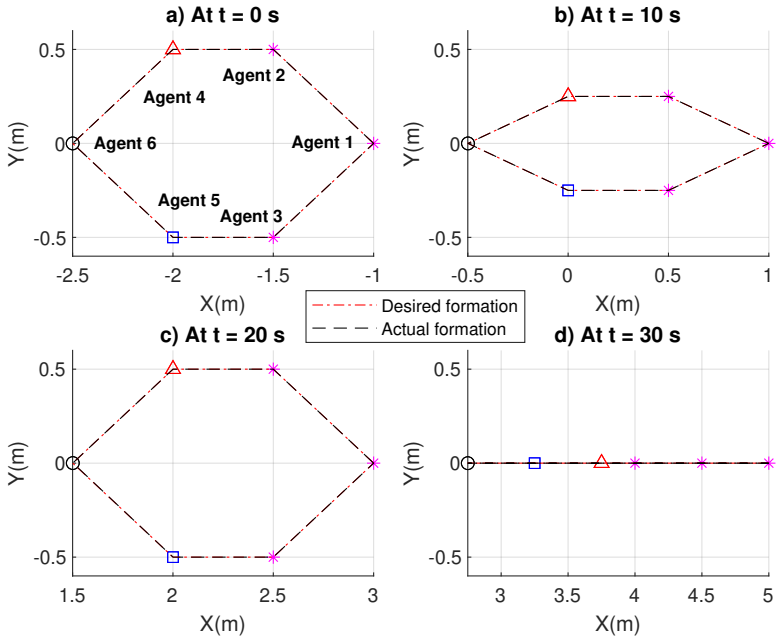

Figure 7.4: Simulation results of snapshots of the group formation in the X-Y plane at: a) t=0 *sec*, b) t=10 *sec*, c) t=20 *sec*, d) t=30 *sec*

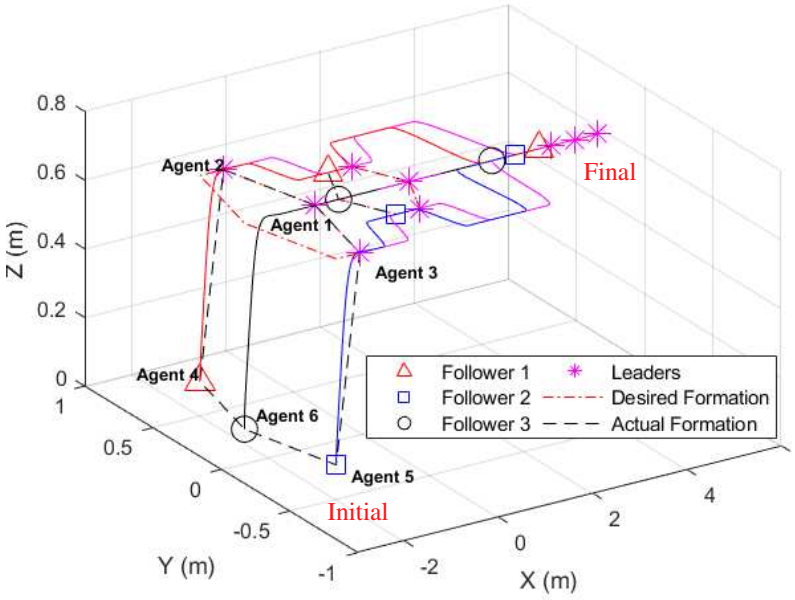

Figure 7.5: Simulation results of the formation evolution in 3D

7.3 Conclusion

This chapter investigated the affine formation control of a group of qaudcopters with experimentally identified dynamics. A two-layer formation control structure was proposed to account for the underactuated nature of quadcopter dynamics. A linear affine formation controller was designed based on the networked virtual double-integrator agents in the formation layer, and a finite-time controller was developed to track the desired virtual inputs in the local controller layer. The developed two-layer affine formation control method was validated in X-Y plane using a group of six quadcopters in simulations.

Chapter 8

Conclusions and Future Research

8.1 Conclusions

Chapter 4 investigates the leader-follower formation tracking control problem for MASs consisting of one autonomous leader and multiple general linear homogeneous followers with a sampled-data-based ECM using Lyapunov-based LMI methods. In particular, the formation control problem was transformed into a stability analysis problem of a closed-loop time-delayed system under the proposed formation protocol and ECM. The communication event generator and the controller were then co-designed based on the formulated sufficient conditions that ensure an asymptotic convergence to the neighborhood of the desired formation. Numerical simulations and experimental implementations were conducted using a group of unicyle-type mobile robots with linearized dynamics to validate the proposed method.

The leader-follower formation tracking control problem for linear MASs with a non-autonomous leader was studied in Chapter 5. A novel state-estimate-based event generator was established for each follower agent to regulate the inter-agent communication at each sampling instant. A new formation tracking controller was then designed based on the event generator regulated information, and new LMI conditions that guarantee the ultimate boundedness of the closed-loop formation error dynamics were derived. It was observed in both simulation and experiment that, for the conditions used in this research, the developed estimate-error-based ECM introduces fewer communication instants than the traditional state-error-based mechanisms or PCM without any notable differences in the formation control performance.

The same formation control problem from Chapter 5 was studied in Chapter 6 using a novel locally-computable asynchronous edge-based ECM. A new distributed

formation tracking controller was then designed based on the edge-event-generator-regulated information. Sufficient LMI conditions that guarantee asymptotic and exponential convergence are derived, respectively. In addition, the exponential convergence rate is explicitly expressed in the derived exponential convergence conditions and can be tuned based on design requirements. Simulation and experimental results show that, for the conditions used in this research, the newly-proposed edge-based ECM can, in general, generate less triggering events than the node-based ECMs.

Chapter 7 studies the time-varying formation control problem of a multi-quadcopter system using affine formation control strategies. Given the underactuated nature of quadcopters, a two-layer (formation layer and local control layer) formation control design is proposed. In the formation layer, a quadcopter is treated as a virtual double-integrator and affine formation controllers were designed based on the networked virtual double-integrator agents. The resultant virtual affine formation control inputs were then converted to the desired attitudes based on the quadcopter dynamics, and a sliding mode controller was then proposed to ensure finite-time tracking convergence to the desired attitude in the local control layer. Simulations were conducted in the XY-plane to successfully validate the proposed controllers.

8.2 Future Research

Although collision avoidance and obstacle avoidance are important for practical implementable formation controllers, they are not explicitly considered in this thesis. Control barrier functions have been found to be successful in several collision avoidance scenarios [100, 101]. The main idea involves designing a safety controller that ensures the forward invariance of a pre-designed safety set, and the safety controller can then be united with other nominal formation controllers using quadratic programming to achieve safety-critical formations. Centralized formulation is the main drawback of this method, thus it would be interesting to investigate the application of control barrier functions in collision avoidance using a distributed manner.

It should be noted that the formation controllers in Chapters 5 and 6 require absolute velocity information from neighboring agents; however, velocity information is not easily obtained (more communication load) in practical MAS settings. It would be interesting to design formation controllers without using velocity measurements.

Alternatively, velocity estimators could be designed based on the information locally available.

As mentioned in Chapter 1, the requirement of sampling synchronization across all agents imposes a major limitation on the sampled-data-based ETC design. In addition to distributedly synchronizing the agents' clocks, it is also possible to design formation controllers that are robust to sampling asynchronization. In particular, measurements from an agent with asynchronized sampling may be modeled as measurements with constant long-delays, and tools from delayed-systems can possibly be applied to analyze system stability.

Other interesting future research directions include: experimental validation of the two-layer affine formation controllers developed in Chapter 7, affine formation control for MASs with more complex agent dynamics (e.g. general linear dynamics and Euler-Lagrange dynamics), event-triggered affine formation control, and fully distributed (without explicit knowledge of the communication topology and total number of agents) sampled-data-based formation tracking controller design.

Bibliography

[1] J. E. Noronha, *Development of a swarm control platform for educational and research applications*. PhD thesis, Iowa State University, 2016.

[2] D. Mellinger, M. Shomin, N. Michael, and V. Kumar, "Cooperative grasping and transport using multiple quadrotors," in *Distributed Autonomous Robotic Systems*, pp. 545–558, Springer, 2013.

[3] M. Debord, "Tesla is going to have to spend an absolutely staggering amount of money in the next few years (TSLA)." `https://sg.finance.yahoo.com/news/tesla-going-spend-absolutely-staggering-125700396.html`, 2018.

[4] P. B. Lissaman and C. A. Shollenberger, "Formation flight of birds," *Science*, vol. 168, no. 3934, pp. 1003–1005, 1970.

[5] Z. Hou and I. Fantoni, "Distributed leader-follower formation control for multiple quadrotors with weighted topology," in *2015 10th System of Systems Engineering Conference (SoSE)*, pp. 256–261, IEEE, 2015.

[6] K. A. Ghamry and Y. Zhang, "Cooperative control of multiple uavs for forest fire monitoring and detection," in *2016 12th IEEE/ASME International Conference on Mechatronic and Embedded Systems and Applications (MESA)*, pp. 1–6, IEEE, 2016.

[7] M. A. Lewis and K.-H. Tan, "High precision formation control of mobile robots using virtual structures," *Autonomous robots*, vol. 4, no. 4, pp. 387–403, 1997.

[8] J. R. Lawton, R. W. Beard, and B. J. Young, "A decentralized approach to formation maneuvers," *IEEE Transactions on Robotics and Automation*, vol. 19, no. 6, pp. 933–941, 2003.

[9] W. Ren, "Consensus strategies for cooperative control of vehicle formations," *IET Control Theory & Applications*, vol. 1, no. 2, pp. 505–512, 2007.

[10] W. Ren and R. W. Beard, *Distributed consensus in multi-vehicle cooperative control*, vol. 27. Springer, 2008.

[11] M. Ji and M. Egerstedt, "Distributed coordination control of multiagent systems while preserving connectedness," *IEEE Transactions on Robotics*, vol. 23, no. 4, pp. 693–703, 2007.

[12] D. V. Dimarogonas and K. J. Kyriakopoulos, "A connection between formation infeasibility and velocity alignment in kinematic multi-agent systems," *Automatica*, vol. 44, no. 10, pp. 2648–2654, 2008.

[13] K.-K. Oh and H.-S. Ahn, "Distance-based undirected formations of single-integrator and double-integrator modeled agents in n-dimensional space," *International Journal of Robust and Nonlinear Control*, vol. 24, no. 12, pp. 1809–1820, 2014.

[14] H. G. De Marina, B. Jayawardhana, and M. Cao, "Distributed rotational and translational maneuvering of rigid formations and their applications," *IEEE Transactions on Robotics*, vol. 32, no. 3, pp. 684–697, 2016.

[15] S. Zhao and D. Zelazo, "Translational and scaling formation maneuver control via a bearing-based approach," *IEEE Transactions on Control of Network Systems*, vol. 4, no. 3, pp. 429–438, 2015.

[16] S. Zhao, Z. Li, and Z. Ding, "Bearing-only formation tracking control of multiagent systems," *IEEE Transactions on Automatic Control*, vol. 64, no. 11, pp. 4541–4554, 2019.

[17] S. Coogan and M. Arcak, "Scaling the size of a formation using relative position feedback," *Automatica*, vol. 48, no. 10, pp. 2677–2685, 2012.

[18] M.-C. Park, K. Jeong, and H.-S. Ahn, "Formation stabilization and resizing based on the control of inter-agent distances," *International Journal of Robust and Nonlinear Control*, vol. 25, no. 14, pp. 2532–2546, 2015.

[19] T. Han, Z. Lin, R. Zheng, and M. Fu, "A barycentric coordinate-based approach to formation control under directed and switching sensing graphs," *IEEE Transactions on Cybernetics*, vol. 48, no. 4, pp. 1202–1215, 2017.

[20] Z. Han, L. Wang, Z. Lin, and R. Zheng, "Formation control with size scaling via a complex laplacian-based approach," *IEEE Transactions on Cybernetics*, vol. 46, no. 10, pp. 2348–2359, 2015.

[21] X. Li and L. Xie, "Dynamic formation control over directed networks using graphical laplacian approach," *IEEE Transactions on Automatic Control*, vol. 63, no. 11, pp. 3761–3774, 2018.

[22] Z. Lin, L. Wang, Z. Chen, M. Fu, and Z. Han, "Necessary and sufficient graphical conditions for affine formation control," *IEEE Transactions on Automatic Control*, vol. 61, no. 10, pp. 2877–2891, 2015.

[23] S. Zhao, "Affine formation maneuver control of multiagent systems," *IEEE Transactions on Automatic Control*, vol. 63, no. 12, pp. 4140–4155, 2018.

[24] J. A. Fax and R. M. Murray, "Information flow and cooperative control of vehicle formations," *IEEE Transactions on Automatic Control*, vol. 49, no. 9, pp. 1465–1476, 2004.

[25] X. Dong, J. Xi, G. Lu, and Y. Zhong, "Formation control for high-order linear time-invariant multiagent systems with time delays," *IEEE Transactions on Control of Network Systems*, vol. 1, no. 3, pp. 232–240, 2014.

[26] X. Dong, Q. Li, Q. Zhao, and Z. Ren, "Time-varying group formation analysis and design for general linear multi-agent systems with directed topologies," *International Journal of Robust and Nonlinear Control*, vol. 27, no. 9, pp. 1640–1652, 2017.

[27] X. Dong and G. Hu, "Time-varying formation control for general linear multi-agent systems with switching directed topologies," *Automatica*, vol. 73, pp. 47–55, 2016.

[28] R. Wang, X. Dong, Q. Li, and Z. Ren, "Distributed adaptive time-varying formation for multi-agent systems with general high-order linear time-invariant dynamics," *Journal of the Franklin Institute*, vol. 353, no. 10, pp. 2290–2304, 2016.

[29] Y. Hua, X. Dong, Q. Li, and Z. Ren, "Distributed time-varying formation robust tracking for general linear multiagent systems with parameter uncertainties and external disturbances," *IEEE transactions on cybernetics*, vol. 47, no. 8, pp. 1959–1969, 2017.

[30] Y. Hua, X. Dong, G. Hu, Q. Li, and Z. Ren, "Distributed time-varying output formation tracking for heterogeneous linear multiagent systems with a nonautonomous leader of unknown input," *IEEE Transactions on Automatic Control*, vol. 64, no. 10, pp. 4292–4299, 2019.

[31] C. Nowzari, E. Garcia, and J. Cortés, "Event-triggered communication and control of networked systems for multi-agent consensus," *Automatica*, vol. 105, pp. 1–27, 2019.

[32] D. V. Dimarogonas, E. Frazzoli, and K. H. Johansson, "Distributed event-triggered control for multi-agent systems," *IEEE Transactions on Automatic Control*, vol. 57, no. 5, pp. 1291–1297, 2011.

[33] Y. Zhu, X. Guan, X. Luo, and S. Li, "Finite-time consensus of multi-agent system via nonlinear event-triggered control strategy," *IET Control Theory & Applications*, vol. 9, no. 17, pp. 2548–2552, 2015.

[34] M. Ghodrat and H. J. Marquez, "An integral based event triggered control scheme of distributed network systems," in *2015 European Control Conference (ECC)*, pp. 1724–1729, IEEE, 2015.

[35] G. S. Seyboth, D. V. Dimarogonas, and K. H. Johansson, "Event-based broadcasting for multi-agent average consensus," *Automatica*, vol. 49, no. 1, pp. 245–252, 2013.

[36] Y.-Y. Qian, L. Liu, and G. Feng, "Distributed event-triggered adaptive control for consensus of linear multi-agent systems with external disturbances," *IEEE transactions on cybernetics*, vol. 50, no. 5, pp. 2197–2208, 2018.

[37] E. Garcia, Y. Cao, and D. W. Casbeer, "Decentralized event-triggered consensus with general linear dynamics," *Automatica*, vol. 50, no. 10, pp. 2633–2640, 2014.

[38] P. Yu, C. Fischione, and D. V. Dimarogonas, "Distributed event-triggered communication and control of linear multiagent systems under tactile communication," *IEEE Transactions on Automatic Control*, vol. 63, no. 11, pp. 3979–3985, 2018.

[39] B. Cheng and Z. Li, "Fully distributed event-triggered protocols for linear multiagent networks," *IEEE Transactions on Automatic Control*, vol. 64, no. 4, pp. 1655–1662, 2018.

[40] Q. Liu, M. Ye, J. Qin, and C. Yu, "Event-triggered algorithms for leader–follower consensus of networked euler–lagrange agents," *IEEE Transactions on Systems, Man, and Cybernetics: Systems*, vol. 49, no. 7, pp. 1435–1447, 2017.

[41] T.-H. Cheng, Z. Kan, J. M. Shea, and W. E. Dixon, "Decentralized event-triggered control for leader-follower consensus," in *53rd IEEE Conference on Decision and Control*, pp. 1244–1249, IEEE, 2014.

[42] C. Nowzari and J. Cortés, "Distributed event-triggered coordination for average consensus on weight-balanced digraphs," *Automatica*, vol. 68, pp. 237–244, 2016.

[43] D. Yang, W. Ren, X. Liu, and W. Chen, "Decentralized event-triggered consensus for linear multi-agent systems under general directed graphs," *Automatica*, vol. 69, pp. 242–249, 2016.

[44] T.-H. Cheng, Z. Kan, J. R. Klotz, J. M. Shea, and W. E. Dixon, "Decentralized event-triggered control of networked systems-part 1: Leader-follower consensus under switching topologies," in *2015 American Control Conference (ACC)*, pp. 5438–5443, IEEE, 2015.

[45] T.-H. Cheng, Z. Kan, J. R. Klotz, J. M. Shea, and W. E. Dixon, "Event-triggered control of multiagent systems for fixed and time-varying network topologies," *IEEE Transactions on Automatic Control*, vol. 62, no. 10, pp. 5365–5371, 2017.

[46] Y. Fan, L. Liu, G. Feng, and Y. Wang, "Self-triggered consensus for multi-agent systems with zeno-free triggers," *IEEE Transactions on Automatic Control*, vol. 60, no. 10, pp. 2779–2784, 2015.

[47] J. Wang, C. Wang, D. Wang, and F. Deng, "Event/self-triggered consensus control of multiagent systems with undesirable sensor signals," *IEEE Transactions on Cybernetics*, 2020.

[48] B. Cheng and Z. Li, "Coordinated tracking control with asynchronous edge-based event-triggered communications," *IEEE Transactions on Automatic Control*, vol. 64, no. 10, pp. 4321–4328, 2019.

[49] B. Wei, F. Xiao, and M.-Z. Dai, "Edge event-triggered control for multi-agent systems under directed communication topologies," *International Journal of Control*, vol. 91, no. 4, pp. 887–896, 2018.

[50] G. Guo, L. Ding, and Q.-L. Han, "A distributed event-triggered transmission strategy for sampled-data consensus of multi-agent systems," *Automatica*, vol. 50, no. 5, pp. 1489–1496, 2014.

[51] C. Nowzari and J. Cortés, "Team-triggered coordination for real-time control of networked cyber-physical systems," *IEEE Transactions on Automatic Control*, vol. 61, no. 1, pp. 34–47, 2015.

[52] X. Meng, L. Xie, and Y. C. Soh, "Asynchronous periodic event-triggered consensus for multi-agent systems," *Automatica*, vol. 84, pp. 214–220, 2017.

[53] X. Yi, K. Liu, D. V. Dimarogonas, and K. H. Johansson, "Distributed dynamic event-triggered control for multi-agent systems," in *2017 IEEE 56th annual conference on decision and control (CDC)*, pp. 6683–6698, IEEE, 2017.

[54] J. Berneburg and C. Nowzari, "Robust dynamic event-triggered coordination with a designable minimum inter-event time," *arXiv preprint arXiv:1903.04734*, 2019.

[55] L. Ding, Q.-L. Han, X. Ge, and X.-M. Zhang, "An overview of recent advances in event-triggered consensus of multiagent systems," *IEEE Transactions on Cybernetics*, vol. 48, no. 4, pp. 1110–1123, 2017.

[56] G. S. Seyboth, "Event-based controlfor multi-agent systems," 2010.

[57] W. Zhu, Z.-P. Jiang, and G. Feng, "Event-based consensus of multi-agent systems with general linear models," *Automatica*, vol. 50, no. 2, pp. 552–558, 2014.

[58] B. Mu, H. Li, W. Li, and Y. Shi, "Consensus for multiple euler-lagrange dynamics with arbitrary sampling periods and event-triggered strategy," in *Proceeding of the 11th World Congress on Intelligent Control and Automation*, pp. 2596–2601, IEEE, 2014.

[59] C. Peng, J. Zhang, and Q.-L. Han, "Consensus of multiagent systems with nonlinear dynamics using an integrated sampled-data-based event-triggered communication scheme," *IEEE Transactions on Systems, Man, and Cybernetics: Systems*, vol. 49, no. 3, pp. 589–599, 2018.

[60] C. Nowzari and J. Cortés, "Zeno-free, distributed event-triggered communication and control for multi-agent average consensus," in *2014 American Control Conference*, pp. 2148–2153, IEEE, 2014.

[61] A. Gollu and P. Varaiya, "Hybrid dynamical systems," in *Proceedings of the 28th IEEE Conference on Decision and Control,*, pp. 2708–2712, IEEE, 1989.

[62] J. Berneburg and C. Nowzari, "Distributed dynamic event-triggered coordination with a designable minimum inter-event time," in *2019 American Control Conference (ACC)*, pp. 1424–1429, IEEE, 2019.

[63] X.-M. Zhang and Q.-L. Han, "Event-triggered dynamic output feedback control for networked control systems," *IET Control Theory & Applications*, vol. 8, no. 4, pp. 226–234, 2014.

[64] X. Ge and Q.-L. Han, "Distributed formation control of networked multi-agent systems using a dynamic event-triggered communication mechanism," *IEEE Transactions on Industrial Electronics*, vol. 64, no. 10, pp. 8118–8127, 2017.

[65] X. Yin, D. Yue, and S. Hu, "Adaptive periodic event-triggered consensus for multi-agent systems subject to input saturation," *International Journal of Control*, vol. 89, no. 4, pp. 653–667, 2016.

[66] E. Garcia, Y. Cao, and D. W. Casbeer, "Cooperative control with general linear dynamics and limited communication: Centralized and decentralized event-triggered control strategies," in *2014 American Control Conference*, pp. 159–164, IEEE, 2014.

[67] W. Ren and Y. Cao, *Distributed coordination of multi-agent networks: emergent problems, models, and issues.* Springer Science & Business Media, 2010.

[68] M. Mesbahi and M. Egerstedt, *Graph theoretic methods in multiagent networks.* Princeton University Press, 2010.

[69] R. Connelly, "Generic global rigidity," *Discrete & Computational Geometry*, vol. 33, no. 4, pp. 549–563, 2005.

[70] R. Connelly and S. Guest, "Frameworks, tensegrities and symmetry: understanding stable structures," *Cornell University, College of Arts and Sciences*, 2015.

[71] R. A. Horn and C. R. Johnson, *Matrix analysis.* Cambridge university press, 2013.

[72] J. G. VanAntwerp and R. D. Braatz, "A tutorial on linear and bilinear matrix inequalities," *Journal of Process Control*, vol. 10, no. 4, pp. 363–385, 2000.

[73] A. De Luca and G. Oriolo, "Modelling and control of nonholonomic mechanical systems," in *Kinematics and dynamics of multi-body systems*, pp. 277–342, Springer, 1995.

[74] T. Luukkonen, "Modelling and control of quadcopter," *Independent research project in applied mathematics, Espoo*, vol. 22, 2011.

[75] G. V. Raffo, M. G. Ortega, and F. R. Rubio, "An integral predictive/nonlinear h-infinity control structure for a quadrotor helicopter," *Automatica*, vol. 46, no. 1, pp. 29–39, 2010.

[76] J. J. Craig, *Introduction to robotics: mechanics and control, 3/E*. Pearson Education India, 2009.

[77] H. A. Gonzalez, *Robust tracking of dynamic targets with aerial vehicles using quaternion-based techniques*. PhD thesis, Université de Technologie de Compiègne, 2019.

[78] M. Blösch, S. Weiss, D. Scaramuzza, and R. Siegwart, "Vision based mav navigation in unknown and unstructured environments," in *Proceedings of IEEE International Conference on Robotics and Automation*, (Alaska, USA), pp. 21–28, May. 2010.

[79] Z. Huang, R. Bauer, and Y.-J. Pan, "Closed-loop identification and real-time control of a micro quadcopter," *IEEE Transactions on Industrial Electronics*, 2021.

[80] M. Quigley, K. Conley, B. Gerkey, J. Faust, T. Foote, J. Leibs, R. Wheeler, A. Y. Ng, *et al.*, "Ros: an open-source robot operating system," in *ICRA workshop on open source software*, vol. 3, p. 5, Kobe, Japan, 2009.

[81] L. Joseph and J. Cacace, *Mastering ROS for Robotics Programming: Design, build, and simulate complex robots using the Robot Operating System*. Packt Publishing Ltd, 2018.

[82] E. Fernandez, L. S. Crespo, A. Mahtani, and A. Martinez, *Learning ROS for robotics programming*. Packt Publishing Ltd, 2015.

[83] W. Hönig and N. Ayanian, "Flying multiple uavs using ros," in *Robot Operating System (ROS)*, pp. 83–118, Springer, 2017.

[84] K. Gu, J. Chen, and V. L. Kharitonov, *Stability of time-delay systems*. Springer Science & Business Media, 2003.

[85] P. Park, J. W. Ko, and C. Jeong, "Reciprocally convex approach to stability of systems with time-varying delays," *Automatica*, vol. 47, no. 1, pp. 235–238, 2011.

[86] C. Ma and J. Zhang, "On formability of linear continuous-time multi-agent systems," *Journal of Systems Science and Complexity*, vol. 25, no. 1, pp. 13–29, 2012.

[87] D. Yue, E. Tian, and Q.-L. Han, "A delay system method for designing event-triggered controllers of networked control systems," *IEEE Transactions on Automatic Control*, vol. 58, no. 2, pp. 475–481, 2012.

[88] Y. Fan, G. Feng, Y. Wang, and C. Song, "Distributed event-triggered control of multi-agent systems with combinational measurements," *Automatica*, vol. 49, no. 2, pp. 671–675, 2013.

[89] M. Franceschelli, A. Gasparri, A. Giua, and C. Seatzu, "Decentralized laplacian eigenvalues estimation for networked multi-agent systems," in *Proceedings of the 48h IEEE Conference on Decision and Control (CDC) held jointly with 2009 28th Chinese Control Conference*, pp. 2717–2722, IEEE, 2009.

[90] P. Di Lorenzo and S. Barbarossa, "Distributed estimation and control of algebraic connectivity over random graphs," *IEEE Transactions on Signal Processing*, vol. 62, no. 21, pp. 5615–5628, 2014.

[91] L. Schenato and F. Fiorentin, "Average timesynch: A consensus-based protocol for clock synchronization in wireless sensor networks," *Automatica*, vol. 47, no. 9, pp. 1878–1886, 2011.

[92] E. Rohmer, S. P. Singh, and M. Freese, "V-rep: A versatile and scalable robot simulation framework," in *2013 IEEE/RSJ International Conference on Intelligent Robots and Systems*, pp. 1321–1326, IEEE, 2013.

[93] Z. Huang, Y.-J. Pan, and R. Bauer, "Formation control with dynamic non-autonomous leader using sampled-data event-triggered communication," in *2021 American Control Conference (ACC)*, pp. 2643–2648, IEEE, 2021.

[94] A. Seuret and F. Gouaisbaut, "Wirtinger-based integral inequality: application to time-delay systems," *Automatica*, vol. 49, no. 9, pp. 2860–2866, 2013.

[95] A. Selivanov and E. Fridman, "Observer-based input-to-state stabilization of networked control systems with large uncertain delays," *Automatica*, vol. 74, pp. 63–70, 2016.

[96] H. K. Khalil and J. W. Grizzle, *Nonlinear systems*, vol. 3. Prentice hall Upper Saddle River, NJ, 2002.

[97] K. Liu, V. Suplin, and E. Fridman, "Stability of linear systems with general sawtooth delay," *IMA Journal of Mathematical Control and Information*, vol. 27, no. 4, pp. 419–436, 2010.

[98] K. Liu and E. Fridman, "Wirtinger's inequality and lyapunov-based sampled-data stabilization," *Automatica*, vol. 48, no. 1, pp. 102–108, 2012.

[99] S. P. Bhat and D. S. Bernstein, "Finite-time stability of continuous autonomous systems," *SIAM Journal on Control and Optimization*, vol. 38, no. 3, pp. 751–766, 2000.

[100] A. D. Ames, X. Xu, J. W. Grizzle, and P. Tabuada, "Control barrier function based quadratic programs for safety critical systems," *IEEE Transactions on Automatic Control*, vol. 62, no. 8, pp. 3861–3876, 2016.

[101] L. Wang, A. D. Ames, and M. Egerstedt, "Safe certificate-based maneuvers for teams of quadrotors using differential flatness," in *2017 IEEE International Conference on Robotics and Automation (ICRA)*, pp. 3293–3298, IEEE, 2017.

Appendix A

Author's Publications

Journal Papers

1. **Z. Huang**, R. Bauer, and Y.-J. Pan, "Closed-Loop Identification and Real-Time Control of a Micro Quadcopter", *IEEE Transactions on Industrial Electronics*, 2021. (DOI: 10.1109/TIE.2021.3065613).

2. **Z. Huang**, Y.-J. Pan, and R. Bauer, "Sampled-Data Event-Triggered Control with Application to Quadcopter Formations", *International Journal of Control*, 2021. (https://doi.org/10.1080/00207179.2021.1978554)

3. **Z. Huang**, R. Bauer, and Y.-J. Pan, "Event-Triggered Formation Tracking Control with Application to Multiple Mobile Robots", *IEEE Transactions on Industrial Electronics*, Submitted. (Paper number: No. 21-TIE-3368)

4. **Z. Huang**, Y.-J. Pan, and R. Bauer, "Multiple Mobile Robots Formation Tracking Control with Edge-Triggered Communication Mechanism", *IEEE Transactions on Industrial Electronics*, In preparation.

5. **Z. Huang**, Y.-J. Pan, and R. Bauer, "Leader-Follower Consensus Control of Multiple Quadcopters under Communication Delays", *ASME Journal of Dynamic Systems, Measurement and Control*, Vol.141, No.10, pp. 1-10, 2019.

6. Y.-J. Pan, H. Werner, **Z. Huang** and M. Bartel, "Distributed Cooperative Control of Leader-Follower Multi-Agent Systems under Packet Dropouts for Quadcopters", *Systems and Control Letters*, Vol.106, pp.47-57, 2017.

Conference Papers

1. **Z. Huang**, Y.-J. Pan, and R. Bauer, "Multi-Quadcopter Formation Control Using Sampled-Data Event-Triggered Communication With Gain Optimization",

In Proceedings of the 47th Annual Conference of the IEEE Industrial Electronics Society, October 2021, Toronto, Canada.

2. **Z. Huang**, R. Bauer, and Y.-J. Pan, "Distributed Formation Tracking Control with Edge-Triggered Communication Mechanism", *In Proceedings of the 47th Annual Conference of the IEEE Industrial Electronics Society*, October 2021, Toronto, Canada.

3. **Z. Huang**, Y.-J. Pan, and R. Bauer, "Formation Control with Dynamic Non-Autonomous Leader Using Sampled-Data Event-Triggered Communication", *In Proceedings of the 2021 American Control Conference (ACC)*, May 2021, New Orleans, USA.

4. **Z. Huang**, R. Bauer, and Y.-J. Pan, "Distributed Robust Finite-Time Containment Control of Euler-Lagrange Systems", *In Proceedings of the 4th IEEE International Conference on Industrial Cyber-Physical Systems (ICPS)*, Victoria, BC, Canada.

5. **Z. Huang** and Y.-J. Pan, "Observer based Leader Following Consensus for Multi-Agent Systems with Random Packet Loss", *In Proceedings of the IEEE Conference on Control Technology and Applications*, August 2017, Hawaii, USA, pp. 1698-1703.